Complexity, segregation, and pattern formation in rotating-drum flows

G. Seiden*

Max Planck Institute for Dynamics and Self-Organization, D-37073 Göttingen, Germany

P. J. Thomas†

Fluid Dynamics Research Centre, School of Engineering, University of Warwick, Coventry, CV4 7AL, United Kingdom

(published 17 November 2011)

Rotating-drum flows span a variety of research areas, ranging from physics of granular matter through hydrodynamics of suspensions to pure liquid coating flows. Recent years have seen an intensified scientific activity associated with this unique geometrical configuration, which has contributed to our understanding of related subjects such as avalanches in granules and segregation in suspensions. The existing literature related to rotating-drum flows is reviewed, highlighting similarities and differences between the various flow realizations. Scaling laws expressing the importance of different mechanisms underlying the observed phenomena have been focused on. An emphasis is placed on pattern formation phenomena. Rotating-drum flows exhibit stationary patterns as well as traveling and oscillating patterns; they exhibit reversible transitions as well as hysteresis. Apart from the predominant cylindrical configuration, this review covers recent work done with tumblers having other geometries, such as the sphere and the Hele-Shaw cell.

DOI: 10.1103/RevModPhys.83.1323 PACS numbers: 89.75.−k, 45.70.Vn, 47.54.−r, 45.70.Qj

CONTENTS

I. INTRODUCTION

There are a few examples of experimental configurations that have been instrumental in the investigation of a wide range of physical phenomena. The rotating horizontal drum is one such example. From phenomena observed in pure liquids, such as solitary waves (Melo and Douady, 1993), through segregation in dilute suspensions (Boote and Thomas, 1999), to avalanches in granular matter (Jaeger, Liu, and Nagel, 1989), this simple geometric configuration has served as a unique experimental tool which contributed to our understanding of various physical systems. In addition to the importance of the rotating horizontal drum from a basic science perspective, it has a valuable contribution in industrial applications. The rotating drum is used in different processes, such as mixing in the pharmaceutical industry and wood debarking in the papermaking industry.

The goal of this article is to review the existing literature on flows associated with the rotating horizontal drum

*Current address: Weizmann Institute of Science, Rehovot 76100, Israel.
gabriel.seiden@weizmann.ac.il
†pjt1@eng.warwick.ac.uk

configuration. We consider partially and completely filled systems. We discuss flows with homogeneous liquids and flows with particle-laden liquids carrying varying amounts of small solid particles, including the limiting case of purely granular flow. We highlight particular characteristics, as well as similarities and differences between flows associated with different parameter regimes. Emphasis is placed on pattern formation phenomena. The types of patterns considered here are those that are established either when the fluid itself adopts certain characteristic flow states or those patterns that form in particle-laden flow as a result of, or in connection with, particle segregation.

The vast majority of results summarized in this article originally appeared in the literature during the last two decades. While a few recent reviews focused on the particular case of granular flows within a rotating horizontal drum [see, e.g., Ottino and Khakhar (2000) and Meier, Lueptow, and Ottino (2007)], we are not aware of the existence of previous works that summarize, compare, and interrelate studies on the different realizations of rotating-drum flows.

The remainder of the article is arranged as follows. Section II describes a typical experimental setup, sets the nomenclature used in the article, and gives a general dimensional analysis. Section III deals with phenomena related to pure liquids. Sections IV and V describe particle-laden flows in partially and completely filled drums, respectively. Section VI is devoted to dense granular flows, and Sec. VII presents results on noncircular cylindrical tumblers. Section VIII closes with a few concluding remarks.

II. GENERAL ASPECTS

A. Experimental configuration

A typical experimental setup used in the investigation of rotating-drum flows is shown in Fig. 1. A transparent circular cylinder of length L and inner radius R is fitted horizontally into ball bearings which are mounted onto a rigid stand. The cylinder is driven at a constant rotation rate Ω by a dc (or stepper) motor. The cylinder may contain a liquid, a mixture of granular materials, or a suspension. Images of the tube are recorded via a CCD camera positioned either on the axis of rotation, facing a transparent side wall, or at right angles to the tube axis. These images are then analyzed in order to explore segregation dynamics (radial or axial) and, in the case of a partially filled cylinder, surface profiles.

In certain cases it is insightful to probe the flow and/or concentration fields in the interior of the bulk. For dilute suspensions the flow field can be studied by adding tracer particles and illuminating the desired region with a thin light sheet. The CCD camera is positioned perpendicular to the plane of the light sheet and records the streaks produced by the tracer particles as they move through the illuminated region (Matson, Ackerson, and Tong, 2003). In the investigation of granular flows, it is important to complement the dynamics observed on the surface of the mixture with information on the concentration field of the different constituents in the bulk. This can be achieved by the use of magnetic-resonance imaging (MRI) measurements, providing at least one of the components contains hydrogen (Hill, Caprihan, and Kakalios, 1997a).

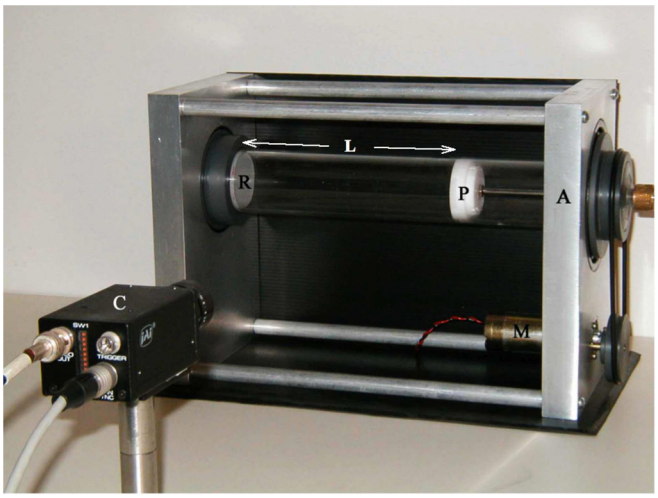

FIG. 1 (color online). An experimental system used in the investigation of rotating-drum flows. Here A is an aluminum stand, P is a Teflon piston that allows the effective length L to be varied, R is a rubber plug sealing the tube end, through which the fluid and/or granular material are inserted, and M is the motor. C is the charged-coupled-device (CCD) camera used to record the flow. From Seiden, Ungarish, and Lipson, 2005.

B. Dimensional analysis

The large variety of complex systems that exhibit pattern formation in the configuration of a rotating horizontal drum corresponds to the large number of parameters involved. If one considers a rather general case, in which the rotating-drum content consists of both fluid and two different kinds of spherical particles, then apart from the three parameters associated with the rotating cylinder (i.e., L, R, and Ω) one has the fluid density ρ_f, viscosity η, surface tension σ, and volume V_f, and the disperse phase densities ρ_1, ρ_2, dimensions d_1, d_2, and volumes V_{p_1}, V_{p_2}.[1] Thus, together with the gravitational acceleration g, the system is defined by as many as 14 dimensional parameters.

Insight into the different dynamics observed for a given system can be gained by considering the dimensionless numbers associated with the dimensional parameters that define the system. In the case described above there are three fundamental units involved (length, time, and mass) and therefore, according to Buckingham's theorem (Buckingham, 1914), one can derive $14 - 3 = 11$ independent dimensionless numbers. As a particular example (incorporated in the previous general scenario), which involves less parameters, consider the case where the drum is partially filled with an aqueous suspension of monodisperse nonneutrally buoyant spheres. In this scenario there are 11 dimensional parameters, which give rise to 8 dimensionless numbers (Guyez and Thomas, 2009). Yet another concrete example is the partially filling mixture of (dry) granular materials (e.g., glass beads and sand particles) (Zik *et al.*,

[1]The different volumes obey $V_f + V_{p_1} + V_{p_2} \leq \pi R^2 L$.

TABLE I. List of dimensionless parameters associated with the case of two kinds of spherical particles suspended in a liquid. The set is constructed in a compact way which enables implementation to less general realizations, namely, pure liquid, monodisperse suspension, and (dry) binary granular mixture. The dimensionless set can also be easily generalized to incorporate a larger number of granular species and/or liquids, as well as additional details regarding the constituents such as ellipticity for oblate particles, surface roughness of particles [important in dense granular flows (Lai, Jia, and Cham, 1997)], and non-Newtonian characteristics (e.g., the Weissenberg number).

Group	Symbol	Definition
Cylinder	Π_1	L/R
	Π_2, Fr^{-1}	$g/\Omega^2 R$
	Π_3, V_f^*	$V_f/\pi R^2 L$
Fluid	Π_4, Re^{-1}	$\eta/\rho_f \Omega R^2$
	Π_5, We^{-1}	$\sigma/\rho_f \Omega^2 R^3$
	Π_6	d_1/R
Particle 1	Π_7, $V_{p_1}^*$	$V_{p_1}/\pi R^2 L$
	Π_8	$(\rho_1 - \rho_f)/(\rho_f + \rho_1)$
	Π_9	d_2/R
Particle 2	Π_{10}, $V_{p_2}^*$	$V_{p_2}/\pi R^2 L$
	Π_{11}	$\rho_2/(\rho_f + \rho_1)$

1994). Here one has 10 dimensional parameters that yield 7 dimensionless parameters.[2] The set of independent dimensionless numbers associated with a given system is not unique. It is nevertheless more physically insightful to utilize numbers that result from comparison of different characteristic quantities, such as forces, densities, and length scales (Thoroddsen and Mahadevan, 1997).

While the different phenomena related to the rotating-drum configuration have different physical origins, there are intrinsic similarities which stem from the mutual experimental setup. From a dimensional analysis perspective, these similarities are related to two dimensionless numbers, shared by all realizations of rotating-drum flows: the Froude number $\mathrm{Fr} = \Omega^2 R/g$ and the geometrical aspect ratio L/R. The rich variety observed for different systems results from the rest of the dimensionless set, which completely describes the system. Thus, one has dimensionless numbers related to the volume fraction of the constituents, their densities, as well as numbers conveying dynamical aspects such as the Reynolds number.

Indeed, one can consider the dimensionless parameter space in which the different realizations occupy different regions. Table I presents a set of dimensionless parameters associated with the general case described above. Note that the dimensionless parameters are arranged in groups (cylinder, fluid, and particles) in a compact way which allows a straightforward implementation to the various systems corresponding to the rotating-drum geometry. Note also that the parameters associated with density ratios were chosen in order to construct a generic set.[3]

[2]For dense granular flows a more comprehensive analysis should also include friction properties [see, e.g., Lai, Jia, and Cham (1997)].

[3]Using a particular density instead (e.g., ρ_f) would lead to a set which would not be applicable to all scenarios.

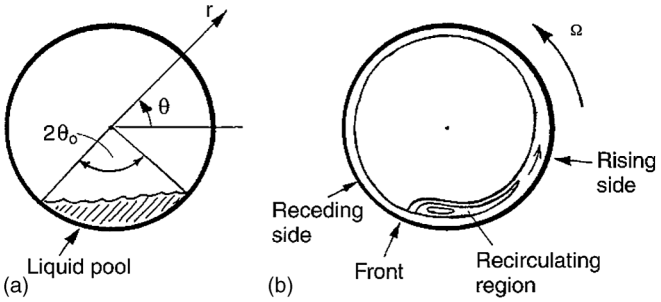

FIG. 2. Schematic of the cylinder cross section and the coordinate system. (a) The pool of liquid at the bottom of the stationary cylinder; (b) formation of a front on the receding side of the cylinder accompanied by a recirculating region of liquid during low and moderate rotation rates. Adapted from Thoroddsen and Mahadevan, 1997.

To date, different investigations have focused on particular systems (e.g., granular mixtures) and have accordingly used specific dimensionless sets which correspond to the systems under study. Moreover, even with respect to the same system, different dimensionless numbers were used [cf. Alonso, Satoh, and Miyanami, 1991 and Jain, Ottino, and Lueptow, 2005a]. This fact might naturally lead to some confusion, especially for the nonspecialist. In this review we present the different scalings as they were introduced in the original works and, when appropriate, elaborate on their relationship to the comprehensive scaling approach presented previously.

The different systems related to the rotating-drum configurations can be most naturally distinguished by the volume fractions of their constituents (i.e., fluid and disperse phases). Accordingly, the following three sections, reviewing results on the predominant circular cylinder geometry, are arranged with respect to the different rotating-drum flows corresponding to different regimes associated with V_f^*, $V_{p_1}^*$, and $V_{p_2}^*$.

III. PURE LIQUID PHENOMENA: RIMMING FLOW

Rimming flow is the flow established by a fluid inside a partially filled cylinder when the cylinder rotates about a horizontal axis of rotation. While the cylinder is stationary the liquid rests in a quiescent pool inside the cylinder as illustrated in Fig. 2(a). When the cylinder rotates with low to moderate rotational velocities its rising side drags out a thin film of liquid from the pool as indicated in Fig. 2(b). This thin film then coats the inner cylinder surface above the liquid pool. The cylinder rotation, mediated by viscosity and the restorative action of gravity, establishes a recirculating region of liquid as shown in Fig. 2(b). Facing the receding side of the cylinder the recirculating liquid region is bounded by a front. When the cylinder rotates sufficiently fast, such that restorative effects of gravity are weak, the entire pool of liquid redistributes itself to form an almost uniform layer of liquid coating the entire inner surface of the cylinder; this is known as the rimming state. The mean thickness of this liquid layer is $h = V_f/(2\pi RL)$. A Reynolds number for rimming flow is commonly defined as $\mathrm{Re}_h = \Omega R h/\nu$, where ν is the

kinematic viscosity [see, e.g., Thoroddsen and Mahadevan (1997)].[4]

It appears that the terminology "rimming flow" for this type of flow was first introduced by Deiber and Cerro (1976) and Ruschak and Scriven (1976). Rimming flow is one example of a class of flows referred to as coating flows. In general, a coating flow is a fluid flow that results in a thin film of liquid forming on a surface. For general overviews regarding the literature on coating flows see, for instance, Kistler and Schweizer (1997) and Weinstein and Ruschak (2004).

A. Early studies of rimming flow of homogeneous liquids

The earliest experiments using the rimming-flow configuration were those conducted by Malkin (1937a, 1937b). He studied the flow in the context of investigating the behavior of condensate in paper machine dryers under operating conditions. Malkin used a partially water-filled large-scale drum with radius $R = 0.762$ m and length $L = 6.604$ m. He presented photographs (Malkin, 1937a) of the flow and described that at a certain drum speed, referred to as the *balancing speed*, the water began to cascade right across the dryer. He elaborated that it then suddenly formed a complete film and that the film was maintained for any further increase of speed.[5]

Modern research on rimming flow originates with the experimental study of White (1956) who was, similar to Malkin (1937a, 1937b), interested in the flow due to its technical relevance to the pulp and paper industries. White (1956) commented that the general behavior of condensate in a cylindrical dryer is fairly well known but that little quantitative data had been published. White (1956) conducted experiments with water-filled metal drums with radii of the order of $0.3 \leq R \leq 0.6$ m. While the length of the drums is not explicitly stated by White (1956), the photographs contained in the paper indicate that the typical ratio of length to radius was around $L/R \approx 1$–2. White (1956) identified three main flow states and referred to these as the pond, the cascading condition, and the rimming condition. He conducted experiments for different filling levels of the cylinders and investigated under what experimental conditions the three flow states were adopted. White and Higgins (1958) followed up this study by performing additional experiments to investigate the effects of the fluid properties.

Yih (1960) elaborated further that the phenomenon of instability of a rotating liquid film with a free surface is of importance to the paper industry since it occurs on the table rolls underneath a wire screen carrying the pulp in a Fourdrinier machine. These devices are the basis for most modern papermaking; they accomplish all the steps required to transform a source of wood pulp into a final paper product. Moreover, in the process of coating, rotating cylinders are often used to carry the coating material in the form of liquid films.

While the cylinder is stationary, as in Fig. 2(a), or when it rotates very slowly, the contact or front line marking the edge of the free surface of the liquid pool inside the cylinder is a straight line [cf. Fig. 6(a)]. However, when the rotation rate is slightly increased an instability can develop. This instability reveals itself through the regular wavy deformations of the contact line shown in Fig. 6(b).

Motivated by the practical relevance of rimming flow, Yih (1960) performed the first theoretical stability analysis for this initial wavy liquid-film instability that exists before the contact line breaks up [cf. Fig. 6(c)] at higher rotational velocities and before it subsequently disappears entirely at the highest rotation rates when the rimming condition is adopted. Yih (1960) found satisfactory agreement between the analytical results of his stability analysis and concurrent experiments for low Reynolds numbers. He concluded that the critical wave number of the stability analysis displayed a substantially stronger dependence on the surface tension than on the viscosity, the primary effect of viscosity being to reduce the rate of amplification. Viscosity effects on the critical wave number are overshadowed by those of surface tension, particularly when the Reynolds number is large.

Phillips (1960) approached the flow from a more fundamental point of view. His particular interest focused on the wave motion on the free surface of the liquid for the case when it is *rapidly* rotating and in the rimming state with almost rigid-body motion and cylindrical interior free surface of radius cR with $0 < c < 1$. Phillips concluded that if the flow is to be stable, the condition $\mathrm{Fr} > 3/c$ has to be satisfied. Phillips (1960) experimentally confirmed this stability criterion under varying conditions of water depth and rotational velocity of the cylinder and then proceeded to investigate modes of oscillation of the free surface. Interestingly, the article by Phillips (1960) does not contain a single reference to any other publication.

The first theoretical studies investigating steady rimming flow with the goal of determining the shape of the liquid film covering the inner surface of the rotating cylinder were conducted by Deiber and Cerro (1976), Ruschak and Scriven (1976), Gans (1977), and Orr and Scriven (1978).

Gans (1977) commented that the theoretical work available at the time was inadequate for understanding the time-dependent processes that had been documented. He remarked that the experiments and observations available (Phillips, 1960, Karweit and Corrsin, 1975, Greenspan, 1976) indicated that steady-state phenomena were often submerged in a welter of time-dependent phenomena. The theoretical analysis of Gans (1977) accounted for viscous effects, nonlinear effects, and effects of the finite container length. He obtained solutions displaying steady-state circulations within the liquid film coating the inner cylinder wall and Stewartson layers at its inner and outer boundaries.

Ruschak and Scriven (1976) considered the two-dimensional limiting case when the motion of the liquid is a small perturbation from a rigid-body motion, and they considered both large and small Reynolds-number limits of their solution. Deiber and Cerro (1976) solved the corresponding boundary-layer equations numerically using a streamline coordinate system, and Orr and Scriven (1978) presented exemplary two-dimensional finite-element numerical solutions of the full Navier-Stokes equations with free-boundary conditions accounting for gravity and surface

[4]Note that $\mathrm{Re}_h = \mathrm{Re} V_f^*/2$.

[5]Currently Malkin's articles are available at the British Library, London.

tension. Their study represents one of the first numerical calculations of a Newtonian free-surface flow. Deiber and Cerro (1976) speculated on the existence of discontinuous solutions when their numerical scheme failed to converge. Some of these discontinuous solutions were subsequently clearly identified for the first time by Johnson (1988). Lin (1986) described a least-squares method with finite elements to simulate viscous rimming flow with surface tension. He discussed the advantages of his method, with regards to locating the free boundary of the liquid film, in comparison to the techniques previously used by Orr and Scriven (1978). While all previous theoretical studies considered two-dimensional flows, Preziosi and Joseph (1988) first addressed the issue of three dimensionality associated with the large axial variations of the interface shape observed in experiments along the axis of the cylinder.

B. Pattern formation in rimming flow of homogeneous liquids

The dynamic regime of rimming flow, between the limiting cases of very slow and very fast cylinder rotation or, equivalently, low and high Reynolds numbers, is characterized by the development of a sequence of different characteristic flow patterns. From the perspective of pattern formation rimming flow was first studied by Balmer (1970) who documented the regular cell patterns shown in Fig. 3. Balmer (1970) suggested the Greek word "hygrocysts" (fluid cell) as a general descriptive label for the cellular configurations that appear in all fluid phenomena of this type. He presented results only of a short preliminary investigation of the hygrocysts using two different motor oils (SAE-30, SAE-40-50, i.e., kinematic viscosities of $\nu = 350$–950 cS at 20° C) and three different tubes for his experiments. He commented that hygrocysts have been observed in spherical, triangular, annular, and square rotating containers and that the critical rotational speed for the onset of hygrocyst formation was lower in rectangular tubes than in circular tubes. Balmer (1970) concluded that, within the accuracy of the correlation of his data points, surface tension did not appear to have been an important factor in his experiments. Note that this conflicts with the theoretical result of Yih (1960) for the initial onset of the liquid-film instability discussed in Sec. III.A. Yih's theoretical results showed that the critical wavelength depended substantially stronger on the surface tension than on viscosity. Nevertheless, Balmer (1970) pointed out that in small tubes, when the surface-to-volume ratio becomes high, the Weber number ($\mathrm{We} = \Pi_5^{-1}$) will undoubtedly become important. Karweit and Corrsin (1975) published a short qualitative research note describing the cellular patterns (hygrocysts) developing in rimming flow and two other possible patterns referred to as periodic bores and "fingers." Karweit and Corrsin (1975) did not provide values for the kinematic viscosities of the liquids used, but their photographs suggest low viscosities with maximum values of at most a few hundred cS.

It appears that Karweit and Corrsin (1975) were not aware of the earlier publication of Balmer (1970), since their article does not contain a reference to his article. Subsequently, Balmer and Wang (1976) presented a more thorough experimental study of the hygrocyst phenomenon. They

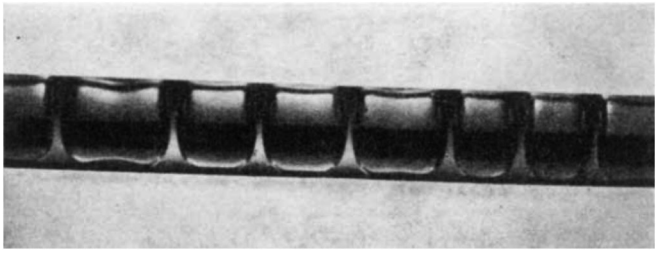

FIG. 3. Hygrocysts in a rotating circular tube. SAE-30 motor oil occupies 70% of the tube volume. Rotational speed is about 4 rev s^{-1}. From Balmer, 1970.

summarized nearly 500 sets of data, obtained from 13 fluid systems, and analyzed these using a number of different empirical dimensionless correlation models. Also note that Kovac and Balmer (1980) experimentally addressed the complementary problem of external hygrocyst formation in a brief study. While Balmer (1970), Karweit and Corrsin (1975), and Balmer and Wang (1976) all focused on the hygrocyst cell structures, Karweit and Corrsin (1975) did, in fact, point out that a whole continuum of periodic events are passed through before the complete cell structure is achieved; see also the comment by Karweit at the end of Balmer and Wang (1976).

Benjamin and Pathak (1987) provided the first theoretical approach in an attempt to explain the cell patterns described by Balmer (1970). They pointed out that the full hydrodynamic problem was too complicated to be amenable to quantitative theoretical treatment, except by numerical analysis which was not available at the time. Benjamin and Pathak (1987) developed a general, abstract qualitative dynamical-systems theory investigating a model system that is, similar to rimming flow, controlled by dissipative effects and free from inertial effects. The model system represents a finite-dimensional analog of the complete problem and is determined by n general coordinates resulting in n ordinary differential equations. Benjamin and Pathak (1987) emphasized that their analysis did not give any quantitative information. However, they concluded that the stable steady-state solutions of their model succeed in providing a reasonably clear qualitative picture by capturing all the essentials of the behavior found in their concurrent experimental study of rimming flow.

Johnson (1988) computationally studied steady-state rimming flow inside a horizontal rotating cylinder. Four possible steady-state liquid-film configurations identified by Johnson (1988) are shown in Fig. 4. Two of the cases correspond to a continuous coating where films cover the entire inner surface of the cylinder [Figs. 4(c) and 4(d)]. The other two cases involve partial films covering a limited portion of the cylinder surface [Figs. 4(a) and 4(b)]. Of the two continuous films, one is the expected rimming-mode configuration involving a coating that gradually changes in thickness as one moves around the cylinder, the film being thicker on the ascending portion of the cylinder and thinner on the descending portion. The second continuous-film configuration has regions on the rising side of the cylinder displaying a rapid change in film depth. Johnson (1988) discussed that the latter case also has the potential to have recirculating zones where a portion of the fluid is trapped in either one or two eddies at fixed locations on the rising side of the cylinder.

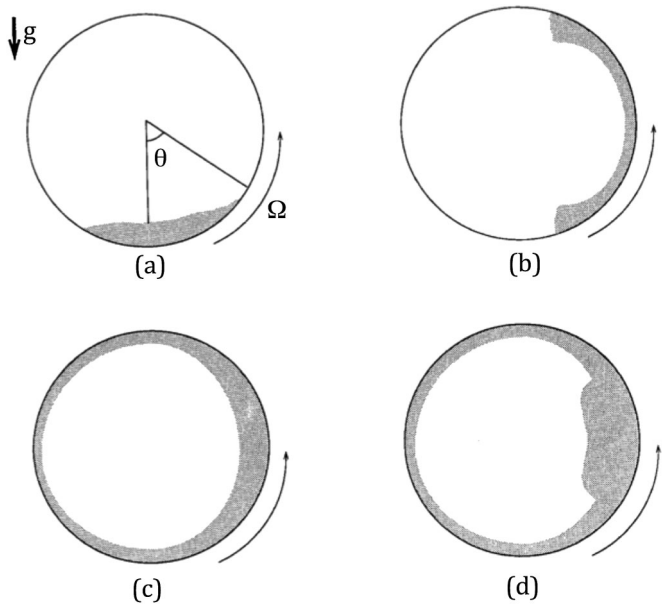

FIG. 4. Sketch of four possible steady-state, continuous, and partial film configurations. Adapted from Johnson, 1988.

Motivated by Johnson (1988), Benjamin, Pritchard, and Tavener (1993) conducted an unpublished theoretical and experimental study investigating steady and unsteady rimming flow of a highly viscous liquid. Based on lubrication-type approximations they rederived equations, previously also noted by Moffatt (1977), for the thickness of the film coating the inner cylinder wall under steady-flow conditions. Benjamin, Pritchard, and Tavener (1993) noted that several of the theoretically possible steady states of film flow [see, e.g., Fig. 4(d)] identified by Johnson (1988) had no practical relevance. Moreover, they commented that Johnson (1988) neither examined the stability of the flow nor did he report any experimental confirmation of the possible behavior predicted. Benjamin, Pritchard, and Tavener (1993) demonstrated that the leading-order lubrication model is neutrally stable and stated that the rederived simple solutions needed new interpretations to account for their concurrent experimental observations. Benjamin, Pritchard, and Tavener (1993) proceeded to explore second-order effects including that of surface tension and examined the stability of steady flows for both two-dimensional and three-dimensional disturbances. Benjamin, Pritchard, and Tavener (1993) described numerical solutions of various lubrication approximations and compared these with one another. In particular, they also showed how the discontinuous shock solutions to the basic lubrication model, first identified by Johnson (1988), are smoothed by second-order approximations including surface tension and gravity. Discontinuous solutions were subsequently studied in more detail by Wilson and Williams (1997) and O'Brien and Gath (1998).

The seminal study of Benjamin, Pritchard, and Tavener (1993), originally motivated by Johnson (1988), led to a series of publications that further considered the effects of higher-order corrections such as inertia, surface tension, and the hydrostatic pressure gradient on the stability of the thin film of viscous fluid on the inside of a horizontally rotating cylinder. A summary of these studies is contained in Hosoi and Mahadevan (1999) and Ashmore, Hosoi, and Stone (2003). More recent theoretical and computational studies and studies mainly involved with resolving issues regarding the existence, uniqueness, and stability of the solutions for the various types of models employed are O'Brien (2002a, 2002b), Wilson, Hunt, and Duffy (2002), Acrivos and Jin (2004), Villegas-Díaz, Power, and Riley (2003, 2005), Shrager *et al.* (2005), Bae and Kim (2007), and Tougher, Wilson, and Duffy (2009) as well as Benilov and coworkers (Benilov, 2004, 2006; Benilov and O'Brien, 2005; Benilov, O'Brien, and Sazonov, 2003; Benilov, Kopteva, and O'Brien, 2005; Benilov, Lacey, and O'Brien, 2005 Benilov, Benilov, and Kopteva, 2008, Benilov, Benilov, and O'Brien, 2008).

The experiments described by Benjamin, Pritchard, and Tavener (1993) were conducted using highly viscous silicone oil with a nominal kinematic viscosity of $\nu = 10\,000$ cS. Benjamin, Pritchard, and Tavener (1993) observed a multiplicity of steady and time-dependent dynamic flow modes of the contact line between the liquid pool inside the cylinder and the inner cylinder wall breaking the left-right symmetry about the vertical plane midway between the ends of the cylinder. Benjamin, Pritchard, and Tavener (1993) found that most of their unsteady flows observed were periodic, with periods many times that of the rotation also exhibiting period doubling and even chaotic behavior in narrow speed ranges. Similar experiments with a viscous fluid (golden syrup) were previously described by Aitta *et al.* (1988) who reported the observation of cell formation while Aitta (1991) described cell formation and observations of solitary waves on the air-liquid interface of a viscous silicone oil ($\nu = 12\,700$ cS). However, the whole spectrum of patterns that rimming flow can display for liquids with lower viscosities, hinted at by Karweit and Corrsin (1975), was not investigated further until the experiments of Melo (1993), Melo and Douady (1993), Thoroddsen and Mahadevan (1997), and Vallette, Edwards, and Gollub (1994, 1997).

Melo (1993) was interested in rimming flow from the viewpoint of pattern formation in nonlinear dissipative systems driven far from equilibrium by an external force. In such systems the simplest spatial pattern is a localized structure consisting of two spatially homogeneous states that can coexist in an interval range of an associated control parameter. The central questions of the field concern the mechanism responsible for the stabilization of localized structures and the selection of their size. Melo (1993) interpreted the rimming mode of Fig. 4(c) and the front state of Fig. 2(b) as the two homogeneous states involved. At low rotation rates the system adopts the state when a front is established near the pool. At high rotation rates the front disappears and the coverage of the inner cylinder surface is uniform. However, at intermediate rotation rates these two states can coexist along the horizontal axis of the system. This coexistence state is illustrated in Figs. 5(a)–5(c), where two lateral regions of completely uniform azimuthal coverage surround a central region of nonuniform coverage. The domains of stability of coexisting states were characterized by the angular velocity of the cylinder and its filling level as two control parameters. Melo (1993) extended the lubrication approximation of Moffatt (1977), originally developed to describe the behavior of a viscous film on the outer surface of a rotating cylinder,

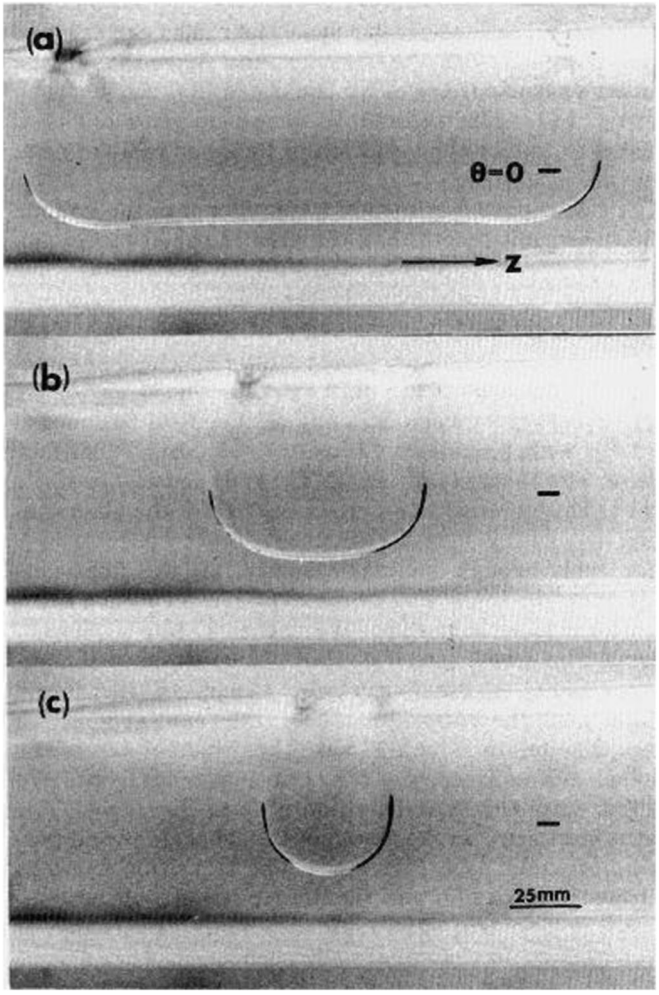

FIG. 5. Photographs showing localized structures that can be adopted by the contact line of surface of the pool of liquid inside the rotating cylinder and the inner cylinder wall; the filling level is 18.2%. (a) $\Omega = 12.1\ \mathrm{rad\,s^{-1}}$, (b) $\Omega = 13.06\ \mathrm{rad\,s^{-1}}$, and (c) $\Omega = 14.45\ \mathrm{rad\,s^{-1}}$. From Melo, 1993.

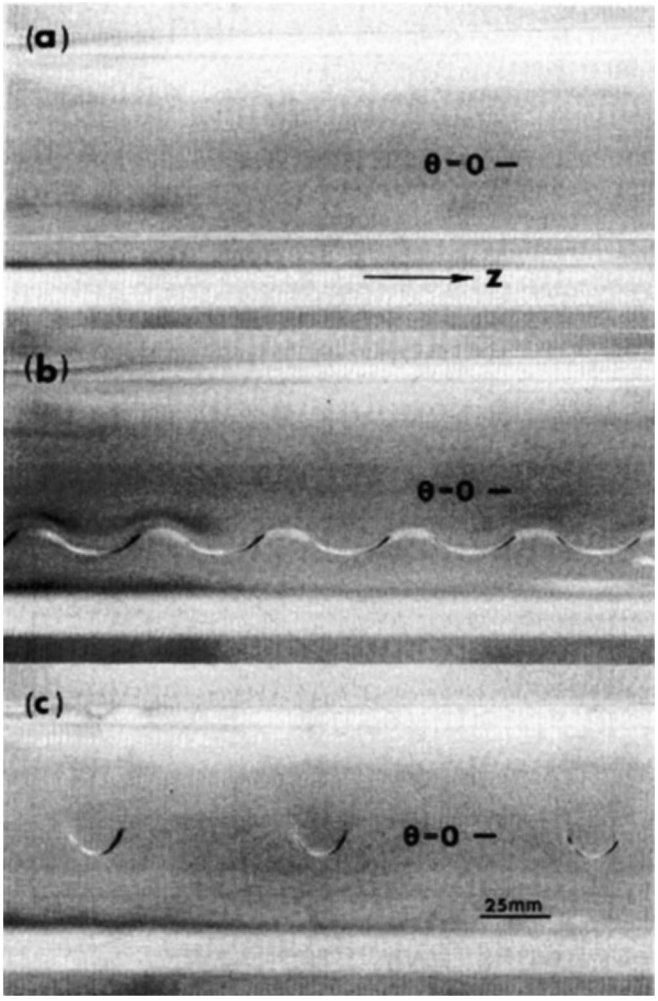

FIG. 6. Photographs showing patterns that can be adopted by the contact line of surface of the pool of liquid inside the rotating cylinder and the inner cylinder wall; the filling level is 13.6%. (a) A stable front at $\Omega = 6.9\ \mathrm{rad\,s^{-1}}$, (b) a stationary wavy front at $\Omega = 7.3\ \mathrm{rad\,s^{-1}}$, and (c) quasiperiodic pattern of bumps (u-shaped structures) at $\Omega = 8.0\ \mathrm{rad\,s^{-1}}$. From Melo, 1993.

for his rimming flow to study the dynamics of disturbances of the viscous layer. By investigating the profile and the dynamics of disturbances of the viscous film, Melo (1993) found that the independent states are well described by the lubrication approximation but that it failed to explain the coexistence of the two states.

Melo (1993) moreover considered how the shape of the contact line between the pool of liquid inside the horizontal cylinder and the inner cylinder surface changes as the rotational velocity of the cylinder was slowly increased from rest. As discussed in Sec. III.A this instability was first analyzed theoretically by Yih (1960). Figure 6(a) shows the contact line at rotation rate of approximately 1 revolution per second, when it is still a straight line, as is the case when the cylinder is at rest. At the slightly higher rotational speed in Fig. 6(b) the initially straight front has developed its characteristic wavy instability. As the rotational velocity of the cylinder is increased the wave amplitudes on the wavy front increase. At some critical rotation rate the waves break up and develop into a quasiperiodic pattern of bumps (localized u-shaped structures) that is illustrated in Fig. 6(c). It appears that the u-shaped structures had not been documented in the literature prior to the study of Melo (1993). Similarly there does not appear to exist a visualization of the wavy instability of Fig. 6(b) prior to the investigation by Melo (1993), despite Yih (1960) having considered it theoretically.

The wavy-front state and u-shaped structures of Melo (1993) in Figs. 6(b) and 6(c) are typical for a fluid with values of the kinematic viscosity around $\nu = 500$ cS at rotation rates of $\Omega = 7\ \mathrm{rad\,s^{-1}}$. We observed equivalent state-transition scenarios, and photographs similar to those shown here in Fig. 6 are contained in Boote and Thomas (1999).

In this context it appears timely to briefly comment on the apparent doubling of the wavelength between the wavy-front state in Fig. 6(b) and the state displaying the localized u-shaped structures in Fig. 6(c). We found that in our apparatus a strict wavelength doubling is usually difficult to observe and it is, in this sense, not a reproducible effect. Our own observations have shown that the increase of the pattern wavelength results from the disappearance of troughs on the wavy contact line during their transition toward developing into u-shaped structures. However, this process

appears to be sensitive to the overall flow field and, as such, a rather random process; see Figs. 2(a), 2(b) of Boote and Thomas (1999). The photo in Boote and Thomas displays a transition equivalent to that shown here in Figs. 6(b) and 6(c) but with an imperfect wavelength doubling.

For the experiments of Melo (1993) in Figs. 6(a)–6(c) one determines Reynolds numbers of 2.35, 2.49, and 2.55, respectively. Thoroddsen and Mahadevan (1997) conducted experiments with liquids of substantially lower viscosity and documented flow structures similar to, but more complex than, the wavy fronts of Melo (1993). Figures 7(a) and 8, from Thoroddsen and Mahadevan (1997), show patterns for a liquid with dynamic viscosities of $\eta = 49$ and $\eta = 25$ cP. The two photographs illustrate the fact that the comparatively simple wavy front of Melo (1993) that was shown in Fig. 6(b) has changed into a more complex three-dimensional flow pattern. One can estimate the values of the Reynolds number associated with the two experiments of Thoroddsen and Mahadevan (1997) in Figs. 7(a) and 8 for comparison with the results of Melo (1993). In both experiments of Thoroddsen and Mahadevan (1997) the liquid used was a glycerin-water mixture. The comparison requires values for the densities ρ_f of the glycerin-water mixtures but these are not given in Thoroddsen and Mahadevan (1997). We contacted Thoroddsen who has supplied us with density values of $\rho_f = 1.20$ and $\rho_f = 1.18\ \mathrm{g\,cm^{-3}}$ for the experiments of Figs. 7(a) and 8, respectively. With these densities the associated kinematic viscosities for the two experiments are $\nu = 41$ and $\nu = 21$ cS. Thoroddsen and Mahadevan (1997) do not explicitly state the radius of the cylinder for the experiments of Figs. 7(a) and 8, but they commented that the cylinder primarily used had a diameter of $R = 62.5$ mm and that their discussion always referred to this cylinder unless otherwise stated [Note that the cylinder radius of $R = 62.5$ mm for Fig. 7(a) was also reconfirmed to us by Thoroddsen]. Using this information one can infer that the Reynolds numbers for the experiments in Figs. 7(a) and 8 are $\mathrm{Re}_h = 58$ and 111, respectively. Both these values are over 1 order of magnitude larger than those for the experiments of Melo (1993) in Figs. 5 and 6. This implies, as one would expect, that it is the decreasing, stabilizing, effects of viscosity that have led to the more complex flow structures in Fig. 7(a).

Thoroddsen and Mahadevan (1997) referred to the modified flow structures in Figs. 7(a) and 8 as "shark teeth" and "fishlike" patterns, respectively. As part of a short study investigating the entrainment of small air bubbles into liquid shark-teeth fronts, Thoroddsen and Tan (2004) subsequently published the first photograph revealing the local flow structure in the troughs between two successive shark teeth in Fig. 7(a). Their photo displaying this local flow structure is reproduced in Fig. 7(b). The flow is visualized by the small bubbles that have been entrained across the liquid front from the ambient air and then act as tracers. The photo shows that the region within the trough is dominated by vortices connecting to the free surface, with one vortex being located on each side of the center line of the trough.

Recently Chen *et al.* (2007) conducted an experimental study focusing on the dynamics of the shark-teeth pattern of Thoroddsen and Mahadevan (1997), and on the transition to

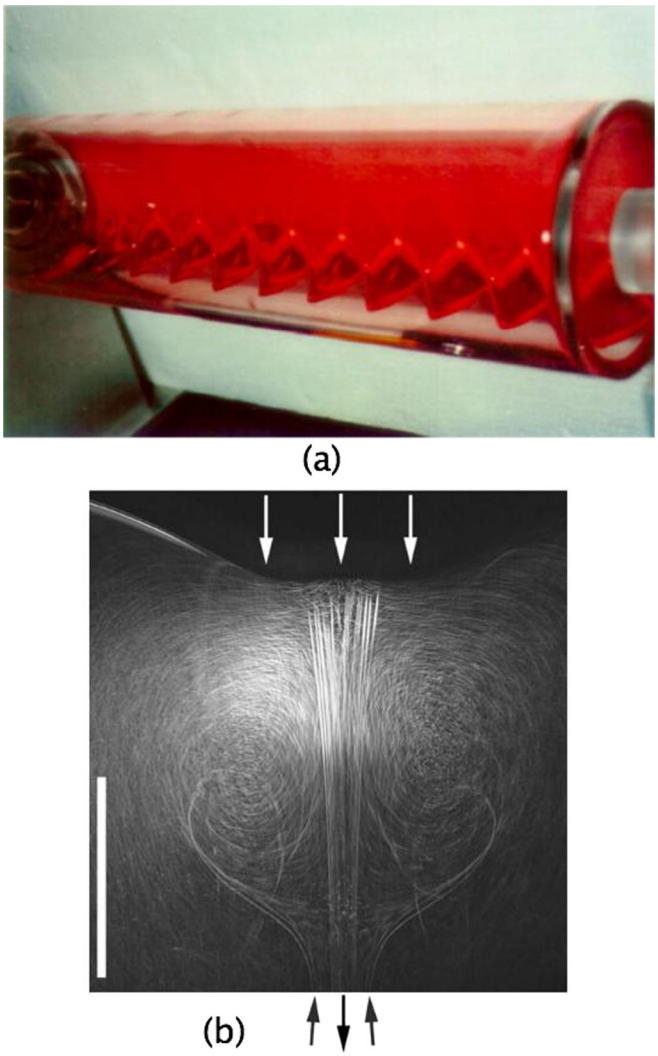

FIG. 7 (color online). (a) Shark teeth along the entire cylinder. The fluid has a dynamic viscosity of $\eta = 49$ cP, the rotational velocity is $\Omega = 20.1\ \mathrm{rad\,s^{-1}}$, and the volume fraction is $V_f^* = 0.06$. From Thoroddsen and Mahadevan, 1997. (b) Bubble tracks visualizing the flow structure in the trough between two successive shark teeth. The view is from above and the white arrows indicate the direction of the cylinder rotation. The scale bar in the bottom left corner is 10 mm long. Adapted from Thoroddsen and Tan, 2004.

the rimming state, when the volume fraction of an aqueous low viscosity (1–3 cS) Newtonian solution inside the rotating cylinder is reduced to low values in the range of $V_f^* = 0.0025$–0.05 of the total cylinder volume. Chen *et al.* (2007) reported the surprising result that there exists a certain critical volume fraction V_c^*, for each solution, where the rotational velocity required to achieve uniform rimming flow adopts a minimum. Thus, for volume fractions above and below this critical value it required higher rotational velocities of the cylinder to reach the rimming state. For volume fractions above V_c^* the observed structures were mainly shark-teeth and turbulent structures. For volume fractions below V_c^* they reported the observation of structures referred to as fingers. Moreover, they documented the ring pattern shown in Fig. 9 and indicated that the pattern results from the surface shape of the liquid film on the inner cylinder

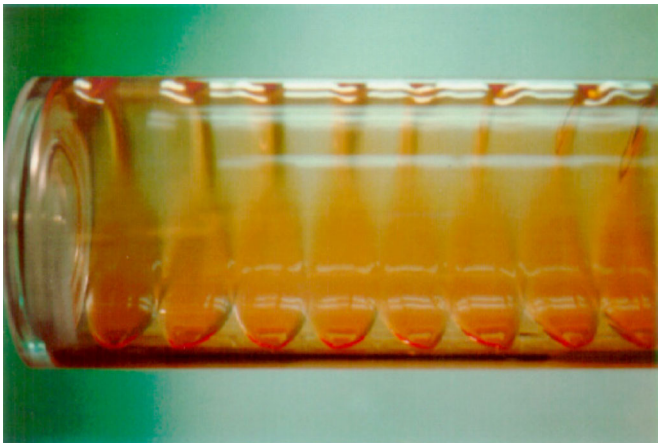

FIG. 8 (color online). Fishlike patterns along the entire cylinder. The fluid has a dynamic viscosity of $\eta = 25$ cP, the rotation rate is $\Omega = 24.5\ \mathrm{rad\,s^{-1}}$, and the volume fraction is $V_f^* = 0.049$. From Thoroddsen and Mahadevan, 1997.

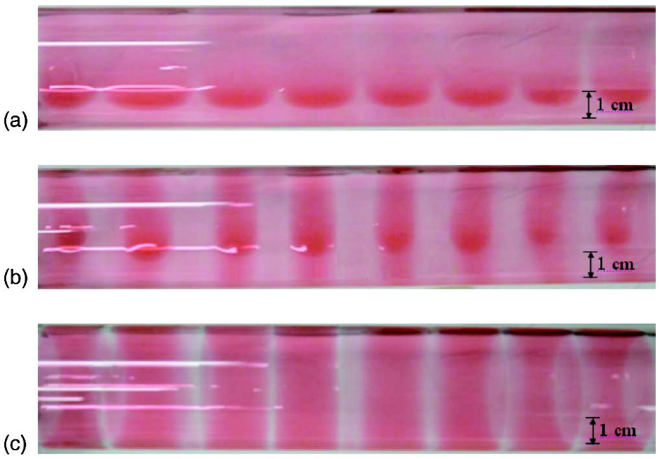

FIG. 9 (color online). A surface-shape ring pattern for a glycerol-water solution with dynamic viscosity $\eta = 13.2$ cP at a volume fraction of 1.5% and (a) $\Omega = 3.14\ \mathrm{rad\,s^{-1}}$. Rings with large pools. (b) $\Omega = 6.91\ \mathrm{rad\,s^{-1}}$. Rings are becoming narrower and pools are shrinking. (c) $\Omega = 27.0\ \mathrm{rad\,s^{-1}}$. Rings are expanding. From Chen *et al.*, 2007.

wall. Chen *et al.* (2007) discussed that the rings initially became narrower when the rotational velocity was increased and the size of the liquid pool reduced [cf. Figs. 9(a) and 9(b)]. Upon further increase of the rotational velocity the liquid pool disappeared while the rings expanded and coalesced with other rings until the rimming-flow condition was established [cf. Fig. 9(c)]. Note that this description implies that the wavelength of the pattern is independent of, or at least not sensitive to, the rotational velocity, as is also suggested by reference to Figs. 9(a)–9(c). Based on our own experience, gained from observations of transition between flow states at higher liquid volume fractions, as described by Boote and Thomas (1999) [see also Melo (1993) and Fig. 6], it appears that the dynamics outlined by Chen *et al.* (2007) represent a new dynamical scenario.

Melo (1993) considered how the critical values of the rotational velocity Ω for the state transitions between the different flow states are affected by the cross-section area A of the cylinder occupied by the fluid. Melo defined a new nondimensional parameter

$$\Lambda = \frac{\Omega \nu R}{g h^2}, \tag{1}$$

where h is the mean thickness of the viscous layer coating the inner cylinder wall. The parameter Λ characterizes the competition between viscous stress and gravity. Using the expression for h from above and definitions from Table I the parameter becomes $\Lambda = 4\,\mathrm{Fr}\,\mathrm{Re}^{-1} V_f^{*-2} = 4\Pi_2^{-1}\Pi_3^{-2}\Pi_4$. Melo (1993) then wrote the parameter as a function of the area A yielding $\Lambda = (2\pi)^2 \nu R^3 \Omega / g A^2$. This expression reveals that Λ is constant along a straight line in the plane (Ω, A^2). Consequently, in a phase diagram displaying the critical state-transition values of Ω as a function of A^2, each state transition is associated with a constant value of Λ.

Thoroddsen and Mahadevan (1997) conducted rimming-flow experiments for a wide range of fluid volumes and viscosities. Their discussion of the patterns that rimming flow can display represents the most comprehensive description to date. Their associated phase diagrams illustrate in what regimes of the parameter space the different patterns are observed to occur. Similar to Chen *et al.* (2007), the studies of Melo and Douady (1993), Vallette, Edwards, and Gollub (1994), and Vallette, Jacobs, and Gollub (1997) focused on the dynamics of the fluid fronts in rimming flows established for low volume fractions in the range of 0.01–0.04 but, rather than aqueous low viscosity solutions [i.e., 1–3 cS used by Chen *et al.* (2007)], they used oils with higher viscosities in the range of 10–20 cS. Figure 10, reproduced from Vallette, Jacobs, and Gollub (1997), displays three examples of highly symmetric stationary and time-dependent patterns of the liquid front observed in these experiments.

Melo and Douady (1993) documented the first observation of a continuous transition from solitary waves on the liquid front to static spatially periodic patterns. They reported that between these two extreme situations, a regime of colliding solitary waves exhibiting chaos with spatiotemporal intermittency can be observed. Melo and Douady (1993) noted their observations suggested that the static periodic pattern can be described as being the result of a dense packing of propagating solitary waves, and its destabilization to spatiotemporal intermittency as the attempt of some solitary waves to propagate. They concluded by emphasizing they were confident that the general idea of considering some periodic patterns, not as a whole but constituted of a packing of localized structures, could help to understand some of their particular dynamics.

Vallette, Edwards, and Gollub (1994) and Vallette, Jacobs, and Gollub (1997) investigated the transition of the steady, primary wavy-front state to chaotic time dependence through secondary transitions at different volume fractions. For one particular highly symmetric transition to spatially subharmonic oscillations they discussed model equations that well represented the flow. The subsequent transition of the oscillatory state to spatiotemporal chaos was explored qualitatively through the use of spectral analysis and complex demodulation to extract slowly varying amplitudes and phases. Their analysis revealed that many features of the

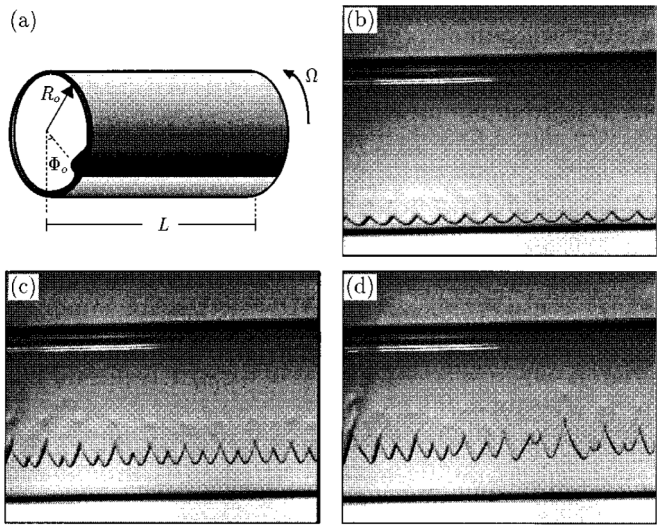

FIG. 10. Highly symmetric stationary and time-dependent patterns on the falling front inside the rotating cylinder (a), (b) Cellular, time-independent pattern; (c) spatially subharmonic oscillatory state; and (d) spatiotemporally chaotic state. From Vallette, Jacobs, and Gollub, 1997.

chaotic state are at least qualitatively described by the model employed.

Contrary to the dynamical-system approaches of Melo and Douady (1993), Vallette, Edwards, and Gollub (1994), and Vallette, Jacobs, and Gollub (1997), the axial instability of the free-surface front in rimming flow was readdressed numerically by Hosoi and Mahadevan (1999) on the basis of the Navier-Stokes equations. They derived and solved a simplified model equation for the evolution of the free surface that includes effects of gravity, capillarity, inertia, and viscosity. This equation was solved numerically to determine the base state with no axial variation, and a numerical linear stability analysis was carried out to examine the onset of unstable axial modes. Hosoi and Mahadevan (1999) found that inertia plays an important role in the onset of instability and that the wavelength is related to surface tension through a power-law proportionality. Their numerical simulations showed that the simplified evolution equation can capture the steady shark-teeth patterns described by Johnson (1990) and Thoroddsen and Mahadevan (1997).

The early research summarized in this section was originally motivated primarily by the relevance of rimming flow to the pulp and paper industry. While rimming flow remains to be of interest in this industrial context [see, e.g., Wilhelmsson *et al.* (1995)], many of the newer studies were probably curiosity driven, inspired by the numerous complex phenomena displayed by the conceptually simple rimming-flow geometry. However, rimming flow is also of interest in other technological contexts as encountered, for instance, in the aeronautical industry. Here the flow bears relevance to issues associated with heat transfer from the relatively hot modern aero-engine bearing chambers containing bearing lubrication oil. Heat transfer issues in rimming flow were investigated by, for instance, Chew (1996), Peng *et al.* (1997), and Baker *et al.* (2001).

In conclusion it is noted that recently two studies appeared that addressed a new fundamental issue of rimming flow that has, as we are aware of, not been studied by any others in the past. Ivanova, Kozlov, and Polezhaev (2005) and Kozlov and Polezhaev (2008) described experimental investigations of the stability of a rimming-flow system subject to transverse translational vibration relative to the axis of rotation. Ivanova, Kozlov, and Polezhaev (2005) studied the average flow of a centrifuged fluid layer in a transversely vibrating system where gravity induces fluid oscillations. They reported the observation of azimuthal waves propagating in a direction opposite to the direction of rotation of the cylinder and with a velocity comparable to the rotation velocity of the cylinder. Ivanova, Kozlov, and Polezhaev (2005) discussed that substantial intensification of these waves, and hence intensification of the average flows, was observed in resonance regimes. They elaborated that the excitation of standing inertial waves leads to the development of intense three-dimensional flows characterized by the appearance of the circular or helical vortical structures shown in Fig. 11. Kozlov and Polezhaev (2008) discussed that the structure of the vortices, and the threshold of their appearance, did not depend on the direction of the induced mean flow and reported that the onset of the pattern formation was determined by the intensity of oscillatory liquid flow in the Stokes boundary layer on the inner cylinder wall.

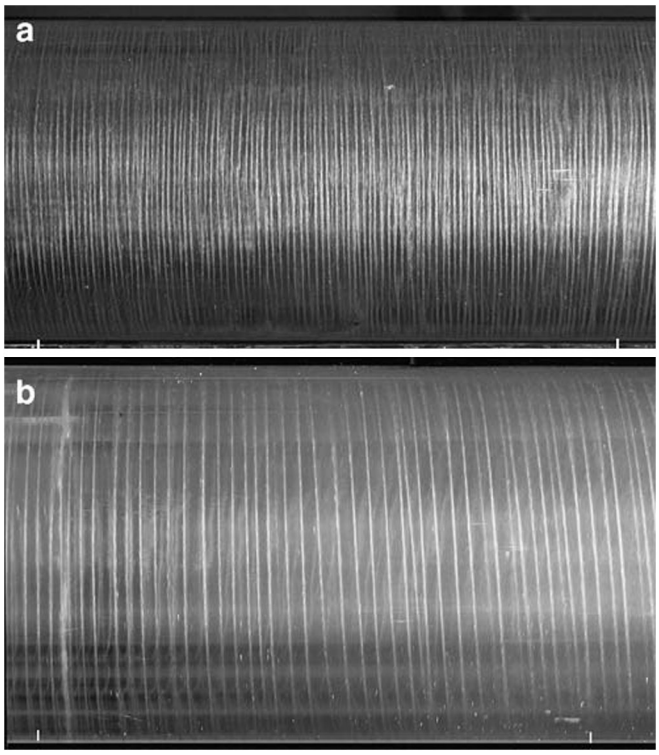

FIG. 11. Vortical structures in a rotating cylinder with radius 2.5 cm. (a) Circular, $\nu = 1.0$ cS and (b) helical, $\nu = 4.2$ cS. The light stripes correspond to the zones of visualizer concentration. The distance between the pairs of small white marks at the bottom of each photo is 10 cm. From Kozlov and Polezhaev, 2008.

C. Rimming flow of non-Newtonian liquids

While the existing literature dealing with rimming flow of Newtonian fluids is quite substantial, the literature for

rimming flow of non-Newtonian fluids is comparatively sparse. It appears that rimming flow of a non-Newtonian fluid was first considered by Sanders, Joseph, and Beavers (1981), Johnson (1988), and Rajagopalan *et al.* (1992). Sanders, Joseph, and Beavers (1981) discussed that for the non-Newtonian case, general constitutive equations were known only in the sense of perturbations. Global numerical results were possible only under some more-or-less arbitrary assumption that the constitutive equation of the fluid is described by some particular model.

Sanders, Joseph, and Beavers (1981) developed a perturbation solution for the case of rimming flow of a viscoelastic liquid. One of their main goals was to show how their solution leads to a simple, practical method for the measurement of the complex viscosity of the liquid by measuring the thickness of the liquid film coating the inner cylinder wall. The complex viscosity obtained from the free-surface shape and the theory was compared with the corresponding results obtained from measurements using an oscillating cone-and-plate rheometer. Sanders, Joseph, and Beavers (1981) used two different viscoelastic polymer solutions, STP and TLA 227, for their experiments. STP is a solution of polyisobutylene in petroleum oil while TLA 227 is a solution of methacrylate copolymer in oil.

Sanders, Joseph, and Beavers (1981) concluded with some brief general qualitative observations on the stability of the flow showing the formation of liquid cells for the case when the cylinder is rotating slowly. They discussed that the effects observed in their experiments did not seem to be greatly influenced by the non-Newtonian characteristics of the liquids used in comparison to the behavior of viscous Newtonian liquids.

Rajagopalan *et al.* (1992) investigated the influence of viscoelasticity on the existence of steady solutions in two-dimensional rimming flow. They stated that previously numerical simulation of viscoelastic, free-surface flows had received limited attention because of the difficulties associated with developing convergent calculations for much simpler viscoelastic flows. Rajagopalan *et al.* (1992) elaborated that initial attempts at the numerical simulation of viscoelastic flows all suffered from the so-called ''high Deborah number problem'' (Brown *et al.*, 1986; Keunings, 1989). Brown *et al.* (1986) stated that the major obstacle in the numerical analysis of complex viscoelastic flows arises from the amount of elasticity in the constitutive model for the fluid stresses being significant. They discussed that the symptoms of the numerical failure seemed to be the same irrespective of the numerical method, flow geometry, and constitutive equation. Brown *et al.* (1986) elaborated that the iteration scheme for computing steady flows diverges beyond a critical value of the elasticity of the fluid, as measured by the Deborah number. The possible causes for the loss of convergence were attributed to either excessive approximation error or the mathematical loss of existence of the steady solution beyond the limiting value of the Deborah number. A summary discussing how the breakthrough in the formulation of appropriate numerical methods for viscoelastic flows was subsequently prompted by a mixture of theory and numerical models is provided by Rajagopalan *et al.* (1992).

Rajagopalan *et al.* (1992) investigated rimming flow by conducting viscoelastic flow calculations based on a elastic-viscous split stress formulation for differential constitutive models. They used a single-mode Giesekus differential constitutive equation (Giesekus, 1982) to study steady, two-dimensional rimming flow and interface shapes of Newtonian and viscoelastic liquid films by means of a finite-element analysis. Rajagopalan *et al.* (1992) elaborated that the Giesekus model describes the polymeric part of the deviatoric stress along with an additional Newtonian contribution to the stress tensor that accounts for the presence of a solvent. With reference to Bird, Armstrong, and Hassager (1987), they stated that the Giesekus model is one of the simplest differential constitutive equations that qualitatively describes the rheological behavior of polymer solutions. Rajagopalan *et al.* (1992) concluded that the Giesekus constitutive equation leads to the existence of steady solutions at lower rotation rates and they presented contour plots for velocities and stresses within the liquid film coating the inner cylinder wall.

Johnson (1988), Fomin *et al.* (2001, 2002), Fomin, Hashida, and Watterson (2003), and Fomin (2006) numerically investigated rimming flow of generalized Newtonian fluids. These are fluids for which the shear stress is a function of the shear rate at the particular time but not dependent upon the history of deformation. Hence, the Deborah number that characterizes memory effects of the liquid is sufficiently small such that these effects are negligible (Fomin, Hashida, and Watterson, 2003).

While Johnson (1988) was mainly involved with Newtonian fluids the derivation of his model equations described the stresses by means of an unconventional formulation, in terms of two material parameters, in such a way that an extension to power-law fluids became straightforward. Johnson (1988) discussed continuous films and partial films (cf. Fig. 4) for the rimming flow of power-law fluids. However, as discussed, Benjamin, Pritchard, and Tavener (1993) noted that several of the theoretically possible steady states of film flow [see, e.g., Fig. 4(d)] identified by Johnson (1988) had no practical relevance.

Fomin *et al.* (2001) determined the runoff condition for rimming flow of a power-law fluid and found continuous solutions for the regime of thin liquid layers by applying lubrication theory. For the supercritical case, outside this regime, they found that discontinuous solutions are possible. Here a hydraulic jump (shock) may occur and they calculated its location and height. Fomin *et al.* (2002) summarized numerical results for power-law liquids and liquids described by the Carreau-Yasuda model and the Ellis model. Carreau-Yasuda liquids display a transition from Newtonian behavior at low shear rates to power-law behavior at high shear rates. This behavior is typical for most polymeric liquids and Fomin, Hashida, and Watterson (2003) stated that the Carreau-Yasuda model is the most appropriate model for viscous flows with free surfaces. For liquids complying with the Ellis model the shear rate is a function of the shear stress, incorporating shear thinning effects and simulating Newtonian features for the low shear rates. The properties of the Carreau-Yasuda model and the Ellis model mean that liquids of these types exhibit Newtonian behavior near the

free surface and power-law behavior near the wall of the rotating cylinder (Fomin, Hashida, and Watterson, 2003).

Similar to Johnson (1988), Fomin, Kilpatrick, and Hubbard (2010) studied steady-state rimming flow for a power-law fluid at low Reynolds numbers. They considered the thickness of a power-law liquid along the cylinder wall for the case of high Weissenberg number when non-Newtonian effects dominate and the flow can be modeled by the power-law constitutive equation. They discussed that under these conditions their mathematical model reduces to a simple set of algebraic equations regarding the thickness of the liquid film. Their qualitative analysis revealed the existence of two possible solutions. Different regimes of the rimming flow were defined and analyzed analytically. For the particular case, when the flow index in a power-law constitutive equation is equal to $\frac{1}{2}$, the problem reduced to a fourth order algebraic equation which was solved analytically.

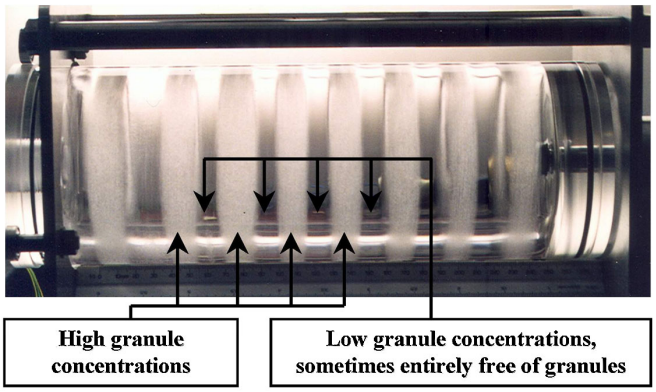

FIG. 12 (color online). The primary banding pattern. The granules that were initially uniformly distributed throughout the liquid have segregated and have established a sequence of alternating circumferential regions containing high and low particle concentrations. Adapted from Guyez and Thomas, 2008.

IV. DILUTE SUSPENSION: PARTIALLY FILLED DRUM

A. Rimming flow of particle-laden liquids

As discussed in Sec. III.B, Melo (1993) demonstrated that the state-transition boundaries of rimming flow in phase space are characterized by associated constant values of a nondimensional parameter Λ, characterizing the competition between viscous stress and gravity. This result motivated Boote and Thomas (1999) to begin investigating rimming flow of particle-laden liquids. Initially, their main goal was to experimentally investigate how the particular values of Λ, for the different state-transition boundaries, are affected when the liquid inside the horizontal cylinder contains successively increasing amounts of small solid particles. The underlying rationale for the study of Boote and Thomas (1999) was that small numbers of particles added to the liquid should not measurably affect the values of Λ, but larger amounts must be expected to have some influence since the liquid properties will change substantially as it turns into a slurry. Boote and Thomas (1999) used small glass spheres with a density higher than that of the liquid for their study. Their experimental results showed that, for each particular state transition, the value of Λ decreases with the amount of particles added. With regard to the physical interpretation of Λ this implied that gravitational effects become increasingly more prominent. Boote and Thomas (1999) further observed that granular additives can lead to the stabilization of certain flow states and to an increased parameter range over which states can be observed. In particular, it was found that the effects on the investigated transition boundaries appear to be due to an increased bulk density associated with increasing granule concentrations of the solid-liquid flow.

B. Pattern formation and segregation in rimming flow of particle-laden liquids

The most surprising result of the study of Boote and Thomas (1999) was the discovery that the particles in the particle-laden rimming flow display a tendency to segregate. While the particles were initially uniformly distributed throughout the liquid they were observed to redistribute themselves into a characteristic pattern of successive, equally spaced circumferential particle-rich regions separated by regions of liquid devoid of particles. A typical photograph illustrating this pattern is shown in Fig. 12. The banding pattern is established within minutes for high particle concentrations but it can take several hours for distinct bands to become visible for low particle concentrations.

At the same time that Boote and Thomas (1999) conducted their experiments on particle-laden rimming flow, Tirumkudulu, Tripathi, and Acrivos (1999) coincidentally conducted an independent study using a liquid carrying neutrally buoyant particles in a partially filled horizontal Taylor-Couette system. In these experiments with neutrally buoyant particles they observed a banding pattern similar to that reported by Boote and Thomas (1999) for rimming flow and particles denser than the carrier fluid. Subsequently Tirumkudulu, Mileo, and Acrivos (2000) reported results showing that segregation bands also form in rimming flows when the liquid carries neutrally buoyant particles, rather than particles denser than the ambient fluid.

Thomas *et al.* (2001) conducted experiments using particles with a density substantially lower than that of the carrier liquid. Here they discovered that the primary granular bands seen in Fig. 12 can develop a compound structure whereby each one of these bands splits up into a set of three narrower, secondary rings as illustrated in Fig. 13.

Figure 13 reveals that each granular triplet-band structure is centered around a cusp of the wavy contact line between the liquid in the pool inside the cylinder and the inner cylinder wall. Boote and Thomas (1999), and also Thomas *et al.* (2001), expressed that the waviness of the contact line in the homogeneous system [cf. Fig. 6(b)] and in the particle-laden system probably results from different physical mechanisms. In the particle-laden system the wavelength of the contact line deformation is always equal to the wavelength of the banding pattern and it increases systematically and continuously with the rotation rate of the cylinder. In the homogeneous system, however, where a continuous wavy contact line exists only in a relatively narrow parameter regime, the disturbance wavelength does not depend on the rotation rate of the cylinder.

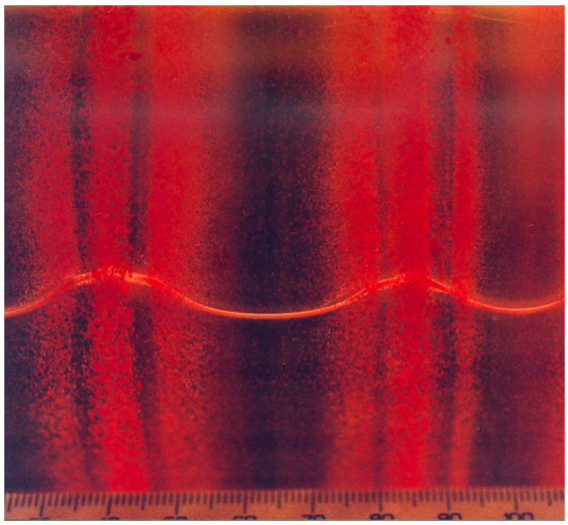

FIG. 13 (color online). The secondary banding pattern on two adjacent primary bands. Each of the primary granular bands of Fig. 12 has developed a compound structure consisting of three narrower secondary rings. From Thomas *et al.*, 2001.

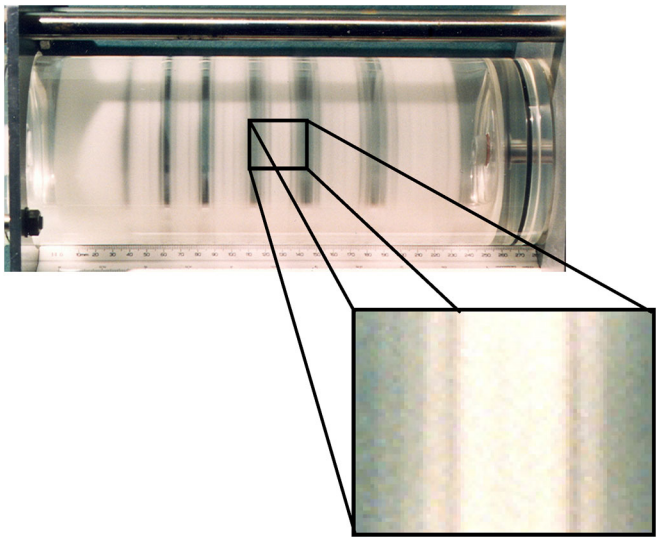

FIG. 14 (color online). Photograph showing evidence that the primary bands of Fig. 12 are split up into compound structures consisting of more than the three narrower bands shown in Fig. 13. From Thomas, 2011a.

Tirumkudulu, Mileo, and Acrivos (2000) referred to the remark of Boote and Thomas (1999) addressing the issue of the origin of the waviness of the contact line. Thomas *et al.* (2001) elaborated that Tirumkudulu, Mileo, and Acrivos (2000) concluded that their latest experimental results supported the view that the waviness of the contact line in homogeneous and in particle-laden systems is of a different origin.

Thomas *et al.* (2001) commented that they did not know whether the triplet structure of Fig. 13 is the only possible stable fine structure or whether it was possible that each primary band might split up into a compound structure displaying more than three rings. In the meantime we obtained experimental evidence that this is indeed possible. The previously unpublished photograph in Fig. 14 reveals clear evidence of each primary band having split into a whole sequence of narrower bands.

Thomas *et al.* (2001) also conducted experiments with particles of different sizes, and their data revealed that the wavelength of the banding pattern is independent of the particle size. The independence of the wavelength on the particle properties is illustrated here in the, previously unpublished, photograph in Fig. 15. For the particular experiment shown in the figure the silicone carrier liquid, viscosity $\nu = 500$ cS, contained two substantially different types of particles. One particle class consisted of a sample of glass spheres with diameters $250 \leq d_G \leq 425$ μm and density $\rho_p = 2.5\ \mathrm{g\,cm^{-3}}$, while the other particle class was a sample of cylindrical nylon rods with dimensions $1 \times 5\ \mathrm{mm^2}$ and density $\rho_p = 1.4\ \mathrm{g\,cm^{-3}}$. Figure 15 clearly reveals that each band contains glass spheres and nylon rods. This suggests that the banding wavelength is not only independent of the particle size, as already discussed by Thomas *et al.* (2001), but it is also independent of the particle density and the particle shape.

The discovery that the wavelength of the granular segregation bands in rimming flow does not depend on the particle properties has substantial implications with regards to the underlying physical mechanisms responsible for the formation of the granule bands. The result implies that the primary cause of the banding pattern must be associated with the flow dynamics of the liquid phase, possibly in combination with particle-liquid interactions. However, it cannot be a consequence of purely granular dynamics, i.e., its primary origin cannot reflect particle-particle interactions. For purely granular flows, i.e., when no liquid phase is present, it is known that particles display size segregation. If a horizontal rotating cylinder is filled with a mixture of granules comprising two different size classes then these segregate into an axial band pattern (see Sec. VI.B.2) that shares superficial similarities with that for the particle-laden flow in Fig. 15. However, for purely granular flow each two successive bands alternatingly contain larger or smaller particles only, whereas in particle-laden rimming flow one finds particles from different size, or shape, classes in each band.

In an experimental study similar to those of Boote and Thomas (1999) and Thomas *et al.* (2001), Joseph *et al.* (2003) described results for experiments of particle-laden rimming flow for a broad range of experimental conditions.

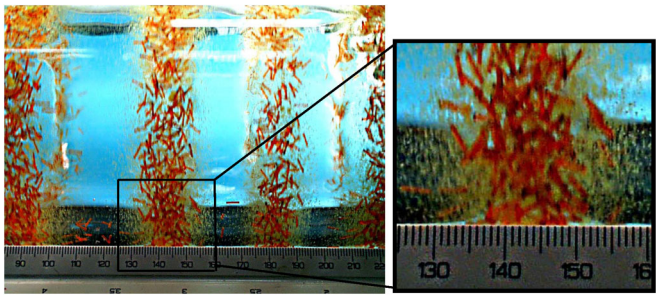

FIG. 15 (color online). The primary banding pattern in an experiment where the liquid contained glass spheres together with nylon rods. Each band contains spheres and rods implying that the pattern wavelength is independent of particle density and shape. From Thomas, 2011b.

They investigated liquids with high and low viscosities, particles lighter and (hydrophobic) heavier than liquids, for small and large particles, and for low and high particle concentrations. Their results confirmed that clustering and band formation occurs under a broad range of conditions and concluded that it is a robustly unstable phenomenon. They identified three different regimes of clustering. The first regime is associated with the case of thin films and slowly rotating cylinders. Joseph *et al.* (2003) concluded that here it is capillarity that causes particles to cluster either into islands or into the typical bands displaying the high particle concentrations. The second flow regime is encountered at moderate rotation rates and higher filling levels. Here the experiments of Joseph *et al.* (2003) displayed cellular structures of air bubbles separated by disks of liquid. The bubbles were not centered and took different shapes depending on the relevant parameters (cf. Fig. 16). In this dynamic regime Joseph *et al.* (2003) attributed the band formation to secondary motions induced by the off- center gas bubbles.

The third regime of segregation is associated with bidisperse suspensions for which it was found that two layers of heavier-than-liquid particles stratify when there is no rotation but segregate into alternate bands of particles when there is rotation.

Note that the result of Joseph *et al.* (2003) that bidisperse suspensions lead to alternating bands of particles is at odds with the observations of Thomas *et al.* (2001). In their experiments particles of different density and shape displayed the same pattern wavelength and remained mixed within each band as illustrated in Fig. 15. The discrepancy between the results of Thomas *et al.* (2001) and Joseph *et al.* (2003) is probably due to the substantially different rotation rates of the cylinder in both studies. The rotation rate in the experiments of Thomas *et al.* (2001) was typically slow and of the order of a few revolutions per minute only. However, in the experiments of Joseph *et al.* (2003) where alternate bands were observed the rotation rate was 306 rpm (see their Fig. 24). While centrifugal forces were negligible for the experiments of Thomas *et al.* (2001) they were substantially more prominent for the experiments of Joseph *et al.* (2003). It appears highly likely that it is the centrifugal forces that are responsible for the bidisperse suspensions with particles of different densities to display the alternate banding observed by Joseph *et al.* (2003). If this interpretation is indeed correct then this prompts the intriguing question with regards to what happens when the experimental conditions are in the intermediate regime between those of Thomas *et al.* (2001) and Joseph *et al.* (2003). Is it possible that there exists a transitional regime where banding disappears entirely? Finally it is noted that none of the experiments conducted by Joseph *et al.* (2003) displayed the fine structure of the banding phenomenon reported by Thomas *et al.* (2001).

C. Models for the granule-band formation in rimming flow of particle-laden liquids

Tirumkudulu, Tripathi, and Acrivos (1999) concluded their study on the flow of liquid carrying a neutrally buoyant part in the partially filled Taylor-Couette system by indicating that they were of the opinion that the banding phenomenon represented a further example of a mechanism known as shear-induced diffusion (Leighton and Acrivos, 1987a, ; 1987b). According to this mechanism particles migrate from regions of high shear to regions of low shear and from regions of high particle concentrations to regions of low particle concentrations. However, in their follow-up study (Tirumkudulu, Mileo, and Acrivos, 2000) with neutrally buoyant particles in rimming flow, their conclusions were that they believed that the observed particle segregation is initiated by some as yet unknown mechanism. They speculated on the mechanism being associated with fluctuations in the local particle concentration modifying the local effective viscosity and, thereby, the local value of a parameter

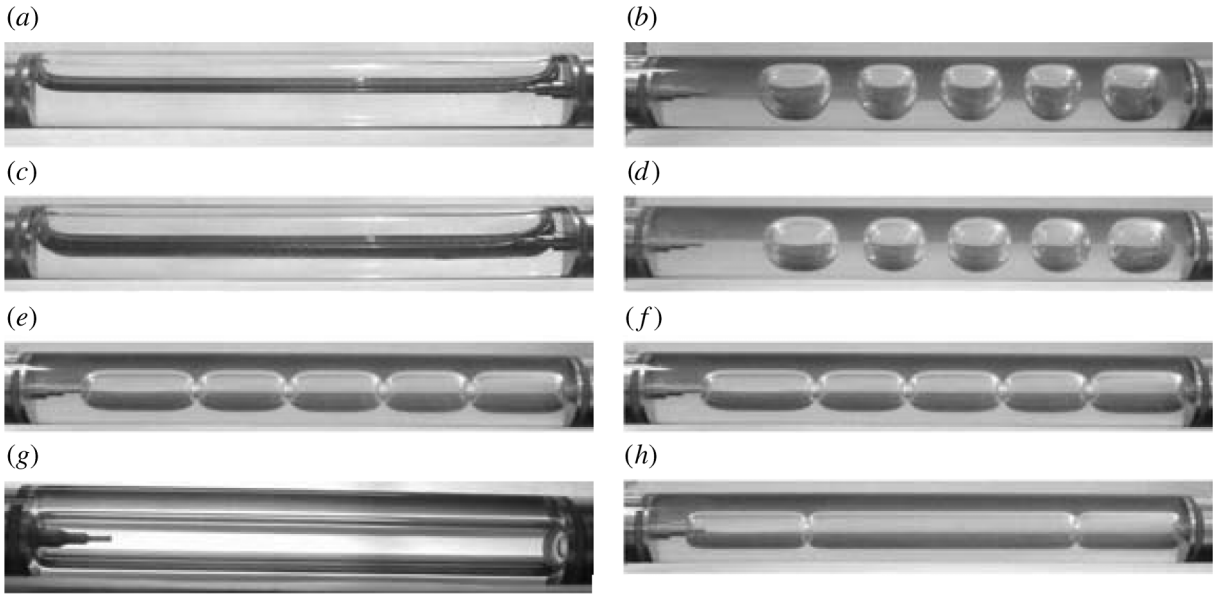

FIG. 16. Comparison of bubble formation in (a), (c), (e), and (g) soybean oil and (b), (d), (f), and (h) Triton mixture (2950 cP). (a), (b) $\Omega = 200$ rpm; (c), (d) 300 rpm; (e), (f) 600 rpm; and (g), (h) 900 rpm. From Joseph *et al.*, 2003.

$$\beta = V_f^* \left(\frac{gR}{\Omega \nu}\right)^{1/2} \tag{2}$$

which follows from standard lubrication analysis (Moffatt, 1977; Johnson, 1988; O'Brien and Gath, 1998; Tirumkudulu and Acrivos, 2001). The parameter β of Tirumkudulu, Mileo, and Acrivos (2000) relates the fluid volume fraction V_f^* and the ratio of gravitational forces to viscous forces and can be expressed as $\beta = V_f^* \mathrm{Fr}^{-1/2} \mathrm{Re}^{1/2} = \Pi_3 \Pi_2^{1/2} \Pi_4^{-1/2}$ using the definitions of Table I. Note also that β and the parameter Λ used by Melo (1993) are related through $\Lambda = 4\beta^{-2}$.

The first attempt to provide a mathematical description for the formation of the granule bands was, however, due to Govindarajan, Nott, and Ramaswamy (2001). Their theoretical approach was, in fact, based on the concept of shear-induced diffusion, combined with a concentration dependent viscosity and the existence of a free surface. Govindarajan, Nott, and Ramaswamy (2001) claimed that their results provided an explanation of the experiments of Tirumkudulu, Tripathi, and Acrivos (1999) and Tirumkudulu, Mileo, and Acrivos (2000), but their mathematical derivation received substantial criticism in a subsequent comment by Acrivos (2002).

The suggestion of Tirumkudulu, Mileo, and Acrivos (2000) that granule-band formation for neutrally buoyant particles in rimming flow may arise from fluctuations of the local effective viscosity was formulated theoretically and analyzed in detail by Jin and Acrivos (2004a, 2004b). In their analysis Jin and Acrivos (2004a) initially considered rimming flow of a particle-free liquid that did, however, have an axially varying viscosity. Evidently it is not straightforward to develop a real physical system that would satisfy these conditions. However, Acrivos (2005) commented that the idea for their theoretical approach was motivated by experiments conducted by one of his students who cooled the selected circumferential location of the cylinder in order to change the viscosity of the liquid inside the cylinder in these regions. Jin and Acrivos (2004a) showed that, at steady state, the fluid within the pool of liquid in the cylinder moved, on average, toward regions of low viscosity, whereas the liquid integrated across the circumferential region moved, on average, toward regions of high viscosity. The total axial volumetric flow rate is the same in the pool and in the circumferential region.

Jin and Acrivos (2004b) then continued their theoretical analysis by considering rimming flows of suspensions containing neutrally buoyant particles. They assumed that the suspension had already segregated radially in the sense that the particle concentration in the circumferential flow region is everywhere uniform and greater than the (uniform) particle concentration in the pool. Jin and Acrivos (2004b) viewed the radially segregated suspension as a continuum. They performed a linear analysis to examine the stability of the suspension to axial perturbations in the particle concentration. The underlying idea is that axial perturbations in the particle concentration give rise to axial perturbations of the effective viscosity of the suspension. With reference to the analysis in the companion paper (Jin and Acrivos, 2004a) for the homogeneous liquid with axially varying viscosity it was then established that there is a net particle flow rate toward the high viscosity region which, thereby, further enhances the initial particle concentration and the corresponding effective viscosity perturbations. In conclusion, the linear stability analysis performed by Jin and Acrivos (2004b) for dilute suspensions revealed that such a particle distribution is unstable to axial perturbations with the surface tension being responsible for the selection of the wavelength of the most rapidly amplified disturbance. This consequently explains the formation of the bands and Jin and Acrivos (2004b) did indeed find that calculated and measured spacings between the bands were in good agreement.

Jin and Acrivos (2004b) emphasized that they believed that their analysis appeared to leave little doubt regarding the mechanism responsible for the band formation along the axis of the cylinder for the case of a liquid carrying neutrally buoyant particles. However, Jin and Acrivos (2004a) also stressed that their explanation pertains specifically to the conditions of the experiments described by Tirumkudulu, Tripathi, and Acrivos (1999), Tirumkudulu (2001), and Jin (2004). Jin and Acrivos (2004b) further highlighted that their analysis did not address the issue of why, to begin with, the neutrally buoyant particles leave the pool of liquid and, thereby, trigger the radial segregation which then, subsequently, induces the segregation along the cylinder axis.

Timberlake and Morris (2002), who conducted experiments with a horizontal Taylor-Couette system filled with a liquid carrying neutrally buoyant particles, suggested a mechanistic alternative basis for the earliest stages, or onset, of axial segregation to concentrated bands. According to their model the band generation is initiated by differential rates of drainage of particles and fluid by gravity-driven flows from fluctuations in the surface elevation of the film on the inner cylinder wall. The central idea upon which their proposed mechanism rests is that in gravity-driven flow in a thin film of suspension the fluid and the particle phase film-averaged velocities will differ. Timberlake and Morris (2002) attributed the differential drainage to two primary factors. First, the layer of material directly adjacent to the free surface is liquid if the particles are wetted and has the largest gravity-driven velocity. Second, the motion of a particle within a thin film will be hindered by the presence of the solid (and to a lesser degree the free) surface. Both factors will result in fluid flowing ahead of the particles. To illustrate the mechanism that initiates the band formation they considered sinusoidal fluctuations of the free surface of their Taylor-Couette flow along the horizontal axis for a liquid with an initially uniform particle volume fraction. They argued that the more rapid fluid drainage resulted in a slight increase of the local particle volume fraction at the crests of the surface. This, consequently, constituted a self-propagating mechanism in the sense that an increased particle volume fraction leads to an increase in the local effective viscosity, which in turn will cause the free surface to remain elevated at these positions on subsequent cylinder rotations. Timberlake and Morris (2002) pointed out that their arguments were consistent with the results of Tirumkudulu, Mileo, and Acrivos (2000), where the particle size relative to the film thickness in the drainage flow down the cylinder wall was noted to be a controlling factor in the degree of segregation. Timberlake and Morris

(2002) remarked that the two factors they identified as being responsible for the differential drainage would have relatively less influence at film depths which are many times the particle size.

In conclusion, to date, the model of Jin and Acrivos (2004a, 2004b) represents the most elaborate and successful theoretical attempt to explain the banding phenomenon for rimming flow of a liquid carrying neutrally buoyant particles. The suggested physical mechanism for the band formation is plausible and the model yields good agreement between the calculated and measured spacings between the bands. However, as emphasized by Jin and Acrivos (2004b), their model pertains specifically to the conditions of their earlier experiments. Furthermore, a shortcoming of the model is that it does not provide an explanation of why the neutrally buoyant particles leave the pool of liquid on the bottom of the cylinder to begin with.

D. Spatiotemporal dynamics of the segregation bands

Guyez and Thomas (2008) reported results from long-term observations revealing that the granular segregation bands forming in particle-laden rimming flow can display an extremely rich spatiotemporal behavior that emerges as the banding patterns drift slowly along the axis of rotation. They commented that spatiotemporal variability, as such, was not surprising since previous authors also noticed this in related systems (Timberlake and Morris, 2002, 2003; Seiden, Ungarish, and Lipson, 2005). Nevertheless, none of these observed dynamics with the level of complexity and symmetry reported by Guyez and Thomas (2008, 2009). Guyez and Thomas also emphasized that, surprisingly, the spatiotemporal variability can, in fact, disappear entirely under certain experimental conditions.

In order to monitor the long-term spatiotemporal behavior Guyez and Thomas (2008) observed experiments, lasting up to about four weeks, by taking head-on photographs of the system at regular intervals, Δt. For each digital photograph, they scanned and then extracted a horizontal pixel line at a fixed level across the image. Each pixel line was processed such that the location of the granular bands was represented in black whereas the regions free of granules were represented in white. The successive pixel-scan lines for the entire photo sequence of each experiment were then composed into a single image. This yields a space-time diagram revealing the drift of the banding pattern illustrating the overall system dynamics. An example of a typical space-time diagram is shown in Fig. 17.

The abscissa displays the position L along the axis of rotation such that $L = 0$ corresponds to the left-hand side of the cylinder while $L = 27$ cm corresponds to the right-hand side. The left-hand ordinate displays the number of cylinder revolutions t/T, where t is time and T represents the time required for one cylinder revolution. The right-hand ordinate additionally displays time in units of days. Figure 17 illustrates how the bands drifted slowly from positions along the axis of rotation toward the left and right end walls of the cylinder. However, the drift direction of the bands is not directed outward, i.e., toward the end walls, for all experimental conditions. Under certain experimental conditions the

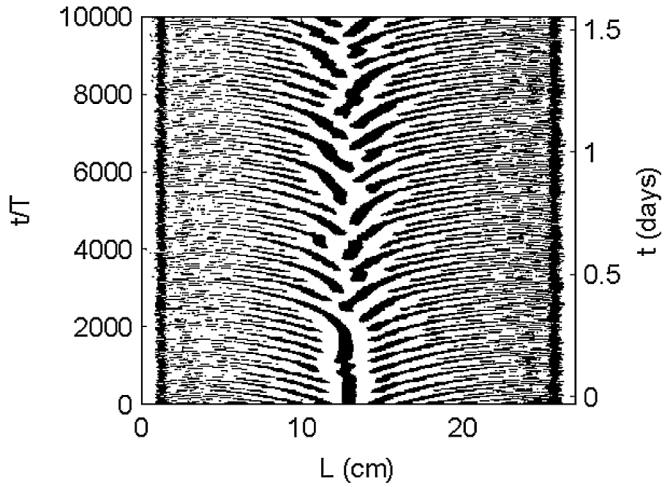

FIG. 17. Spatiotemporal diagram illustrating band drift for an experiment in which the granular segregation bands drifted toward the left and right end walls of the cylinder. From Guyez and Thomas, 2008.

bands can also drift from the end walls toward the center of the cylinder as illustrated in Fig. 18. Guyez and Thomas (2008, 2009) observed several other drift modes and identified eight nondimensional parameters required to characterize the system. The experiments of Guyez and Thomas (2009) were designed to assess the system response to two of these parameters and it was found that they are crucial parameters with regards to the initiation of the band drift. Based on the physical relevance of the two parameters it was concluded that the initiation of the band drift was strongly affected by a competition between capillary forces and gravitational forces. A third nondimensional parameter was identified as being of relevance to controlling the band-drift speed in the parameter regime where band drift exists. It is still entirely unknown which physical mechanisms are responsible for the initiation of the band drift and which processes select the drift mode. However, Guyez and Thomas (2009) discussed the fact that their results indicated that the flow dynamics near the end walls and, consequently, the aspect ratio of the cylinder, play

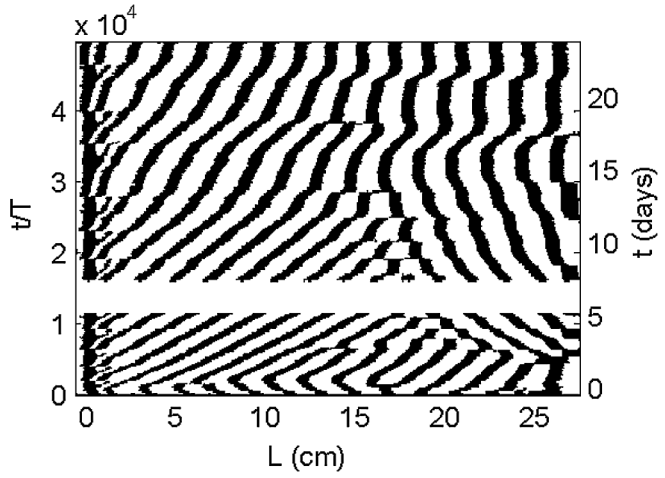

FIG. 18. Spatiotemporal diagram illustrating band drift for an experiment in which the granular segregation bands drifted toward the center of the cylinder. From Guyez and Thomas, 2008.

key roles in establishing and sustaining the band drift. The near-wall flow dynamics are affected by the fluid properties and these may, therefore, also affect the selection of the drift mode.

E. Rimming Flow: Summary and conclusions

The existing literature on pattern formation phenomena in homogeneous and particle-laden rimming flow was reviewed in the last two sections. Regarding the case of homogeneous liquids, this review has shown that the onset of the wavy instability of the contact line between the puddle of liquid inside the cylinder and the inner cylinder wall can be treated theoretically by a linear stability analysis. Similarly it was found that the shape of the film coating the inner cylinder surface, while in the rimming state, is amenable to a computational analysis. However, the higher-order patterns that develop out of the wavy-front state in parameter regimes when the wave amplitudes break up cannot yet be treated analytically or computationally.

The literature on particle-laden rimming flow revealed that adding the particulate phase triggers many new flow phenomena that do not exist for the corresponding flow of homogeneous liquids. The primary new phenomenon is the axial granular-banding pattern that develops when the particles segregate and accumulate to form a series of circumferential azimuthal regions of high particle concentrations. For the particular case of neutrally buoyant particles it is possible to understand the axial banding phenomenon on the basis of a theoretical model based on viscosity variations induced by the increased effective liquid viscosity in regions of high particle concentrations. However, this model assumes that the particles have already segregated radially. Hence, it does not explain why the particles, which are initially uniformly distributed throughout the liquid in the pool, segregate in the radial direction toward the inner cylinder surface. It is presently unknown how far the model for segregation banding of neutrally buoyant particles is also relevant for flow where the particles are denser or less dense than the carrier liquid. Furthermore, the model cannot capture the fine structure of the banding phenomenon where each primary band develops a compound structure consisting of a set of narrower rings. This either indicates that segregation banding for neutrally buoyant and non-neutrally buoyant particles is due to different physical mechanisms or it indicates that the existing model for neutrally buoyant particles may not be complete.

A further aspect associated with the banding phenomenon that is not yet understood theoretically is the slow drift of the granule bands along the axis of rotation. It is entirely unknown what physical mechanisms initiate and sustain the band drift and which mechanisms select the drift mode.

The literature reviewed here deals with flows of dilute suspensions in partially filled horizontally rotating cylinders. We conclude with a brief comment regarding the corresponding case when the cylinder contains a dense suspension. As far as we are aware there exists only one such study (Duong, Hosoi, and Shinbrot, 2004). For their experiments Duong *et al.* used a dense suspension of fine glass beads in water. They reported the spontaneous emergence of a doubly periodic train of sedimented knolls that formed along the cylinder axis on the inside cylinder wall and at its rising side. The solidified knolls were described as rising out of, and coexisting alongside, a sea of freely flowing liquid. Duong, Hosoi, and Shinbrot (2004) briefly discussed a model to calculate the height of the dense suspension on the rising side of the inner cylinder wall in cross-sectional simulations for different particle fractions. However, Duong, Hosoi, and Shinbrot (2004) did not provide any information regarding, for instance, the wavelength of the knoll patterns as a function of the particle volume fraction or how the wavelength compares to the wavelength for segregation bands in dilute suspensions.

V. DILUTE SUSPENSION: COMPLETELY FILLED DRUM

One of the main differences between the previously discussed scenario related to a partially filled cylinder and the fluid-filled case is the absence of a free surface. Both for partially filling suspensions and for partially filling granular mixtures (see Sec. VI), the segregation mechanisms are strongly related to free-surface dynamics (Zik *et al.*, 1994; Jin and Acrivos, 2004a). It is therefore intriguing that apparently similar patterns emerge for a fluid-filled rotating horizontal cylinder (see Fig. 19). Moreover, as we see shortly, even within the category of fluid-filled rotating-drum flows there are more than one segregation mechanisms, which are applicable at different regimes of particle volume fraction (V_p^*) and fluid viscosity (η).

A. Experimental observations

When non-neutrally buoyant particles are suspended at low volume fraction ($V_p^* \approx 0.01$) in a rotating horizontal cylinder three main scenarios are possible, depending on the rotation rate Ω (Seiden, Ungarish, and Lipson, 2007; Matson, Ackerson, and Tong, 2008). For rotation rates below a low critical value Ω_L the buoyancy force dominates and the particles accumulate adjacent to the rising wall of the rotating cylinder. For intermediate values $\Omega_L < \Omega < \Omega_H$ axial segregation takes place and periodically spaced bands of high particle concentration form with a wavelength λ. The transition from a homogeneous (or axially independent) distribution to a well-developed band configuration typically occurs on a time scale $O(\Omega^{-1})$. For large rotation rates $\Omega > \Omega_H$, the centrifugal force dominates and the particles form a uniform thin layer adjacent to the surface of the cylinder. Both the wavelength of the observed patterns and their dynamics (i.e., steady, traveling, or oscillating bands) depend on the fluid

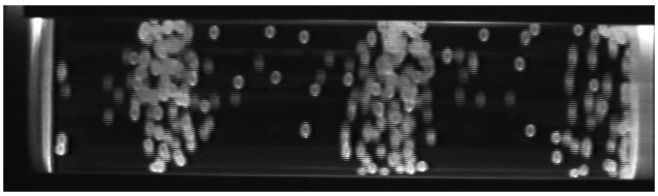

FIG. 19. Axial segregation of 3 mm polystyrene balls suspended in a water-filled drum. The inner tube diameter is $D = 4.5$ cm, the tube length is $L = 18.5$ cm, and the rotation rate is $\Omega = 6.25$ rad/s. Note that in this case $L = 5\lambda/2$. A symmetric configuration with the bands shifted $\lambda/2$ to the left is equally probable. From Seiden, 2011.

viscosity (Breu, Kreulle, and Rehberg, 2004). We therefore distinguish between the low viscosity limit ($\eta < 10$ cP) and intermediate values of viscosity ($10 < \eta < 100$ cP). Segregation and pattern formation in dilute suspensions of non-neutrally buoyant particles at higher viscosities are yet to be explored.

1. The low viscosity limit

Over the last decade, several experimental and theoretical studies focused on pattern formation in the dilute, low viscosity suspension limit. The pioneering observation of axial banding in this case was made by Lipson (2001) with ammonium chloride crystals suspended in a supersaturated solution. In his work, Lipson reported that the phenomenon also occurred for positively buoyant particles [i.e., air bubbles; see also Lipson and Seiden (2002)]. This was followed by more elaborate studies made by Breu, Kreulle, and Rehberg (2003) and Seiden, Lipson, and Franklin (2004). In these investigations the fluid medium was either water ($\eta \cong 1$ cP) or a low viscosity aqueous glycerol solution (i.e., $\eta < 10$ cP), and the particles used ranged from $d \approx 100$ μm to ≈ 1 mm. These mostly experimental investigations not only explored in detail the steady band configuration, but also revealed novel time-dependent dynamics, such as oscillating bands (see Sec. V.A.2).

Seiden, Lipson, and Franklin (2004) investigated the dependency of the phenomenon on the tube length L and on particle characteristics (i.e., size, shape, and specific gravity). The dependency of the phenomenon on tube length revealed a *sawtoothlike* relationship between λ and L, resembling a resonant wave phenomenon, such as a laser resonator. In the latter case the boundary conditions determine the exact value of the wavelength, in accordance with an amplification mechanism centered at a particular frequency (Yariv, 1969). Figure 20 shows the dependency of λ on L for the different particles used. The graph of Fig. 20, in which the abscissa and ordinate were scaled by the tube radius, shows no significant dependency on the characteristics of the particles [in the ranges explored by Seiden, Lipson, and Franklin (2004)]. The oblique dashed lines in Fig. 20, which capture the varying sawtooth slope of the experimental data, represent the following relationship between the observed wavelength and tube length:

$$\lambda = \frac{2L}{n}, \qquad n = 2, 3, 4, \ldots . \tag{3}$$

The mean value of the observed wavelength is $\bar{\lambda} \cong 3.6R$. Also note the tendency at large tube lengths toward an upper limit wavelength $\lambda \approx 4R$.

In accordance with the fact that the compendium of data presented in the scaled graph of Fig. 20 collapses onto the same oblique lines, Seiden *et al.* concluded that the phenomenon scales with the tube radius only. Additional reports, however, indicate that the wavelength depends not only on the tube radius, but also on the particle size. Breu, Kreulle, and Rehberg (2003), who conducted similar experiments with small spherical glass particles ($d = 290$ μm), found in addition to $\lambda = 3.6R$ a shorter, albeit less dominant, wavelength with approximately half the periodicity as a result of splitting of the ring-shaped bands.

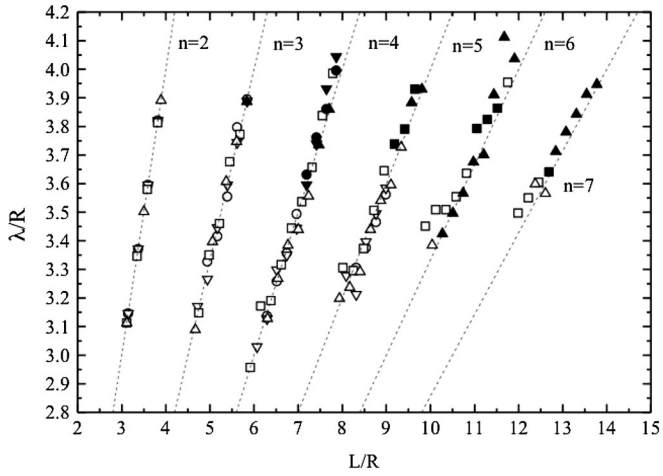

FIG. 20. Dependence of the wavelength on the tube length. By scaling the tube length and observed wavelength by the tube radius the data of different experiments (i.e., different particle characteristics and tube diameters) collapse onto straight lines given by Eq. (3). Solid symbols represent oscillating bands (see Sec. V.A.2). Adapted from Seiden, Lipson, and Franklin, 2004.

Another important result emerged from the investigation of the dependency of the phenomenon on tube length, which has to do with the position of the band pattern with respect to the vertical walls (i.e., at $z = 0, L$). It was found that the bands would form either adjacent to or half a wavelength from the wall. Thus for every tube length there are two possible band configurations (Seiden, Lipson, and Franklin, 2004). An example of a situation where two symmetric and energetically degenerate band configuration occurs is shown in Fig. 19. This double degeneracy is at the origin of a related phenomenon of band oscillations found in the low viscosity limit (Seiden, Lipson, and Franklin, 2004), which will be described in detail in Sec. V.A.2.

An important aspect of pattern forming systems is the transition between qualitatively different states of the system, often depicted through a bifurcation diagram. In the present system there are two main transitions. The first is between the sediment state and the stable band state, and the second is between the band state and the centrifugal state. These transitions occur in the vicinity of Ω_L and Ω_H, respectively. Breu, Kreulle, and Rehberg (2003) experimentally investigated these transitions by varying the control parameter (i.e., rotation frequency) and analyzing the root mean square of the transmitted light, emitted from a source placed behind the rotating drum. The results of their investigation are shown in Fig. 21. The hysteretic character of these transitions is evident from the graph and indicates a subcritical bifurcation. The values of Ω_L and Ω_H are approximately 18.8 and 23.2 rad/s, respectively.

The effect of viscosity in the range $1 < \eta < 10$ cP on the steady banding phenomenon was explored by Seiden, Ungarish, and Lipson (2005). The characteristic sawtoothlike dependency observed for $\eta = 1$ cP (see Fig. 20) carried over to higher values of viscosity. The main consequence of the increase in viscosity was an increase in the mean observed wavelength, from $\bar{\lambda} = 3.6R$ to $4R$. This effect is in agreement with an investigation carried out by Breu, Kreulle, and

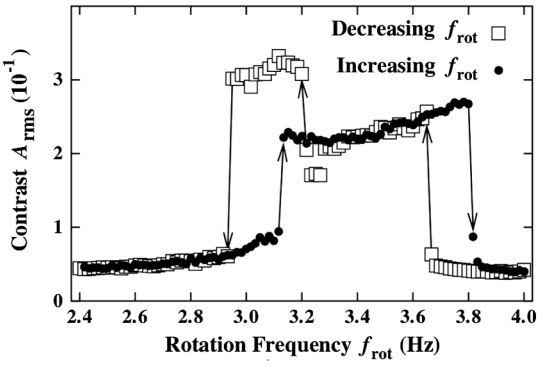

FIG. 21. Bifurcation diagram depicting the frequency dependence of the root-mean-square intensity amplitude. The hysteretic nature of the two transitions is evident. Note that for decreasing rotation rate, there is an intensity jump at 3.25 Hz which corresponds to particles accumulating at either the right or left part of the tube. From Breu, Kreulle, and Rehberg, 2003.

Rehberg (2003) on the effects of viscosity (in the same low viscosity range) on traveling axial bands. However, while in Seiden, Lipson, and Franklin (2004) the effect is moderate (approximately 10% increase), in Breu *et al.* the reported increase is much more substantial (up to 3 times the wavelength observed for pure water).

2. Traveling and oscillating band patterns

As with many other pattern forming systems [e.g., Rayleigh-Bénard convection (Bodenschatz, Pesch, and Ahlers, 2000)], the suspension-filled rotating drum exhibits both steady and dynamical states. Breu, Kreulle, and Rehberg (2004) reported the occurrence of traveling waves for a range of rotation rates between the sediment state and the stable band state. The speed and wavelength of these long-lived, bidirectional waves were found to be almost independent of the rotation frequency. In addition, they note that these waves are nonhysteretic. By altering the viscosity of the interstitial liquid, Breu *et al.* were also able to show that an increase in viscosity causes a decrease in the propagation speed and an increase in wavelength.

Breu, Kreulle, and Rehberg (2004) and Seiden, Lipson, and Franklin (2004) reported an intriguing phenomenon of oscillating band patterns of characteristic time scales $O(10\Omega^{-1})$–$O(100\Omega^{-1})$. Breu, Kreulle, and Rehberg (2004) observed the phenomenon at the transition between the steady band state and the centrifugal limit state. The ring-shaped regions rich in suspended particles were found to periodically expand and shrink along the axis. The frequency of oscillations depended on the rotation rate, with the oscillation frequency increasing as the rotation rate decreased. Seiden, Lipson, and Franklin (2004) reported the oscillation phenomenon for a variety of particles (full symbols in Fig. 20) suspended in water. Here the oscillations consisted in the complete breaking up of each ringlike band and the subsequent merging of adjacent bands. In this way, the band structure oscillated between the two possible configurations determined by the boundary conditions, as discussed in Sec. V.A.1. The phenomenon was found to occur mainly for wavelengths in the range $3.6R$–$4.0R$ (solid symbols in Fig. 20). A dynamical presentation of oscillating axial bands can be found in the supplementary material of Seiden, Ungarish, and Lipson (2005). We note that neither the traveling waves nor the oscillating bands have, to date, been rigorously explained.

3. The intermediate viscosity range

The intermediate viscosity range ($10 < \eta < 100$ cP) has many similar features to the low viscosity range described previously. One example is the similar flow patterns observed in the embedding fluid when steady band patterns occur (Seiden, Ungarish, and Lipson, 2005; Matson *et al.*, 2005). There are, however, fundamental differences between the two regimes. Maybe the most evident difference is the observed wavelength, which for the intermediate range is $\lambda \cong 2.4R$ (compared to $\lambda \cong 3.6R$ for the low viscosity limit). These two regimes also differ in the range of the associated dimensionless numbers. Although the viscosity is typically only an order of magnitude larger in the present case, other parameters such as the rotation frequency corresponding to the occurrence of stable bands are affected as a result of the different values of viscosity. This yields substantial differences in the governing dimensionless parameters. For example, the Reynolds number based on the particle dimension,[6] which takes values $\mathrm{Re}_d \cong 10$ for an aqueous suspension of 100 μm glass beads filling a tube with $R = 1$ cm, here is typically $\mathrm{Re}_d \approx 0.1$ for the same particles and tube. This difference in dimensionless numbers has in turn a profound effect on the theoretical approaches one utilizes in order to understand the segregation mechanisms (see Sec. V.B).

Matson *et al.* (2003, 2005, 2008) carried out detailed experimental investigations into the various states observed as both the rotation rate Ω and the fluid viscosity η were varied. They used 100 μm glass beads suspended at low volume fraction ($V_p^* = 0.023$) in aqueous glycerol solutions, completely filling a tube with $R = 0.95$ cm and $L = 22.75$ cm. Matson *et al.* reported as many as ten different states, ranging from the granular bed state (GB in Fig. 22) found at low rotation rates to the centrifugal limit state (CL in Fig. 22), which characterizes the high rotation rates. The left column in Fig. 22 shows a side view of the ten states observed in the intermediate viscosity range. The photographs were taken with a backlit illumination. The dark areas represent high particle densities. The center and right columns in Fig. 22 show a complementary view of the flow field in the r-θ plane, pertaining to the main states shown in the left column. These photos were taken in an especially designed shorter cell ($L = 2.25$ cm) having a transparent window, with the illuminating light sheet directed through the r-θ and the CCD camera positioned at right angles. Figure 23 depicts a selected region in the η-T (T being the rotation period) phase diagrams.

The flow in the r-θ plane associated with the first three states found at low rotation rates (GB, F1, F2 in Fig. 22) is a rather complex one, resulting from the fact that a relatively large bulk of particles forms a granular bed adjacent to the

[6]Note that $\mathrm{Re}_d = \mathrm{Re}\Pi_6$.

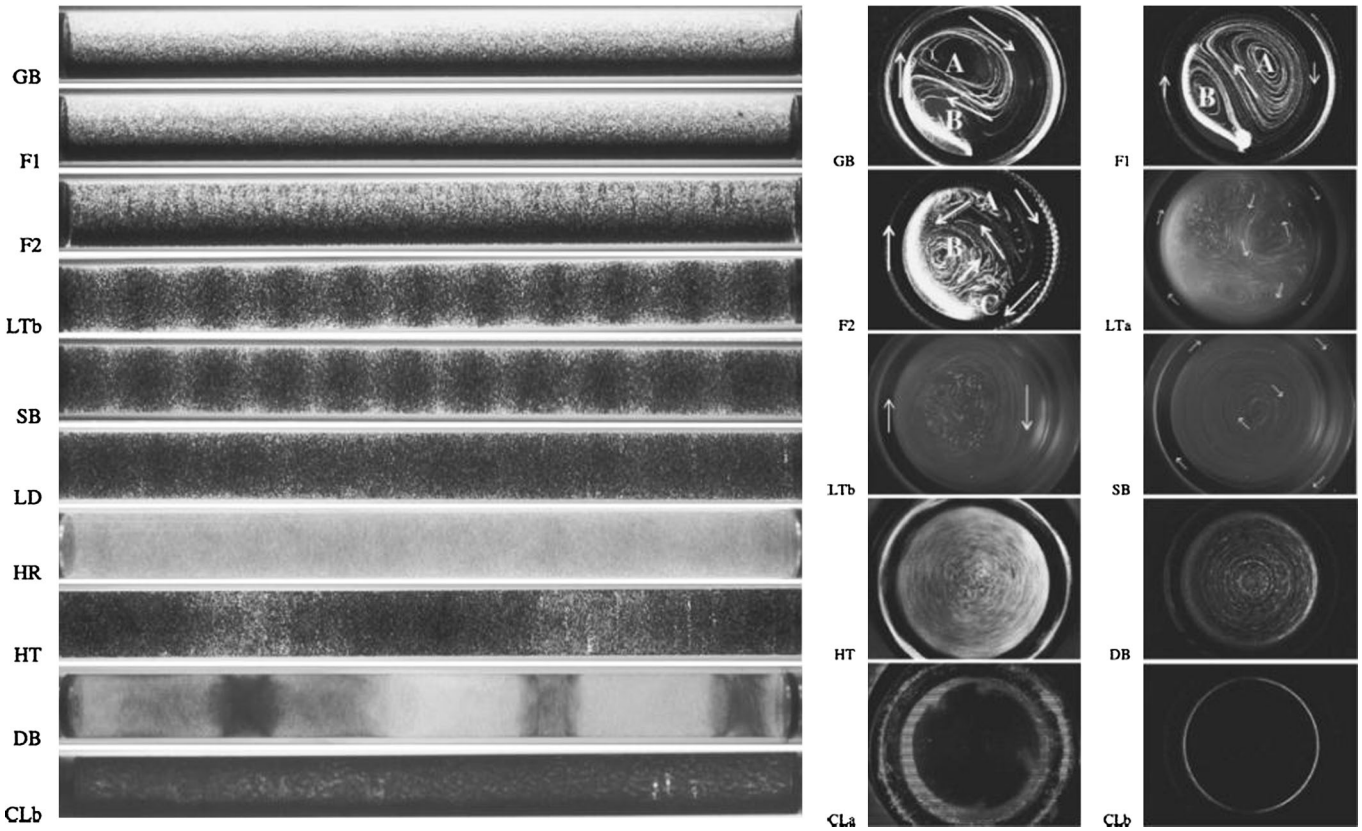

FIG. 22. Different states observed in the intermediate viscosity range as both rotation rate and viscosity are varied. Left column: side view (darker regions have higher particle concentration). Center and right columns: complementing, on-axis view depicting flow field (lighter regions have higher particle concentration). From Matson *et al.*, 2005.

wall of the rotating cylinder. The fourth state, the low-rotation rate transition (LT in Fig. 22), marks the onset of large-scale segregation and the formation of axial bands. While the flow field observed for LT is unsteady, the subsequent steady band state (SB in Fig. 22) is characterized by time-independent, well-defined axial bands. The observed wavelength of SB is $\lambda \cong 2.4R$. The flow pattern in the r-θ plane associated with SB is an off-centered circular motion (see Fig. 22). In the y-z plane, one observes a characteristic convectionlike pattern, which is also typical of the flow field found in the low viscosity limit (see Fig. 26).

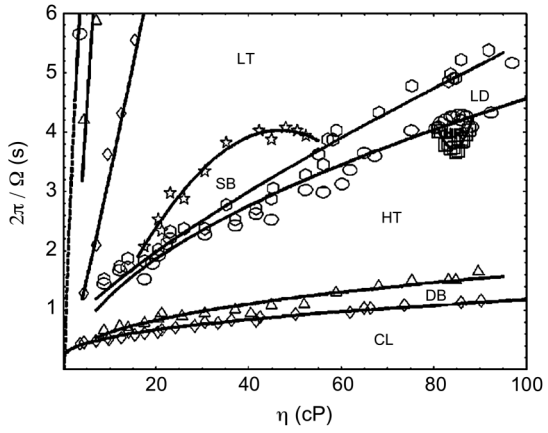

FIG. 23. Phase diagram in η-T plane depicting selected states shown in Fig. 22. The cluster of points on the right represents the homogeneous region (HR) state. From Matson *et al.*, 2005.

For higher rotation rates centrifugal effects are manifested in a growing layer of particles attached to the cylinder inner surface. It is worth noting that the two states found after SB [i.e., the local-structure dropout (LD) and the homogeneous region (HR)] are characterized by no axial patterns, while in the next two states [i.e., the high-rotation-rate transition (HT) and the discontinuous banding (DB)] pattern formation processes again cause axial migration and banding. Here, however, the periodic length is considerably larger than the one observed for SB.

Matson, Ackerson, and Tong (2008) expanded the above investigation in order to study the effects of varying the particle size, concentration, and cylinder radius. Their experiments show that varying the particle dimension has an effect mainly on the transition between states, not on the character and number of observed states. The effect of particle concentration was investigated in the range $0.01 < V_p^* < 0.03$. The results suggest that the dominant effect of increasing the particle concentration is an increase of the gravitational driving force, rather than an increase of the effective viscosity of the suspension. When varying the cylinder radius all states observed by Matson *et al.* (2005) were recovered except for the HR state.

The large range of dimensional parameters explored by Matson, Ackerson, and Tong (2008) enabled them to investigate the scaling laws governing the transitions between the different states. With respect to the transitions in the low-rotation rate regime (states GB, F1, F2, and LT), they found the following power-law dependencies between the Reynolds

number (or Π_4^{-1}), the size aspect ratio (Π_6), and the ratio between buoyancy and centrifugal forces (Π_2):

$$\Pi_4 = \begin{cases} \frac{35}{8}\frac{\Delta\rho}{\rho_f}\Pi_2\Pi_6^3, & \text{GB-F1 transition,} \\ \alpha\frac{\Delta\rho}{\rho_f}\Pi_2\Pi_6, & \text{F1-F2, F2-LT transitions,} \end{cases} \tag{4}$$

where $\alpha = 2.75 \times 10^{-3}$ for the F1-F2 transition and $\alpha = 0.65 \times 10^{-2}$ for the F2-LT transition. Note that the ratio $\Delta\rho/\rho_f$ is different than the corresponding dimensionless parameter of the general set presented in Table I. The latter has $\rho_f + \rho_p$ in the denominator in order to allow for a generic set which is applicable to other rotating-drum flows. In this respect, it should be noted that Matson *et al.* did not explore the ρ_p dependence.

The intermediate and high-rotation-rate transitions were fitted by the following general relationship:

$$\Pi_4 = 1.69 \times 10^{-2}\left(\frac{\Delta\rho}{\rho_f}\Pi_2\right)^{3/2} V_p^{*3/4}. \tag{5}$$

While the above scaling laws were derived empirically, Matson, Ackerson, and Tong (2008) were able to explain the scaling of the centrifugal limit DB-CL transition by viewing it as a Rayleigh-Taylor instability.

B. Theoretical approaches

The fact that the system under study consists not only of a fluid, which is governed by the nonlinear Navier-Stokes equations, but also a large number of suspended particles makes a theoretical analysis extremely difficult. Indeed, without making simplifying assumptions one faces a formidable task. Two different approaches aimed at unraveling the physical origin of segregation and formation of axial bands were made by Lee and Ladd (2002, 2005, 2007) and by Seiden *et al.* (2004, 2005, 2007). These two approaches differ both in the range of dimensionless parameters they attempt to explore and in the conceptual view regarding the role of the suspended particle in causing segregation to occur in a system that would otherwise be in a state of solid body rotation.

1. Stokes flow approximation

Lee and Ladd (2002), 2005, 2007) addressed the experimental observations made by Matson, Ackerson, and Tong (2003) on intermediate viscosity suspensions [$\eta = O(10$ cP)] consisting of 100 μm glass spheres. Their approach is based on the smallness of the Reynolds number $\mathrm{Re}_d = \rho_f d\Omega R/\eta$, which, in the experiments of Matson *et al.*, was $\mathrm{Re}_d \approx 0.01$. Thus the *creeping* flow in the vicinity of a single suspended particle is governed by the Stokes and continuity equations,

$$\eta\nabla^2\mathbf{u} = \nabla p, \qquad \nabla\cdot\mathbf{u} = 0. \tag{6}$$

In this low Reynolds number regime, the motion of the particle in the rotating drum is characterized by two terminal velocities associated with the gravitational and centrifugal forces:

$$\mathbf{v}_g = \frac{m_b}{3\pi\eta d}\,\mathbf{g}, \qquad \mathbf{v}_c = \frac{m_b\Omega^2 r}{3\pi\eta d}\hat{\mathbf{r}}, \tag{7}$$

where $m_b = \pi d^3\Delta\rho/6$ and r is the distance of the particle from the cylinder axis. Superimposing these velocities onto the underlying rigid rotation yields the velocity of the particle at a given point within the drum. Figure 24 depicts different possible trajectories, depending on the dimensionless parameters $P_1 = \Pi_2 = g/\Omega^2 R$ and $P_2 = v_g/\Omega R$.

According to Lee and Ladd (2005, 2007), axial segregation and banding is caused by an attractive, hydrodynamic interaction between the suspended particles. Specifically, axial perturbations in the concentration field lead to faster settling where particles are closer together, which draws more particles toward the high concentration regions. By numerically integrating the equations of motion of $N = O(10^4)$ ($V_p^* \approx 0.01$) spherical particles in a flow field which consists of a superposition of the flow in the vicinity of an isolated particle and the long range contribution of the rest of the suspended particles, they were able to show that axial banding occurred with a wavelength approximately equal to the cylinder diameter (see Fig. 25). We recall that the observed wavelength reported by Matson, Ackerson, and Tong (2003) was $\lambda = 2.4R$. The rotation rate interval pertaining to the occurrence of banding was $0.9v_g/l < \Omega < 1.4v_g/l$, where l is the mean interparticle separation.

Lee and Ladd also identified a dimensionless parameter $Q = \bar{\Theta}/N\Omega$ (where $\bar{\Theta}$ is the total time-averaged angular momentum of the disperse phase), which distinguishes between a transversally (i.e., in the r-θ plane) segregated phase at low rotation rates, and the transversally disperse phase in which the particles go through well-defined closed trajectories. Banding was observed at the transition between those two phases. It is also important to note that the wavelength of

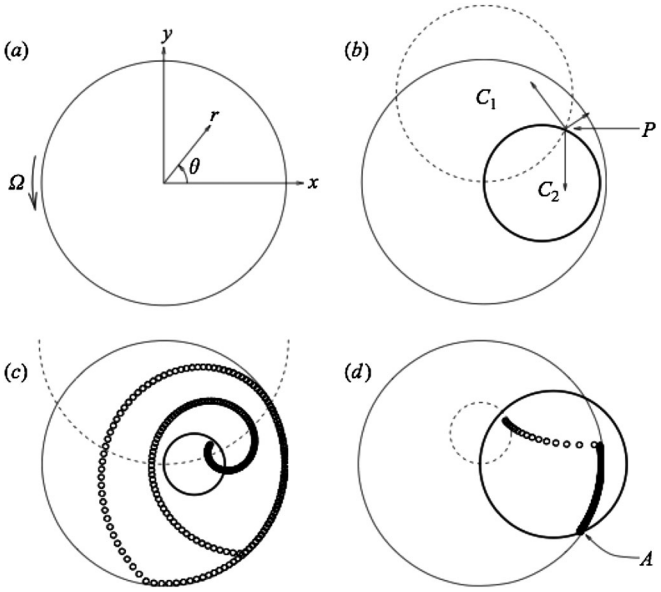

FIG. 24. Different possible trajectories of a single particle in a rotating drum under Stokes flow. (a) Coordinate system used. (b) Loci of points pertaining to vanishing radial (C_1) and tangential (C_2) components of velocity. (c) Closed trajectory bound by cylinder wall reached after spiraling motion from initial point. (d) When $P_2 > 1$ the viscous drag is not sufficient to suspend the particle and the particle reaches a stagnation point on the wall (A). From Lee and Ladd, 2002.

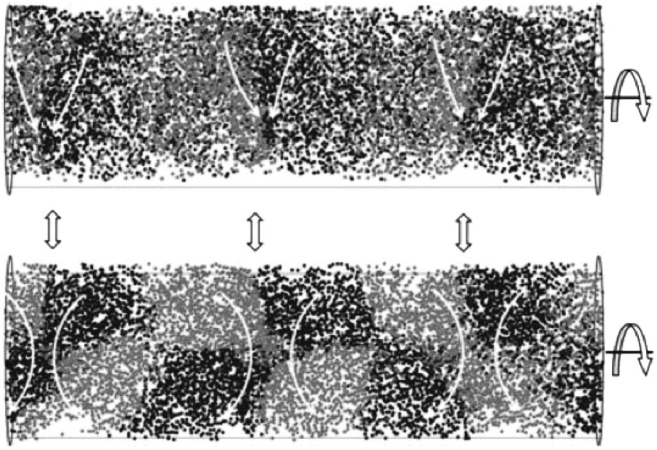

FIG. 25. Axial segregation due to low Reynolds-number hydrodynamic interactions. Upper panel: top view of rotating drum showing axial banding. Lighter particles are moving to the right and darker particles to the left. Bottom panel: front view of drum depicting secondary axial flow. From Lee and Ladd, 2007.

the band pattern was found to be sensitive to the length of the tube. Thus, for $L = 6.2R$ they observed three stable bands while for $L = 7.0R$ the system alternated between three and four bands. This relationship between wavelength and tube length is also a characteristic of banding at the low viscosity range (see Sec. V.A.1).

2. Boundary-layer approximation

Seiden *et al.* (2004, 2005) considered the observations made with suspensions consisting of millimeter-sized particles (e.g., 3 mm polystyrene beads) suspended in water. This scenario yields much larger values of Re_d [$\mathrm{Re}_d = O(100)$], and thus the Stokes approximation is no longer valid. Their approach, in turn, is based on the smallness of the Ekman number $E = \eta/\rho_f \Omega R^2 = \mathrm{Re}^{-1}$. This dimensionless number, which is the reciprocal of the Reynolds number based on the cylinder radius and corresponding velocity, is an indicator of the effects of the boundary layers (Greenspan, 1969). For small values of E one can use a singular perturbation analysis in order to expand the fields ($\mathbf{u}$, p) in powers of E^α ($\alpha < 1$). In particular, when $L = O(R)$ the dominant boundaries are the Ekman boundaries adjacent to the vertical walls at $z = 0$, L and the expansion is in powers of $E^{1/2}$ (Greenspan, 1969). In the experiments of Seiden, Lipson, and Franklin (2004) $E \approx 10^{-3}$, and thus they used a boundary-layer approach to analyze the flow causing the particles to segregate.

In contrast to the approach of Lee and Ladd (2002), Seiden *et al.* (2004, 2005) did not focus on the hydrodynamic interaction between the particles, which for the corresponding values of Re_d is to date unknown.[7] Instead, they investigated the collective effect of the dispersed phase on the continuous phase through looking first at the flow of a single particle in an otherwise unperturbed rigidly rotating flow. While for low Re_d the flow of a single particle is well understood (Roberts, Kornfeld, and Fowlis, 1991), for large values of Re_d the flow in the vicinity of an accelerating particle is complex and only approximate solutions are available (Lawrence and Mei, 1995). Seiden, Ungarish, and Lipson (2007) employed the first approximation for the drag acting on an accelerating particle, namely, the (empirical) drag exerted on an identical particle moving through an infinite fluid with a terminal velocity equal to the instantaneous velocity of the accelerating particle. This approximation leads to an off-centered, almost circular trajectory adjacent to the cylinder wall (Seiden, Ungarish, and Lipson, 2007). The corresponding effective frequency of the suspended particle ω was found to be close to that of the cylinder (i.e., $\omega \cong \Omega$). In light of the fact that one considers dilute suspensions, they further assumed that the effect of hydrodynamic interactions between the suspended particles does not alter in a significant way the overall single-particle dynamics picture and concluded that the collective effect of the suspended particles can be viewed as a persistently perturbing driving force acting on the fluid, with a frequency equal to the effective frequency ω.

In order to explore the fluid response to the gravity-induced perturbation of the suspended particles Seiden *et al.* (2004, 2005) made two simplifying assumptions regarding the governing Navier-Stokes equations, which in a frame rotating at $\mathbf{\Omega} = \Omega\hat{\mathbf{z}}$ read in nondimensional form

$$\frac{\partial \mathbf{u}^*}{\partial t^*} + \mathrm{Ro}(\mathbf{u}^* \cdot \nabla)\mathbf{u}^* + 2\hat{\mathbf{z}}^* \times \mathbf{u}^* = -\nabla \tilde{p}^* + E\nabla^2 \mathbf{u}^*, \qquad \nabla \cdot \mathbf{u}^* = 0. \tag{8}$$

In the above equation, the Rossby number $\mathrm{Ro} = U/\Omega R$ (U being a characteristic velocity in the rotating frame) is the ratio between the inertial term and the Coriolis term, and $\tilde{p}^*$ is the reduced pressure, incorporating the dynamical pressure and the centrifugal and gravity effects.

The first approximation was to neglect the viscous term due to the smallness of the Ekman number in the experiments. The second simplifying assumption was that $\mathrm{Ro} \ll 1$. This approximation can be justified only in the initial stages of axial segregation.

Under these two assumptions Eq. (8) reduced to the inviscid, linear form:

$$\frac{\partial \mathbf{u}^*}{\partial t^*} + 2\hat{\mathbf{z}}^* \times \mathbf{u}^* = -\nabla \tilde{p}^*, \qquad \nabla \cdot \mathbf{u}^* = 0. \tag{9}$$

The solutions of Eq. (9) are termed *inertial waves* (Greenspan, 1969). Inertial waves occur in a variety of natural systems related to bounded rotating fluids, ranging from the Earth's interior (Aldridge and Lumb, 1987) and atmosphere [i.e., Rossby waves (Rossby, 1939)] to accretion disks (Dubrulle and Valdettarol, 1992).

Out of an infinite set of inertial modes associated with ω^* Seiden *et al.* were led to consider a particular family of modes, which when viewed from the laboratory frame of reference appear stationary and thus could cause segregation and a steady pattern to occur. This family of modes is characterized by the dependency $\exp(\theta^* + \omega^* t^*)$. The specific modes that would be excited by the gravity-induced motion of the suspended particles can in general be identified by projection of the driving field seen by the fluid onto the

[7] We note that hydrodynamic interactions between two and three particles in the rotating horizontal drum configuration were recently studied experimentally for $\mathrm{Re}_d = O(1)$ by Mullin *et al.* (2005).

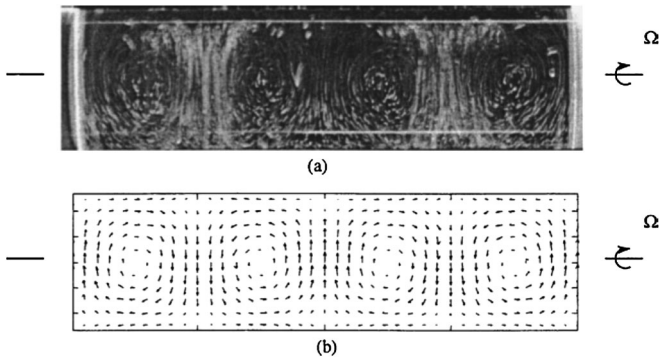

FIG. 26. Comparison between the theoretical prediction of the boundary-layer approach and experimental visualization of the flow field. (a) Experimental flow field manifested by streaks of small tracer particles using a thin light sheet projected from above. (b) Theoretical prediction of flow field in the same plane. From Seiden, Ungarish, and Lipson, 2005.

family of inertial modes (Greenspan, 1969). This projection singles out a dominant mode, which was studied in detail by Seiden *et al.* (2005, 2007). In particular, for an effective frequency $\omega^* = 1$, which corresponds to the gravity-induced relative motion of the suspended particles, the wavelength of this mode is $\lambda_{\text{theory}} = 3.97R$. This theoretical value is in good agreement with the experimental observation.

Seiden, Ungarish, and Lipson (2005) conducted an experiment which further confirmed their theoretical approach. In the experiment two different kinds of particles were used: tracer particles and larger, millimeter-sized, inertial particles. While the large particles segregated and formed axial bands in the regular fashion, the smaller particles traced the flow and were used to visualize the flow field. A thin light sheet was directed from above along the $x = 0$ plane. A CCD camera was placed in the $y = 0$ plane, facing the transparent tube. In this way the tracer particles were illuminated and streaks of their trajectories recorded.

Figure 26 shows the results of this experiment [Fig. 26(a)] together with the theoretical field predicted by the theory [Fig. 26(b)]. The streaks of the tracer particles depict a flow field consisting of four convectivelike cells, which is in good agreement with the predictions of the theoretical flow field. Moreover, from the dynamics recorded via the CCD camera one could also establish that the predicted orientation of the velocity field in the bands was as predicted (upward between bands and downward within the bands).

VI. DENSE GRANULAR FLOWS

The rotating drum is particularly associated with the study of dense granular flows. The lack of constitutive equations for granular matter coupled with the vast industrial applications make granular dynamics a vibrant and expanding area of research (Jaeger, Nagel, and Behringer, 1996; Duran, 1999; Ottino and Khakhar, 2000; Ristow, 2000). The rotating-drum configuration, partially filled with a mixture of granules, has the advantage of being a self-contained apparatus, where grains are continuously being fed to the top part of the pile and allowing for a wide range of dynamics by varying the rotation rate (Henein, Brimacombe, and Watkinson, 1983).

Previous reviews on granular flows in rotating drums include the works of Ottino and Khakhar (2000), Ristow (2000), and Meier, Lueptow, and Ottino (2007). Ristow addressed the rotating-drum configuration in the broader context of pattern formation in granular matter, while Ottino and Meier *et al.* focused on mixing and segregation in rotating tumblers of different shapes. In this work we restrict ourselves to noncohesive granules and to drums rotating at constant frequencies.

A. Single component case

1. Avalanches: A paradigm of self-organized criticality?

Probably the most characteristic phenomenon associated with granular material is avalanches, the intermediate state between the solidlike and fluidlike regimes experienced by dense granules. The last few decades have seen an intensified interest in granular avalanches, following the introduction of the concept of self-organized criticality (SOC). This concept was coined by Bak, Tang, and Wiessenfeld (1987) in an attempt to account for critical behavior (i.e., intermittent intense events) exhibited by large-scale nonequilibrium systems, such as plate tectonics (Gutenberg and Richter, 1956) and turbulence (Frisch, 1995). According to Bak, Tang, and Wiessenfeld (1987), spatially extended dynamical systems self-organize into a set of barely stable states consisting of all length and time scales. These systems are therefore characterized by a power-law spectrum both in time [e.g., the so-called $1/f$ noise (Press, 1978)] and in space.

In their seminal paper, Bak, Tang, and Wiessenfeld (1987) chose avalanches in sand piles as a paradigm of nonequilibrium critical systems. Here a slow input of new grains gradually increases the slope until, when a critical value θ_c is reached, an avalanche occurs which resets the slope to the static angle of repose $\theta_s < \theta_c$. By using a simple numerical sandpile model Bak, Tang, and Wiessenfeld (1987) showed that both the size distribution and the associated duration of avalanches were governed by a power-law dependency.

In an attempt to experimentally explore the statistics of avalanches in granular material Jaeger, Liu, and Nagel (1989), and independently Evesque and Rajchenbach (1988), carried out experiments in a slowly rotating horizontal drum, partially filled with monodisperse granular material. The avalanches were detected either by a parallel-plate capacitor, through which the grains flowed when an avalanche occurred (Jaeger, Liu, and Nagel, 1989), or by a sensitive microphone (Evesque and Rajchenbach, 1988).

In contrast to the predictions and numerical results of Bak, Tang, and Wiessenfeld (1987), these investigators failed to observe a scale free, power-law spectrum. Figure 27 shows the results obtained by Jaeger, Liu, and Nagel (1989) with spherical glass beads of average diameter $\bar{d} = 0.54$ mm placed in an open cylinder of radius $R = 5$ cm and length $L = 8$ cm, rotating about its axis at $\Omega = 3.78 \times 10^{-4}$ rad/s. The dashed line in Fig. 27 is the predicted f^{-1} power-law dependence.

In order to clarify the apparent contradiction between the numerical studies and the experimental results further experimental investigations were performed in various geometries. Bretz *et al.* (1992) used a rotating-drum configuration,

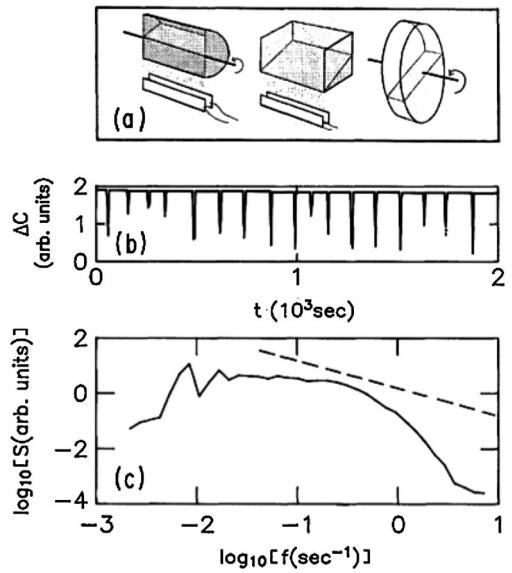

FIG. 27. Statistics of avalanches in a rotating drum. (a) Schematic of different rotating tumblers used in the investigation of avalanches. (b) Time trace of avalanche events detected by a plate capacitor through which the grains fall. (c) Corresponding power spectrum of the sequence in (a). The dashed line represents a $1/f$ spectrum. From Jaeger, Liu, and Nagel, 1989.

similar to the one used by Jaeger, Liu, and Nagel (1989), with the exception that the base was pretextured with a glued layer of grains. The focus of their work was on the spectrum of small avalanches occurring between successive large avalanches. These small scale events were at least in part ignored in previous works due to the measuring techniques used, which were aimed at detecting global effects. By scaling the duration of the small avalanche by the time interval between successive large avalanches Bretz *et al.* (1992) were able to show that these sliding events obey a power-law distribution, with an exponent of -2.134. Held *et al.* (1990) studied the statistics of avalanches in a 2D conical-shaped sandpile. They found that, depending on the size of the sandpile (i.e., the diameter D of the circular base upon which the pile was constructed), the avalanches can exhibit either power-law statistics ($D < 2.5$ cm) or relaxation oscillations ($D > 2.5$ cm). Rosendahl *et al.* (1993, 1994) used a similar setup to the one used by Held *et al.* (1990). They found that small avalanches obey power-law statistics with an exponent of -2.2, independent of the size of the pile. This result is in close agreement with the findings of Bretz *et al.* (1992) for the rotating-drum configuration. Large avalanches, on the other hand, were found to be overly frequent and quasiperiodic. They also demonstrated (Rosendahl, Vekić, and Rutledge, 1994) that the small avalanches can be used to predict the occurrence of large avalanches. Frette *et al.* (1996) investigated avalanches in piles of rice confined between two vertical walls. By using different types of rice, they found that the probability density associated with avalanches of different energy dissipations depends on the shape of the grains (power law for anisotropic grains and stretched exponential for almost isotropic grains).

Thus, while SOC has been reportedly validated as a sound theoretical approach to a variety of nonequilibrium dynamical systems having extended spatial degrees of freedom, such as neural networks (Levina, Herrmann, and Geisel, 2007) and granular high-T_c superconductors (Gerashchenko, 2009), its applicability to avalanches in granular matter is still controversial. Recently, a more comprehensive theoretical framework for driven systems with many degrees of freedom based on the renormalization group has been proposed (Sethna, Dahmen, and Myers, 2001). In particular, this approach extends the power-law predictions to universal scaling functions.

2. Continuous flow

As the rotation rate of the rotating drum increases individual avalanches can no longer be distinguished and one enters the continuous flow regime. Here, the partially filled cylinder consists of a rigidly rotating bottom part and a thin, flowing top layer (see Fig. 28). The free surface of the flowing layer is at first flat (the so-called "rolling" mode) (Henein, Brimacombe, and Watkinson, 1983), but as Ω further increases it acquires an S shape (Rajchenbach, 1990) (the "cascading" mode).

The transition between discrete avalanches and continuous flow was investigated experimentally by Rajchenbach (1990), who reported the hysteretic nature of the transition. Depending on whether one increases or decreases the rotation rate, different values of Ω are associated with the transition. Rajchenbach also reported a square-root dependency of the dynamic angle of repose θ_d on the rotation rate. Further experimental (Dury *et al.*, 1998; Yamane *et al.*, 1998) and numerical (Ristow, 1994) studies, however, found a linear relationship between the rotation rate and the dynamic angle of repose.

Nakagawa *et al.* (1993) utilized MRI as a nonintrusive method for studying the flow in the opaque granular medium. They used mustard seeds due to their strong MRI signal. The MRI measurements produced results on the concentration

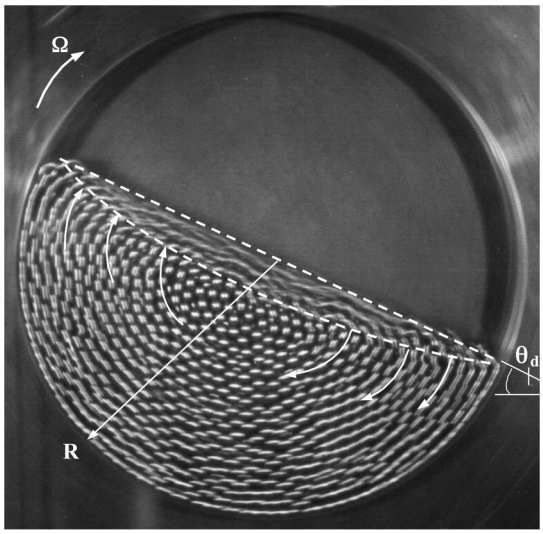

FIG. 28. Continuous flow regime observed for 4 mm steel balls rotated in a cylinder of radius 8 cm. The region bounded by the dashed line is the flowing layer. The rest of the balls experience solid body rotation. The corresponding Froude number is Fr = 0.002. Adapted from Orpe and Khakhar, 2001.

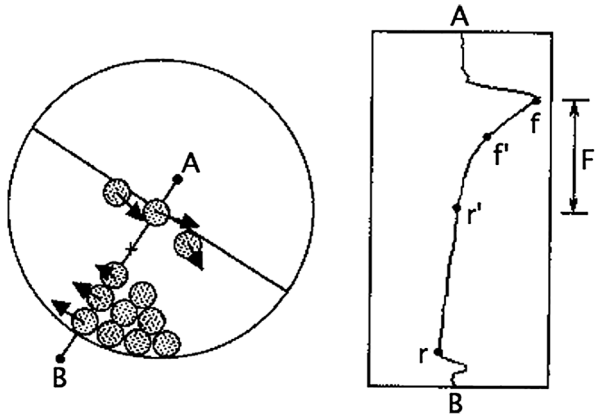

FIG. 29. Velocity profile in rolling regime obtained by MRI measurements. Left: Schematic of granular flow indicating the line segment (AB), along which the velocity was measured. Right: Streamwise velocity profile along the segment AB. The flowing layer is marked F. From Nakagawa *et al.*, 1993.

and velocity fields, as well as on the shape of the flowing layer. The concentration profile across the flowing layer revealed a lower density in the vicinity of the free surface, in accordance with the expected dilatation associated with granular flow (Reynolds, 1885). In the rigidly rotating part, the MRI revealed slight concentration gradients which were attributed to dynamic packing (Nakagawa *et al.*, 1993).

Figure 29 (right) shows the streamwise velocity component across the granular medium. The velocity profile consists of three regions. The first two, between f and f' and between f' and r', correspond to the flowing layer. In the former, the shear rate is almost constant while in the latter the shear rate decreases until, at r', the velocity vanishes. The third region, between r' and r, corresponds to the rigidly rotating bed and is characterized by a small shear rate. Further experimental and numerical investigations of the velocity field in the flowing layer showed that the streamwise component across the layer can be written as (Yamane *et al.*, 1998; Sanfratello and Fukushima, 2008)

$$u(r) = U\left(1 - \frac{r}{h}\right)^2 - \Omega r, \qquad 0 \le r \le h, \tag{10}$$

where h is the thickness of the layer. Both MRI measurements (Nakagawa *et al.*, 1993) and numerical simulations (Ristow, 1996) showed that the streamwise velocity component and the surface flux along the layer are nonsymmetric with respect to the center. The peak of the flux moved downstream from the upper half as the rotation rate increased. Deviations from Eq. (10) for low volume fractions and high rotation rates were reported experimentally by Parker *et al.* (1997) and numerically by Third, Scott, and Scott (2010). These deviations, which were observed for spherical particles, originate due to slip at the cylinder wall and are attributed to the rolling motion of the particles in contact with the wall.

End-wall effects on the dynamic angle of repose and on the streamwise velocity component within the flowing layer were the subject of a number of works. Boateng and Barr (1997) studied end-wall effects using polyethylene pellets. They reported an increase of about 10% in the dynamic angle of repose close to the end walls. The streamwise velocity component was reported to be about 20% higher near the walls, relative to the undisturbed region away from the walls. Dury *et al.* (1998) used both experiments and computer simulations and found that the angle is larger closer to the end caps by up to 5° (about 12%) relative to the center of the drum. Furthermore, by fitting the profile of the dynamic angle of repose along the rotation axis they were able to show that the characteristic length ζ, corresponding to the wall effect, scales with the tube radius and particle dimension in the following way:

$$\zeta = \begin{cases} \alpha_1 R & \text{if } d \le d_c, \\ \alpha_1 R + \alpha_2 (d - d_c) & \text{if } d > d_c, \end{cases} \tag{11}$$

where $\alpha_1 = 0.28$, $\alpha_2 = 3.13$, and $d_c \approx 0.14R$. They found no dependency of ζ on the particle density and gravitational constant. Maneval *et al.* (2005) used MRI measurements to investigate the end-wall effects on the dynamic angle of repose and the velocity profile for two- and three-dimensional drums. They found that the 2D angle of repose and the free-surface velocity are larger than the corresponding ones observed away from the walls in the 3D case. The velocity (at every depth within the flowing layer) close to the walls in the 3D case was found to be smaller than that in the center plane. This last observation seems in contradiction to the findings of Boateng and Barr (1997). Maneval *et al.* (2005) also noted that while in the 2D case mass flux was conserved, in the 3D case mass flux was not conserved in the axial slices examined due to axial flow.

Theoretical studies of the flowing layer used different simplifying assumptions, but were all based on continuum models of the cascading grains. Zik *et al.* (1994) treated the flowing layer as a thin, viscous fluid layer of uniform height. The flow within the layer was assumed tangential to the free surface and the density constant. By balancing the stresses on the layer, Zik *et al.* (1994) were able to reproduce the characteristic S shape of the surface. Khakhar *et al.* (1997a), who sought to investigate not only the flow in the cascading layer, but also the mixing of grains, used a more elaborate approach. They included mass flux from and into the layer, and an explicit expression for the viscosity of the fluid, based on the pioneering work of Bagnold (1954) on nondilute sheared suspensions. They considered three cases, corresponding to plug flow (constant velocity across the layer), Bagnold's profile (Bagnold, 1954), and simple shear. The latter two realistic flow profiles produced averaged velocity and layer thickness along the flowing layer that are in good agreement with the experimental observations for glass spheres. A similar comparison for the case of sugar crystals has, however, revealed qualitative differences, which can be attributed to the nonsphericity of the grains. It should be noted that adopting Bagnold's linear relationship between viscosity and shear rate prompts comparison between phenomena observed in granular flows and those observed for non-Newtonian power-law liquids. While some numerical and theoretical works focused on the latter (mainly, though, on the high Froude number centrifugal limit), experimental investigations are lacking and thus a meaningful comparison is difficult.

Khakhar *et al.* (1997a) studied monodisperse granular mixing by following the advection of individual particles in

the theoretical flow field. The process of mixing was shown to depend on the average velocity in the flowing layer, the distance between the rotation axis and the granular bed, and the diffusivity of the particles perpendicular to the flow direction. The predictions of the theoretical framework were in agreement with experiments. It is important to note that optimal mixing in the continuum flow regime corresponds to bed depth $h/R \approx 0.6$, which is somewhat larger than the value ($h/R \cong 0.5$) obtained by Metcalfe *et al.* (1995) and Peratt and Yorke (1996) for avalanche-induced mixing.

Elperin and Vikhansky (1998) used a boundary-layer approach in order to describe the dynamics in the flowing layer. Their model consists of two adjustable parameters, which depend on the friction in the layer. Gray (2001) derived a theoretical framework based on the avalanche model of Savage and Hutter (1989). He showed that the predicted particle trajectories form closed curves, which pass through both the rigidly rotating bulk and the flowing layer, in agreement with experimental observations. He also performed experiments with monodisperse grains at different volume fractions. The grains were colored in order to visualize mixing. The experimental results are in general agreement with the theoretical predictions, although diffusive mixing, which was not taken into account in the theory, clearly distinguishes the experimental observations.

A number of investigations of scaling laws governing the dynamics and shape of the flowing layer were carried out. Orpe and Khakhar (2001) experimentally studied the dependency of the shape, layer thickness, and dynamic angle of repose on the aspect ratio $\Pi_6 = d/R$ and Froude number $\mathrm{Fr} = \Omega^2 R/g$. They used drums of different sizes, a wide range of rotation rates, and various particles (i.e., steel balls, glass balls, and sand particles) having different dimensions. The shape of the flowing layer and the scaled layer thickness were shown to scale well with Π_6 and the Froude number. The dynamic angle of repose, however, was found to depend also on the material of the grains. They also investigated the scaling of the shear rate and showed that the value at the midpoint of the flowing layer scales as

$$\dot{\gamma} \approx \left[\frac{g \sin(\theta_d - \theta_s)}{d \cos(\theta_s)}\right]^{1/2}. \tag{12}$$

Jain, Ottino, and Lueptow (2004) investigated scaling laws related to the flowing layer under both dry and wet (i.e., slurry) conditions. The scaling laws for the flowing layer thickness, streamwise velocity, and shear rate were found to be *independent* of the interstitial fluid. The former two scaling laws are [the latter given by Eq. (12)]

$$\begin{aligned} \frac{h}{R} &\approx (\mathrm{Fr}\Pi_6)^{1/4}\left[\frac{\sin(\theta_d - \theta_s)}{\cos(\theta_s)}\right]^{-1/4}, \\ \frac{u_{\mathrm{surface}}}{\Omega R} &\approx (\mathrm{Fr}\Pi_6)^{-1/4}\left[\frac{\sin(\theta_d - \theta_s)}{\cos(\theta_s)}\right]^{1/4}. \end{aligned} \tag{13}$$

The above relationship for the surface velocity is consistent with that found by Alexander, Shinbrot, and Muzzio (2002) for relatively high rotation rates. They investigated the dependency of surface velocity on the Froude number and Π_6, but not on the angles θ_d and θ_s. For low-rotation rates they reported the following dependency: $u_{\mathrm{surface}}/\Omega R \approx (\mathrm{Fr}\Pi_6)^{-1/6}$. Midi (2004) analyzed and compared a compendium of experimental data on dense granular flows taken in different geometries, including the rotating-drum configuration. They obtained a similar shear rate dependency ($\dot{\gamma} \approx 0.5\sqrt{g/d}$), and flowing layer thickness: $h/R \propto (\mathrm{Fr}\Pi_6)^{1/4}$.

Sepúlvida, Krstulovic, and Rica (2005) experimentally investigated scaling laws associated with the low volume fraction limit ($V_p^* \ll 1$). The angular extent of the granular front and its depth were examined for a range of microscale particles, drum diameters, and rotation rates. The angular extent of the front was shown to scale with the volume fraction, the Froude number, and the ratio of the tube length and tube radius L/R. In addition, a universal function depending on these three nondimensional parameters was suggested for the front profile (comprised of both angular extent and depth). Recently, Chou and Lee (2008) investigated scaling by a single nondimensional parameter, which combines the Froude number, d/R, and V_p^*. The applicability of the scaling was experimentally examined with respect to the dynamic angle of repose, the flowing layer thickness, the free-surface velocity, and the flowing layer shear rate. The experimental data were shown to collapse when plotted against the nondimensional number, albeit with some scatter.

Kellay, Amarouchene, and Boudet (2007) carried out a detailed experimental investigation of the longitudinal velocity fluctuations on the surface of the flowing layer. Laser Doppler velocimetry was used to accurately measure the 2D velocity field. The results revealed scale invariance in the energy density spectrum with a $-5/3$ power law, similar to the Kolmogorov scaling in 3D turbulence (Kolmogorov, 1941). In addition, the moments of the velocity difference showed a power-law scaling with the exponents saturating at $\frac{2}{3}$, implying strong intermittency. The origin of scale invariance in the velocity fluctuations of the surface flow is yet to be understood.

We close this section with an intriguing example of pattern formation similarity between low volume fraction granular flow and low volume fraction pure liquid rimming flow. Fried, Shen, and Thoroddsen (1998) reported the observation of a variety of wave patterns formed in a thin layer of sand inside the rotating cylinder ($V_p^* \approx 0.01$). In particular, they observed the spanwise spatially periodic wave pattern shown in Fig. 30(a) which is reminiscent of the banding pattern displayed in Fig. 9 for a homogeneous liquid and the segregation bands in Fig. 12 developing in a particle-laden liquid. Fried, Shen, and Thoroddsen (1998) were probably also the first to draw attention to the similarity between some patterns in rimming flows of pure liquids and the flow of a purely granular material inside a horizontal rotating drum. In this context they do, in particular, comment on the remarkable similarity between the stationary granular and frontal wave patterns shown in Fig. 30(b); nevertheless they point out that the patterns do differ in wavelength. The two photos in Figs. 30(b) and 30(c) are not the same scale. The wavelength of the pattern in (c) is approximately twice that of the pattern in (b). The similarities between patterns in fluid flow and granular flow were also highlighted by Krasnapol'skaya *et al.* (2001) who identified, and directly compared, eight

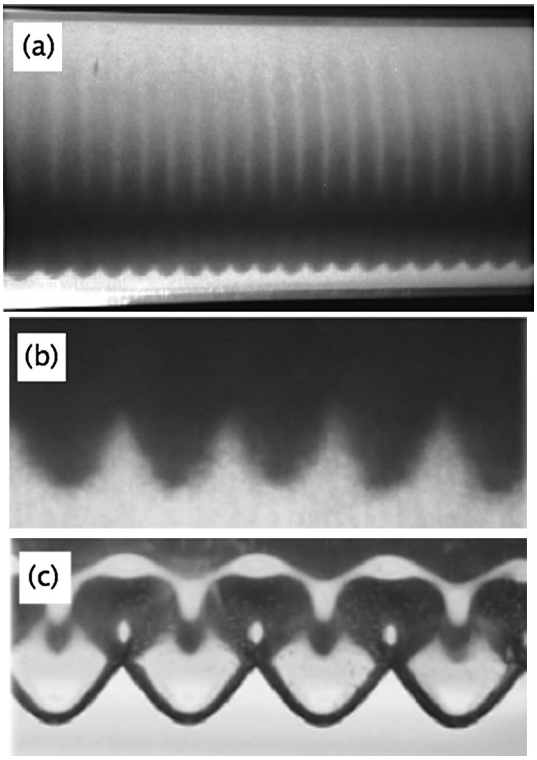

FIG. 30. (a) Stationary periodic wave patterns inside a horizontal cylinder filled with a layer of sand occupying 1.5% of the cylinder volume and rotating with a rotational velocity of $\Omega = 13.8\ \mathrm{rad\,s^{-1}}$ (b) Close-up on the frontal wavy pattern of sand. (c) Frontal pattern observed for a pure liquid, for comparison. From Fried, Shen, and Thoroddsen, 1998.

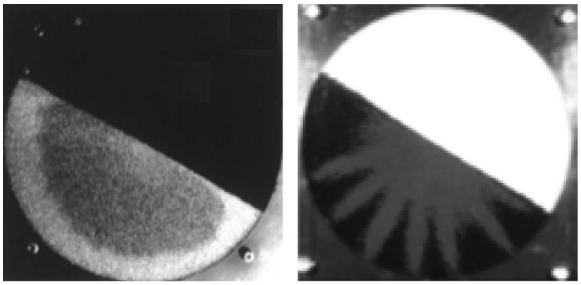

FIG. 31. Different forms of radial segregation in bidisperse granular mixtures (rotation sense is clockwise). (a) Classical radial core observed in a mixture of glass beads ($d_1 = 0.2$ mm, $d_2 = 1$ mm). Adapted from Jain *et al.*, 2001. (b) Radial streaks observed in a mixture of glass beads ($d_1 = 1$ mm, $d_2 = 3$ mm). From Khakhar, Orpe, and Hajra, 2003.

classes of such similar patterns in fluids and granular mixtures.

B. Binary and multicomponent mixtures

1. Radial segregation and streak patterns

A counterintuitive feature of granular mixtures is their tendency to segregate. Differences in particle properties such as size (Drahun and Bridgwater, 1983; Rosato *et al.*, 1987; Cantelaube and Bideau, 1995), density (Ristow, 1994; Khakhar, McCarthy, and Ottino, 1997b), and friction (Lai, Jia, and Cham, 1997; Plantrad, Saadaoui, and Pouligny, 2006) will in general induce segregation, rather than mixing, when a bulk of different particles is subject to vertical shaking (Rosato *et al.*, 1987), horizontal shearing (Schoklitsch, 1933), or is being poured onto a heap (Drahun and Bridgwater, 1983; Prigozhin, 1993). Early studies of granular segregation were motivated primarily by the importance of mixing in industrial applications (Williams, 1976). The rotating-drum configuration, which is a paradigm of industrial tumbling mixers, has been instrumental in shedding light on the physical origin of this intriguing phenomenon.

When a homogeneous binary granular mixture is placed in a quasi-2D rotating drum [$d_1, d_2 = O(L)$] radial segregation is typically observed within a few revolutions (Ristow, 1994; Cantelaube and Bideau, 1995). As mentioned in the previous section, in the rolling regime the granular phase consists of a thin flowing layer and a rigidly rotating bed. The segregation therefore occurs primarily in the flowing layer. The most efficient mechanism, at work when the mixture consists of particles of different sizes, is *percolation* (Williams, 1976). Voids created in the flowing layer are filled with small particles, while the larger granules concentrate at the free surface. This eventually leads to the formation of a core of small particles surrounded by the large particles [Fig. 31(a)]. Another segregation mechanism, relevant when the components are of different densities, is buoyancy. Here heavier particles in the flowing layer sink to lower levels while lighter ones move upward. This process, in a similar manner to that of size induced percolation, leads to a central core of heavy particles engulfed by the lighter grains. Radial segregation induced by friction has also been reported (Lai, Jia, and Cham, 1997).

Size induced radial segregation was investigated independently of other segregation mechanisms by several authors. Clément, Rajchenbach, and Duran (1995) experimentally investigated size segregation in a half-full drum, in the discrete avalanche regime. Segregation was examined by introducing tracer particles of different size into the granular bulk. By tracking the tracer particles they were able to show a clear attraction of small tracer particles to the center of the drum and an opposite tendency of large tracer particles. Cantelaube and Bideau (1995) studied the segregation of millimeter-sized disks in a half-full drum. By recording and analyzing the region occupied by the small disks they were able to show that radial segregation occurs within one revolution. Thomas (2000) investigated size segregation in binary mixtures of glass beads with large aspect ratios. Reverse segregation (i.e., large particles segregating at the center) was reported for $d_L/d_S > 5$ and low composition of large beads, implying that mass effects, rather than percolation, are dominant in this range of parameters. A similar phenomenon was also reported by the author in chute flow and in a flow over a conical heap.

Under certain conditions, the classical semicircular radial core consisting of small particles is observed to develop *radial streaks* [Fig. 31(b)]. Khakhar, Orpe, and Ottino (2001) investigated the formation of streaks in a bidisperse

mixture of glass balls. Streaks were found to form predominantly for $V_p^* \approx 0.5$. In addition, for values of size ratio close to unity (i.e., small differences in size) streak formation was inhibited and only partial streaks were observed. An increase in rotation rate was also observed to suppress streak formation. Recently, Meier *et al.* (2008) reported radial streak coarsening in both circular and square drums. In the former case,[8] they used both size and size-and-density varying binary mixtures. The volume fraction in both cases was $V_f^* = 0.52$. The pattern acquired seven streaks within ten revolutions. The streaks then coarsened to a steady pattern with three streaks after 80 revolutions at a rotation rate of 1 rmp, or one streak after 300 revolutions at 2 rpm. They also reported an orientation periodicity of the streak pattern, whereby the orientation of the pattern coincided with that of the rotating drum after five revolutions. Zuriguel, Peixinho, and Mullin (2009) investigated streak merging in a bidisperse mixture of glass beads and in a binary mixture containing glass particles and sugar crystals. By using angular spatiotemporal diagrams they were able to show that streak merging occurs through the displacement of streaks containing small particles in the counterrotation direction and the deposition of surplus material in the stable streaks. They also reported that the number of streaks in the final stable state is a monotonically decreasing function of the rotation rate. It is important to note that radial streaks were not observed due solely to density difference (i.e., buoyancy).

Several studies used a bidisperse granules mixture of glass beads immersed in water (i.e., slurry condition) in investigating streak formation (Hill *et al.*, 2004, 2005; Zuriguel *et al.*, 2006). The presence of an interstitial liquid eliminates cohesion effects and results in a more smooth, *petal-like* pattern. Hill *et al.* (2004, 2005) investigated the dependency of the waviness index p^2/A (here p is the perimeter of the pattern and A is the area of the pattern), characterizing the petal patterns, on the filling level of the granules. They showed that it peaks at a value which corresponds to a volume fraction slightly larger than $\frac{1}{2}$. Zuriguel *et al.* (2006) experimentally investigated the dependence of the petal pattern on the relative volume fraction, tube diameter, and rotation rate for a half-full drum. Their investigation showed that the dependency of the time period defined through the angular period of the petals $T_{\lambda_\theta} = \lambda_\theta/\Omega$ (here λ_θ is the angular distance between consecutive petals) on the rotation rate has two regimes. For small rotation rates there is a power-law dependency, while for large rotation rates the period saturates to a constant value. Moreover, the former regime does not depend on tube diameter and relative composition while the latter depends on both. The dependency of the saturation period on tube diameter and relative composition was shown to condense into a linear dependency on the radius of the preceding semicircular radial core.

Baumann, Janosi, and Wolf (1994) investigated size segregation of a binary mixture of disks in an almost half-full drum ($V_p^* \approx 0.47$) using a simple numerical model. Their model neglected both inertia and elasticity and utilized a no-slip boundary condition at the drum wall. By studying the trajectories of the small and large particles they observed segregation for particle size ratio in the range $0.5 \leq d_1/d_2 \leq 0.9$. Dury and Ristow (1997) used a molecular dynamics (MD) numerical approach in studying radial segregation of spherical particles half filling a 2D drum. In particular, they investigated the dependency of the phenomenon on the rotation rate and showed that the quality of segregation decreases with increasing Ω and the characteristic segregation time increases.

Theoretical investigations of size induced radial segregation were based on free-surface segregation models (Prigozhin and Kalman, 1998; Makse, 1999; Khakhar, Orpe, and Ottino, 2001; Gray and Thornton, 2005). Prigozhin and Kalman (1998) used a model developed by Prigozhin (1993), whereby a mass transport equation is combined with a phenomenological segregation operator in solving the evolution of the constituent distribution from a prescribed initial condition. The segregation operator was based on the experimental findings of Drahun and Bridgwater (1983), who studied free-surface segregation in a binary mixture poured onto a heap. Prigozhin and Kalman (1998) tested their theoretical predictions using a quasi-2D drum partially filled with a bidisperse mixture of spherical beads made of zirconium oxide and found good agreement.

Khakhar, Orpe, and Ottino (2001) used a more elaborate continuum model, which accounted also for the phenomenon of streak formation. The model consists of mass, momentum, and species balance equations and assumes the difference in size is large enough to allow an almost instantaneous segregation within the flowing layer. Thus, the flowing layer is divided into two parts, with the smaller particles occupying the lower part and the larger ones the upper part. In each layer the velocity profile is assumed to be linear. In addition, the interface between the rigidly rotating bed and the flowing layer is allowed to move, depending on the local composition. This interfacial freedom was found to be crucial to the formation of streaks due to the different angle of repose of the two constituents. Gray and Thornton (2005) used a binary mixture theory approach in order to model size induced segregation. Their theory allowed for the examination of spatiotemporal evolution of the concentration fields. In particular, they reported the formation of three concentration shocks, separating small particles, large particles, and a homogeneous mixture. These three shock lines meet at a triple point.

Hill *et al.* (2004, 2005) explained the formation of radial streaks by a *wave-breaking* mechanism, which is based on the slope of the interface between the large and small particles in the flowing layer. The upper portion consisting of larger particles [dark region in Figs. 32(a) and 32(b)] is, in general, advected faster than the lower part. Therefore, if a positive slope exists, the interface tends to smooth out, while in the case of a negative slope the upper layer overtakes the initially leading lower part. Thus, a gulf of large particles emerges [cf. dark region in Fig. 31(b)], separating regions rich in small particles, which form the radial streaks. Hill *et al.* also accounted for the volume fraction dependence of radial streaks by investigating the oscillating compositions of the flowing layer entering and exiting fluxes. According to their explanation, the amplitude-to-wavelength ratio characterizing the streak pattern, defined through these fluxes, is subject

[8]See Sec. VII.A for details regarding the square tumbler.

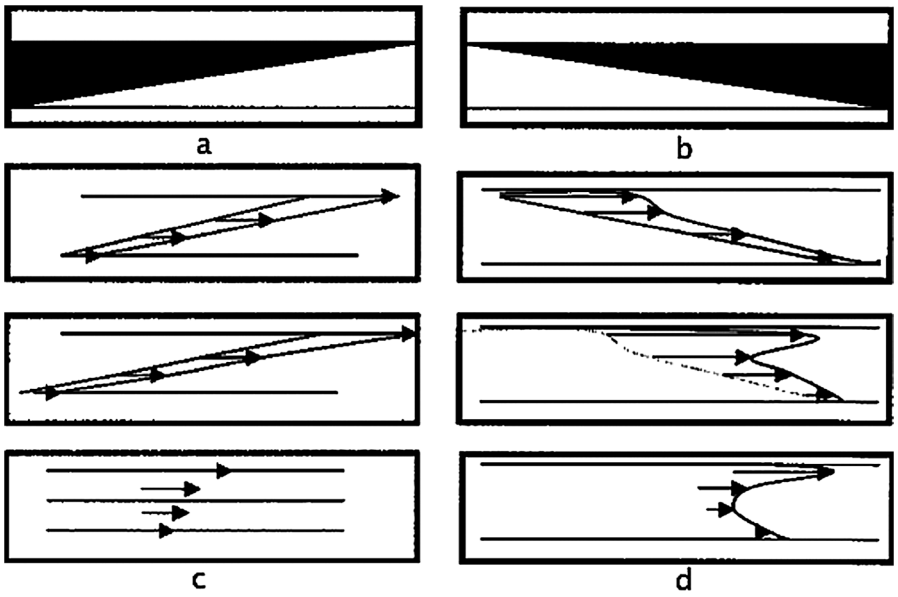

FIG. 32. Wave-breaking model of radial streak formation. Left column (a)–(c): An initial positive slope of the interface between the large (black) and small (white) particles is smoothed out due to the faster advection of large particles. Right column (b)–(d): An initial negative slope of the interface evolves into a gulf of large particles, due to the faster large particles, separating regions rich in small particles. The gulf of large particles [cf. dark region in Fig. 31(b)] eventually outlines the perimeter of the radial streaks. From Hill *et al.*, 2005.

to low pass filtering, with a cutoff frequency which strongly depends on the volume fraction.

Buoyancy induced radial segregation in a quasi-2D drum was investigated by Ristow (1994) and by Khakhar, McCarthy, and Ottino (1997b). Ristow used molecular dynamics simulations to investigate the time evolution of segregation in a binary mixture with $V_p^* \approx 0.4$. By tracking the trajectories of the heavy particles, which constituted 2% of the grains, he was able to study the rate of segregation and its dependence on the density ratio ρ_H/ρ_L. The initial segregation rate was shown to increase as $\log(\rho_H/\rho_L)$. Khakhar, McCarthy, and Ottino (1997b) carried out a comprehensive study which included experimental, numerical, and theoretical investigations. In their experiments, different volume fractions and composition ratios of monodisperse steel and glass balls ($\rho_{\text{steel}}/\rho_{\text{glass}} \approx 3.8$) were used in order to determine their effect on the equilibrium distribution within the mixture. The results showed an increase of the core size with increasing fraction of steel balls, and an independence of the composition profiles on the overall volume fraction. The theoretical model proposed by Khakhar, McCarthy, and Ottino (1997b) is based on a previous analysis of the flowing layer in the single component case (Khakhar *et al.*, 1997a; see Sec. VI.A.2), a species balance equation, and a phenomenological expression for the flowing layer segregation velocity. The model has one free parameter which was determined by the experimental results. With this parameter fixed the theoretical and experimental results were shown to be in quantitative agreement. Khakhar, McCarthy, and Ottino (1997b) utilized the Monte Carlo method and a molecular dynamics simulation in order to further validate their theoretical approach.

Of particular interest and practical importance is the *combined* effect of size and density induced segregation. Alonso, Satoh, and Miyanami (1991) used a simplified theoretical analysis of the flowing layer segregation, taking into account both buoyancy and percolation mechanisms, and proposed a dimensionless parameter which can be used as an indicator of the extent of segregation in a given binary mixture. They tested the prediction of the theoretical approach by plotting the degree of mixing against the segregation parameter for different experiments with binary mixtures in which both size and density were varied. The experimental results confirmed the validity of the proposed parameter as a robust index of the quality of mixing. Metcalfe and Shattuck (1996) used MRI to probe radial segregation in binary mixtures that contained mustard seeds and either glass or sugar balls. The granular volume fraction was $V_p^* = 0.75$. They observed different segregation regimes and, in particular, noted the case in which buoyancy and percolation effects cancel each other resulting in optimal mixing. Jain, Ottino, and Lueptow (2005a) experimentally investigated the competing effects of buoyancy and percolation on radial segregation using steel and glass balls of different sizes. The evolution of segregation was studied through the use of two dimensionless indices: the segregation index, defined as $(A_1A_2)^{1/2}/A$, where A_1, A_2 are the areas occupied by the different balls and $A = A_1 + A_2$, and the shape index p^2/A, where p is the perimeter of the segregated pattern (Hill *et al.*, 1999). From their results, summarized in the diagram of Fig. 33, Jain, Ottino, and Lueptow (2005a) concluded that the regions of segregation and mixing can be distinguished by the size and mass ratios of the particles. Specifically, mixing dominates when

$$d_H/d_L > (m_H/m_L)^{1/4} \tag{14}$$

and vice versa.

Friction is yet another mechanism that can induce segregation in granular mixtures. Lai, Jia, and Cham (1997) used a numerical approach, based on the sandpile model proposed by Bak, Tang, and Wiessenfeld (1987), in order to investigate

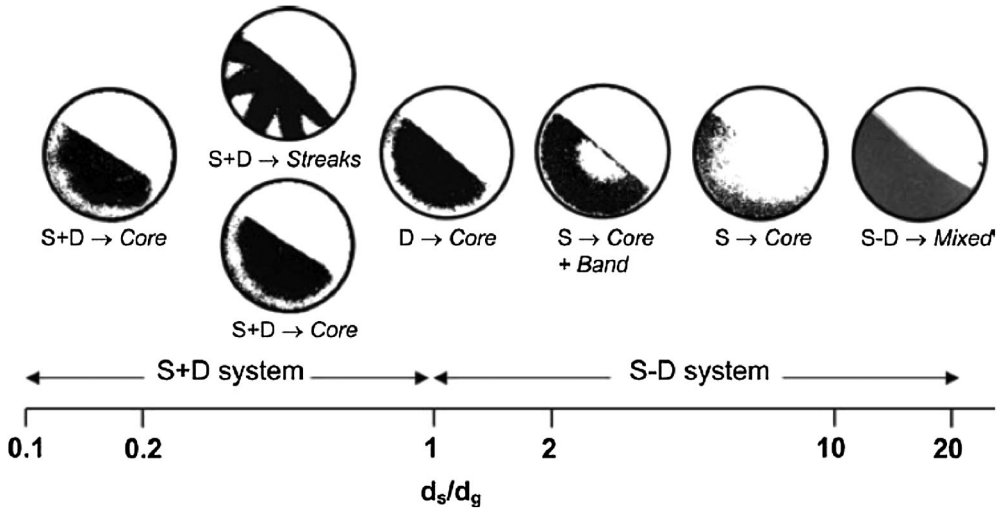

FIG. 33. Dependence of segregation regimes on the aspect ratio d_s/d_g for a binary mixture of glass (white) and steel (dark) beads. *S* and *D* represent mixtures consisting of grains of different sizes and densities, respectively. From Jain, Ottino, and Lueptow, 2005a.

friction induced radial segregation in binary mixtures partially filling a 2D rotating drum. In their model, a difference in friction properties (i.e., surface roughness) between the two constituents was modeled through different angles of repose. The simulations showed that segregation occurred for rotation rates smaller than a critical value, with the rough particles occupying the core and the smooth particles the periphery. However, an experimental study carried out by Pohlman *et al.* (2006) on the effect of surface roughness on the angle of repose and on segregation in a rotating drum was not able to observe radial (or axial) segregation. This is despite the fact that surface roughness did cause an increase in repose angles by as much as 25°.

2. Axial segregation and band patterns

In three-dimensional drums, where an axial transport of particles is possible, another form of segregation is observed in granular mixtures, namely, axial segregation. An initially homogeneous mixture will typically segregate into interleaving axial regions, where the concentration of one component is noticeably higher than that of the other components (see Fig. 34), on a time scale $O(100\ \Omega^{-1})$. The segregation pattern, often referred to as the band pattern, is accompanied by surface undulations (Das Gupta, Khakhar, and Bhatia, 1991) and is observed to slowly evolve, with the number of bands decreasing due to coarsening (Frette and Stavans, 1997; Fiedor and Ottino, 2003).

The phenomenon of axial segregation was first reported by Oyama (1939),[9] who used bidisperse mixtures of limestone particles. The size ratio in Oyama's experiments was $d_1/d_2 = 6.14$. Oyama reported that the observed axial stripes got sharper for longer mixing times and that segregation was enhanced by decreasing the volume fraction ratio $V^*_{p_1}/V^*_{p_2}$. Donald and Roseman (1962) experimentally investigated the effect of size and density on radial and axial segregation using mixtures of sand and Ballotini beads. They reported that axial segregation took place in mixtures, where the smaller (heavier) particles had a larger static angle of repose than the larger (lighter) particles. Segregation occurred initially in the vicinity of the end walls and gradually propagated inward. They concluded that axial segregation and banding result, on the one hand, from end-wall induced velocity gradients which cause small (or heavy) particles to migrate toward faster flowing bands, and on the other hand, from the static angle of repose, which causes the larger (or lighter) beads to flow under gravity in the opposite direction. Recently, Das Gupta, Khakhar, and Bhatia (1991) studied size induced axial segregation using different sieve cuts of sand. They observed that the number of bands increased with the relative concentration of the small particles. They concluded that axial segregation is driven by differences in the *dynamic* angle of repose of the two components, and that radial segregation is a prerequisite for its occurrence. They also pointed out the role of axial dispersion in counteracting the tendency to segregate. Zik *et al.* (1994) experimentally investigated axial banding in binary mixtures of sand and glass beads and of glass beads of different sizes. In the former case axial segregation started throughout the cylinder [rather than adjacent to the end walls (Donald and Roseman, 1962; Hill and Kakalios, 1994)], while in the latter no segregation was observed.

The important role of the dynamic angle of repose in axial segregation and banding was further validated by many others. Hill and Kakalios (1994, 1995), for example, studied the phenomenon with bidisperse mixtures of glass beads in a

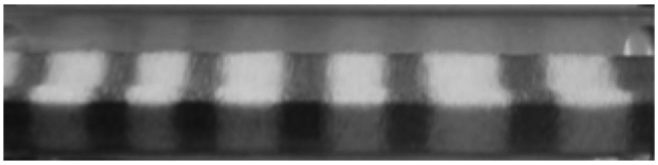

FIG. 34. Axial segregation in a bidisperse sand mixture. The smaller grains (dark) have a larger angle of repose than the larger grains (white). From Caps *et al.*, 2003.

[9]The article is in Japanese. See Weidenbaum (1958) for a detailed account in English of Oyama's work.

half-full drum. By changing the rotation rate, they were able to show that axial segregation is reversible (i.e., segregation is induced from an initially mixed state by increasing the rotation rate and then upon decreasing the rotation rate the mixed state is restored) in mixtures for which the dynamic angle of repose of the mixed state equals that of the segregated phases at a small but finite rotation rate. Reversibility was not observed for mixtures where this condition was not met, e.g., a mixture of glass beads and sand.

While the free surface of the rotating granular media can easily be observed, probing the opaque subsurface composition is difficult, although equally as important. In particular, such measurements complement the free-surface picture. Hill, Caprihan, and Kakalios (1997a, 1997b) investigated the interplay between radial and axial segregation through the use of MRI. They showed that axial segregation is a manifestation of the underlying segregated radial core, which periodically expands and retracts along the cylinder axis, penetrating the free surface at those regions where it is widest. Moreover, when axial segregation is suppressed by lowering the rotation rate the radial core still persists. Santomaso and Petenó (2006) used a solidification technique in order to study the composition of a binary mixture. After a period of rotation, molten wax was poured into the partially filled ($V_p^* = 0.3$) tube. When the wax solidified slices were cut and the composition examined. As a result of their investigation they concluded that an axial surface flow, generated by differences in the dynamic angle of repose, is counterbalanced by a subsurface flow in the opposite direction. Depending on whether the particles differ in density, this convective flow can result in a well-mixed sate when the densities are the same, or in radial and axial segregation for mixtures of different densities.

Numerical investigations of axial segregation were the focus of several works. Yanagita (1999) used a cellular automaton model to investigate both radial and axial segregation. By varying the rotation rate and the model's friction properties, the author was able to reproduce transverse dynamics such as the S shape of the free surface and radial segregation, as well as axial segregation and band pattern coarsening. Shoichi (1998), Rapaport (2002, 2007a), Taberlet, Losert, and Richard (2004), and Taberlet and Richard (2006) used a MD approach in order to investigate axial segregation and banding. An intrinsic feature of this method is the important role of friction in particle-particle and particle-wall collisions. Shoichi (1998) considered binary mixtures with $N = 1000$ particles, in which the two components were distinguishable either by size or by friction properties, or both. The simulations were able to reproduce axial segregation and banding providing that both size and friction properties were different. He also noted that the forces acting on the particles by the end walls stabilize the band structure. Rapaport (2002, 2007a) carried out a more comprehensive MD-based numerical study, in which the parameter range explored included different rotation rates, particle amounts, friction coefficients, volume fractions, cylinder geometry, and densities. He reported that axial segregation was preceded by radial segregation and was observed even when the particles were distinguished only by friction properties. He also noted that the presence of end walls is not necessary for axial segregation to occur. Taberlet, Losert, and Richard (2004) noted that a difference in friction properties was not necessary to observe axial segregation. This was later confirmed by experimental observations made by Pohlman *et al.* (2006). Friction did, however, trigger oscillations in the position or width of the bands. They therefore suggested that similar oscillations found experimentally (Newey *et al.*, 2004) could originate in friction.

Taberlet and Richard (2006) focused on axial diffusion of the small granules from an initially segregated condition. In contrast to previous experimental findings by Khan and Morris (2005), who reported a subdiffusive process with $t^{1/3}$, they observed normal (Fickian) axial diffusion. Further validation of their numerical results was reported recently by Fischer *et al.* (2009) who used MRI measurements to investigate axial transport in bidisperse mixtures immersed in water. Fischer *et al.*, who pointed out that the reliability of the optical technique used by Khan *et al.* in order to observe the hidden core of small grains is questionable, observed normal diffusion. They also reported that the axial transport of large particles, which takes place on the free surface, showed subdiffusive dynamics, in agreement with earlier findings of Khan and Morris (2005). In this respect, it should also be noted that molecular dynamics simulations carried out recently by Third, Scott, and Scott (2010) on monodisperse granules found normal axial dispersion. Hardin *et al.* (2002) used MRI to measure axial dispersion of moist bran in a 20 cm diameter drum and found a diffusion coefficient of 0.51 cm^2/s.

Scaling laws governing the phenomenon of axial segregation include the works of Alexander, Muzzio, and Shinbrot (2004), Charles, Khan, and Morris (2005), and Bielenberg, Gladysz, and Graham (2007). The effects of particle size and tube diameter were investigated by Alexander, Muzzio, and Shinbrot (2004) and Bielenberg, Gladysz, and Graham (2007). Alexander *et al.* carried out experiments with equal volume binary mixtures of spherical glass beads in a half-full drum. Their results, shown in Fig. 35, showed that the size ratio $D/\bar{d}$ ($\bar{d}$ being the mean particle diameter) clearly distinguished between three regions: reversible banding,

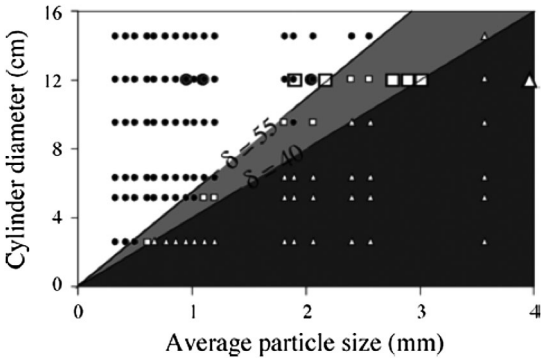

FIG. 35. Different regimes of axial segregation in the $\bar{d}$-D plane. The lines $\delta = D/\bar{d} = 40$ and $\delta = D/\bar{d} = 55$ distinguish between reversible banding (white), nonreversible banding (light gray), and no banding (dark gray). Symbols represent experimental observations (circles always band, squares band reversibly depending on rotation speed, and triangles never band). From Alexander, Muzzio, and Shinbrot, 2004.

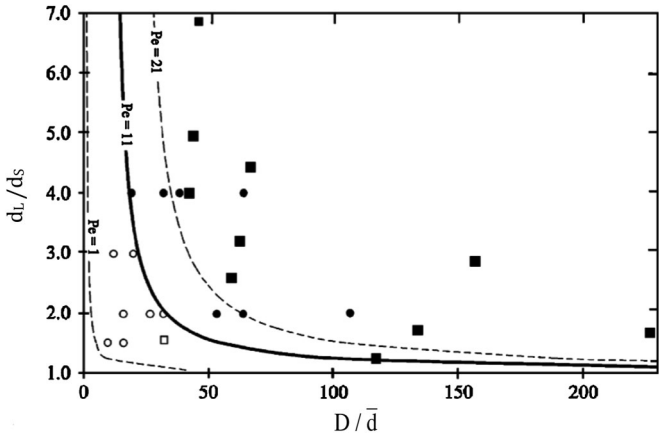

FIG. 36. Segregated and unsegregated states in the $D/\bar{d}$-d_L/d_S plane. Full symbols represent the segregated state and open symbols represent the unsegregated (mixed) state. Lines represent different values of Péclet number (see text). Adapted from Bielenberg, Gladysz, and Graham, 2007.

nonreversible banding, and no banding. Bielenberg *et al.* used equal volume mixtures of acrylic beads with a volume fraction $V_p^* = 0.3$. The Froude number was set to $\mathrm{Fr} = \Omega^2 R/g = 2.6 \times 10^{-3}$ in their experiments. The results of their study were summarized in a phase diagram spanned by the particle size ratio d_L/d_S and the tube-to-particle size ratio $D/\bar{d}$ (see Fig. 36). Bielenberg *et al.* proposed an effective Péclet number, which conveys the ratio between the tendency to segregate (or demix) to the tendency to diffuse (or mix), as an indicator of segregation behavior. The dependence of the band pattern wavelength on tube diameter was investigated by Charles, Khan, and Morris (2005) in a mixture of glass beads of different sizes. The particle size aspect ratio, rotation rate, volume fraction, and relative concentration were all kept constant. The wavelength was observed to scale linearly with the tube diameter.

Under certain conditions, the transient period preceding the occurrence of a saturated band pattern is characterized by wave phenomena. Choo, Molteno, and Morris (1997) reported the observation of traveling waves both from premixed initial conditions and from presegregated conditions, in bidisperse granular mixture. These waves, which were observed when the relative concentration of large grains exceeded one-half, exhibited linear dynamics (i.e., they interpenetrated to form standing waves). The propagation speed of the waves was shown to decrease with wavelength. Khan, Tokaruk, and Morris (2004) studied the interplay between the surface shape, surface concentration, and the thickness of the segregated radial core and observed that these three fields are interdependent and in phase with each other throughout the transient motion.

The saturated band pattern is in general not stable but dynamically evolves on a long time scale. Nakagawa (1994), who carried out experiments with a bidisperse mixture of sand grains, was the first to note that the number of bands decreases with time. He concluded that the final segregation state is comprised of three bands. Frette and Stavans (1997) investigated the long time evolution of band patterns in a binary mixture of sand and glass beads. They investigated both premixed and presegregated initial conditions. In the former case they observed a tendency of the band pattern to coarsen, while in the latter they found that the completely segregated state is not a stable one; glass bands nucleated within the initially homogeneous sand band (but not the other way around). This asymmetric tendency between the two components was found to occur also when the grains were initially premixed. It led them to conclude that there exists a transport mechanism, apart from axial diffusion, mediated by avalanches occurring within the sand bands. These avalanches tend to propagate axially and thus facilitate the transport of glass beads. Fiedor and Ottino (2003) studied the evolution of band patterns with bidisperse mixtures of glass beads ($d_L/d_S = 4$) in a half-full drum. Band coarsening was observed to follow a logarithmic law $N = -k\ln(t)$, with $k = 1.74$.

Theoretical studies of axial segregation and banding were based on continuum models. Zik *et al.* (1994) and Levine (1999) employed a continuum approach, based on mass and momentum conservation, in order to describe the flow in the free surface of a bidisperse mixture. Axial transport and segregation occurred as a result of surface gradients induced by differences in the dynamic angles of repose of the two components. Levitan (1998) used a similar approach to that of Zik *et al.* (1994) but has in addition taken into consideration a noise term conveying the contribution of random collisions. Levitan showed that with the added term the phenomenon of coarsening could be recovered, in agreement with experiments (Frette and Stavans, 1997; Fiedor and Ottino, 2003). Aranson and Tsimring (1999) and Aranson, Tsimring, and Vinokur (1999) used a continuum approach based on averaged mass transport equations and on the assumption that segregation takes place only in the vicinity of the dilated flowing free surface. The governing equations were reduced to two coupled partial differential equations for the relative concentration and dynamic angle of repose. Their analysis not only reproduced axial segregation and banding but also the preceding traveling waves and the subsequent coarsening of the band pattern. It should be noted, however, that while the above fields were predicted to be out of phase by the theory, experiments by Khan, Tokaruk, and Morris (2004) showed them to be in phase.

Axial banding of bidisperse granular mixtures was also investigated under wet conditions (Jain *et al.*, 2001; Fiedor and Ottino, 2003; Arndt *et al.*, 2005; Finger *et al.*, 2006; Finger and Stannarius, 2007; Juarez, Ottino, and Lueptow, 2008; Juarez, Lueptow, and Ottino, 2010). Jain *et al.* (2001) experimentally investigated the effects of interstitial liquid on axial segregation using two different liquids: water and a solution of sodium iodine (NaI). The volume fraction in their experiments was $V_p^* = 0.5$ and the relative granular composition was 1:1. The main difference with respect to dry conditions was that axial segregation took place much faster under wet conditions. Fiedor and Ottino (2003) investigated axial segregation and coarsening both for circular cylinders and for square cross-section cylinders. They observed that banding occurred for higher rotation rates in comparison to dry mixtures. They also reported that the process of coarsening obeys a logarithmic law, in a similar manner to that found for dry conditions. Arndt *et al.* (2005) and Finger *et al.*

(2006) investigated the long-term segregation behavior with water as the interstitial liquid. Arndt *et al.* (2005) reported that, depending on the volume fraction, the core of small particles either remains stable as bands form or completely disappears from within the large granular bands. Finger *et al.* (2006) showed that a logarithmic decay law of the number of bands is only an approximation and that there is an acceleration of the coarsening process after a large number of rotations [$O(10^3)$].

Buoyancy and viscosity effects due to the presence of an interstitial liquid were examined by Finger and Stannarius (2007). Density variations of up to 20% were shown to have no influence on the formation and evolution of bands. Changes in viscosity, on the other hand, had both qualitative and quantitative effects. The range of rotation rate for which bands are observed was found to shift by the same order of magnitude as the change in viscosity. In addition, the viscosity of the liquid tends to stabilize the band structure for long times. Viscosity had little effect, however, on the scaled rate (i.e., in units of Ω) of pattern formation and coarsening. Viscosity effects of the interstitial liquid were also investigated by Fiedor, Umbanhowar, and Ottino (2007), who noted that the area of mixed granules increased linearly with viscosity and that the maximal number of bands reached a peak for $\eta \cong 3$ cP.

Recently, Juarez, Lueptow, and Ottino (2010) investigated the dependence of axial banding on relative concentration and rotation rate for binary mixtures immersed in water. They constructed a detailed phase space which revealed two segregation regimes, analogous to spinoidal decomposition and nucleation observed in binary chemical systems. The former regime occurred for low-rotation rates (10–50 rpm) and relative composition $V_{ps}/(V_{ps}+V_{pL}) \approx 0.4$–$0.8$. The latter regime is observed for low or high small-particle concentrations. Juarez, Lueptow, and Ottino (2010) also studied the scaling law related to the distribution of band thickness $f(s)$. They found that the scaling law associated with the spinoidal decomposition regime is $s^2 f(s) = g[s/S(t)]$, where g is the scaling solution and $S(t)$ is the mean thickness at time t.

An intriguing form of axial segregation was recently reported by Inagaki and Yohsikawa (2010) in an almost completely filled drum ($V_p^* = 0.96$). Although the effect of surface flow was minimized through the high volume fraction, segregation into axial bands, as well as traveling waves, was observed. The granules used were garnet sand grains ($d = 1$ mm) and silica sand grains ($d = 0.15$ mm). The bands first formed in the middle of the drum and then traveled toward the ends. The interior concentration field was carefully examined and revealed three main regions (see Fig. 37). The outer region was found to be completely segregated while the inner core was well mixed. The intermediate region consisted of pure silica grains. They conjectured that a steady, large-scale convective flow causes the bands in the outer region to travel toward the end walls, where the granules mix and flow inward through the inner region. They also suggested a 1D model based on the Cahn-Hilliard equation, which captures the traveling bands dynamics.

Hitherto we considered axial segregation in binary mixtures. Investigations of axial segregation and banding in mixtures consisting of multiple components are few. Das

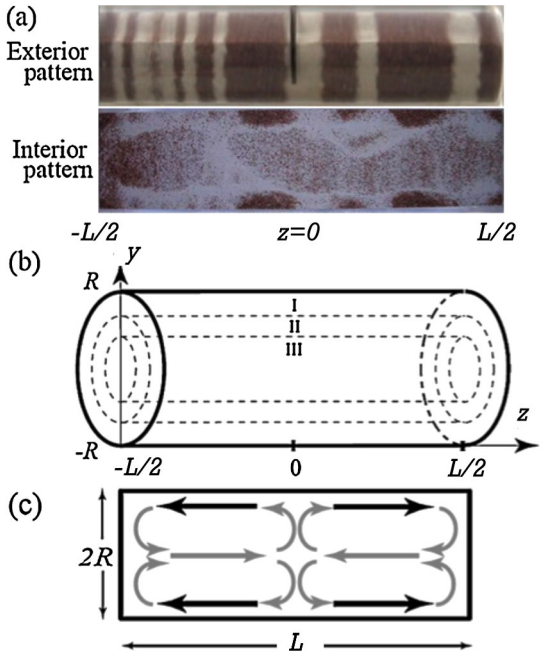

FIG. 37 (color online). Axial segregation in an almost filled drum. (a) Top panel: Side view of axial bands consisting of garnet sand (dark) and silica sand (light). Bottom panel: Interior part of mixture showing three different regions. (b) Sketch of the three radial domains. (c) Schematic of large-scale advection. Adapted from Inagaki and Yohsikawa, 2010.

Gupta, Khakhar, and Bhatia (1991) reported experiments on ternary mixtures consisting of different sieve cuts of sand. Radial segregation was first observed, with the large component occupying the free surface. The middle-size component then segregated and a binary axial band pattern was observed. The small component then axially segregated within the bands of the middle-size component. Newey *et al.* (2004) explored axial segregation for up to six components of glass beads differing in size. The results for the ternary mixture, shown in Fig. 38, were similar to those reported by Das

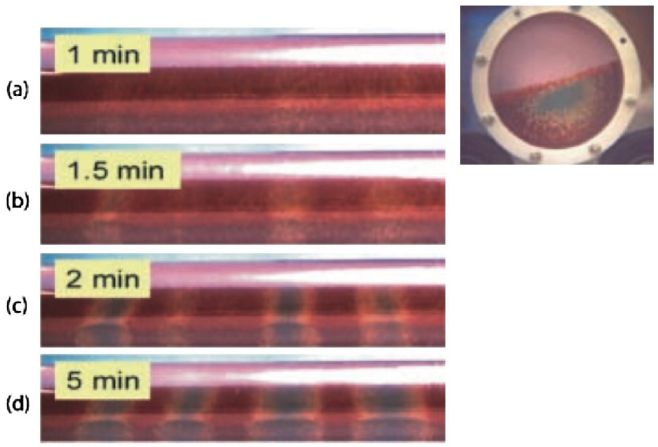

FIG. 38 (color online). Axial segregation in ternary mixture of glass beads (0.6 mm, 1 mm, and 2 mm). The left shows the time sequence of "band within band" formation. The right depicts an on-axis view of radial segregation after 1 min. From Newey *et al.*, 2004.

Gupta, Khakhar, and Bhatia (1991). For mixtures of four components, both radial and axial segregation were observed. However, the banding pattern was not as distinct as for binary and ternary mixtures and the order of the occurrence of bands was not as clear. Five and six component mixtures did show radial segregation, but axial segregation was not observed. Rapaport (2007b) carried out molecular dynamics simulations of ternary mixtures. This work is an extension of a previous investigation of the binary mixture case (Rapaport, 2007a). The results show close agreement with experiments in regard to order of bands (medium particles located between the large and small particles). Radial ordering, however, was not observed in the manner reported in the experiments.

VII. OTHER GEOMETRIES

While the majority of studies on rotating-drum flows focused on the circular cylinder geometry, several works, particularly in the last decade, explored similar phenomenon in tumblers having other geometries. Noncircular cylindrical tumblers are important both from an application perspective, as they are used in various industries, and from a theoretical perspective, to further validate theoretical approaches derived primarily for the simpler cylindrical configuration.

A. 2D tumblers

Noncircular 2D tumblers were used mainly in investigating mixing and segregation of granular materials (Hill *et al.*, 1999; Khakhar *et al.*, 1999; Gilchrist and Ottino, 2003; Jain, Ottino, and Lueptow, 2005b; Cisar, Umbanhowar, and Ottino, 2006; Meier *et al.*, 2006, 2008; Cisar, Lueptow, and Ottino, 2007; Prasad and Khakhar, 2008; Rietz and Stannarius, 2008; Chen *et al.*, 2009; Naji and Stannarius, 2009; Christov, Ottino, and Lueptow, 2010; Prasad and Khakhar, 2010). Unlike circular drums, where under the rolling regime the flow is steady and segregation results in the occurrence of a radial core, noncircular geometries cause the flow to be periodic, with the free-surface length and height oscillating in time (Hill *et al.*, 1999; Khakhar *et al.*, 1999; Jain, Ottino, and Lueptow, 2005b; Cisar, Umbanhowar, and Ottino, 2006). As a result, particle trajectories can be chaotic (Hill *et al.*, 1999) due to streamline crossing and, in the limiting case where the flowing layer is vanishingly small, streamline jumping (Christov, Ottino, and Lueptow, 2010). These systems therefore provide an intriguing example of a dynamical system where order and chaos compete.

Mixing of single component granules in noncircular 2D tumblers was investigated by Khakhar *et al.* (1999), Cisar, Lueptow, and Ottino (2007), Prasad and Khakhar (2008, 2010), and Christov, Ottino, and Lueptow (2010). Khakhar *et al.* (1999) extended the theoretical model derived for the circular configuration (Khakhar *et al.*, 1997a) and compared the predictions to experimental studies carried out with spherical glass beads partially filling elliptic and square tumblers. The main difference in the analysis with respect to the circular geometry lies in the periodic time dependence of the length and depth of the flowing layer, which results in chaotic advection. Both the experimental results and numerical simulations based on the extended continuum model showed that chaotic advection enhances mixing, in comparison with circular containers.

Cisar, Lueptow, and Ottino (2007) used two discrete models in order to investigate avalanche-induced mixing in noncircular tumblers. The first model is based on the cellular automata sandpile model developed by Bak, Tang, and Wiessenfeld (1987). The second is based on the wedge model developed by Metcalfe *et al.* (1995), which successfully reproduced experimental results in the circular configuration. Both models showed that the mixing occurs faster for low volume fractions and in geometries having sharper corners (e.g., triangular versus hexagonal tumblers). Prasad and Khakhar (2008) expanded the treatment of Khakhar *et al.* (1999) using perturbation analysis. The small parameter used in their work was the aspect ratio of flowing layer depth to length. They have considered tumblers having 90° and 180° rotation symmetries. Their analysis showed that the flowing layer thickness is symmetric for all cases and scales with the orientation dependent length of the layer. These predictions were in reasonable agreement with their complementary experiments. Recently, Prasad and Khakhar (2010) investigated mixing in tumblers having square and star shapes, as well as circular drums with two and four wedges. Their results further validated the fact that mixing is enhanced in geometries having sharp corners. In addition, it was observed that the mixing process is nearly the same for particles of different sizes.

Hill *et al.* (1999) studied segregation in square and elliptical tumblers containing mixtures of spherical particles. Both size induced and density induced segregation were explored. Figure 39 shows the experimental results observed for the different geometries, together with a comparison with the theoretical predictions based on a continuum model (Khakhar *et al.*, 1997a) and with the corresponding Poincaré sections. The theoretical treatment is an extension of the derivation made for the circular drum, the main difference being the time dependence of the free-surface length. The Poincaré sections represent a set of trajectories corresponding to different initial conditions, calculated using the single component continuum equations (Khakhar *et al.*, 1997a). The agreement between segregation patterns obtained from the theoretical analysis and the experimental observations is evident from Fig. 39. In addition, there is good agreement between the nonmixing islands (Hill *et al.*, 1999) surrounding periodic elliptic points[10] and the location of segregated lobes observed in the experiment (labeled E in Fig. 39).

Hill *et al.* (1999) also examined the effect of volume fraction on the segregation patterns in the square geometry. Both experimental results and Poincaré section analysis revealed a strong dependency on volume fraction, especially close to the half-full level. Jain, Ottino, and Lueptow (2005b) expanded the investigation of Jain, Ottino, and Lueptow (2005a) on the combined effect of percolation and buoyancy in binary mixtures partially filling a circular drum to a square drum. Experiments were carried out in an equal volume

[10]These islands are known as the Kolmogorov-Arnold-Moser (Kolmogorov, 1954; Arnold, 1963; Moser, 1962) regions in the Poincaré section.

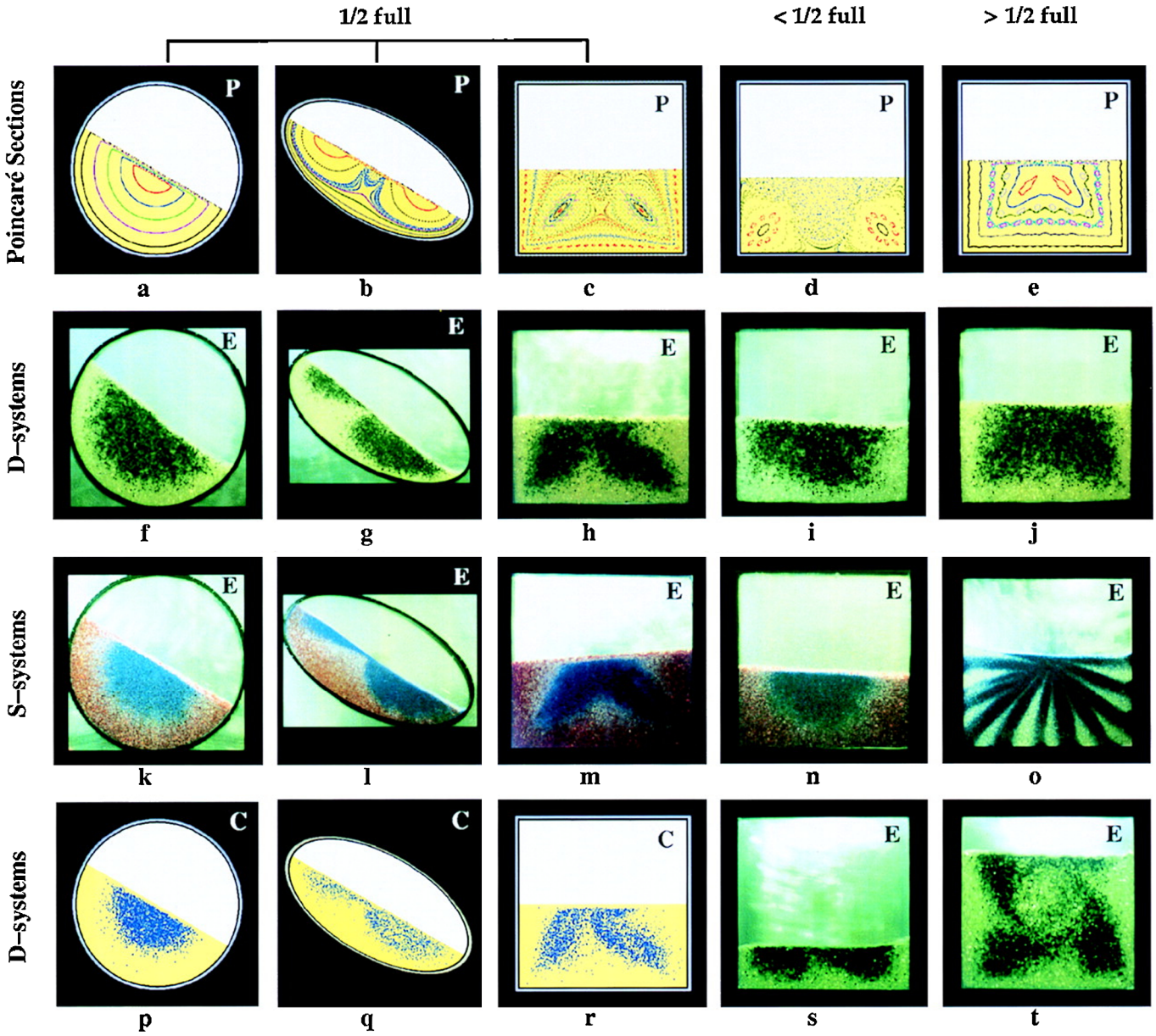

FIG. 39 (color online). Segregation in different 2D tumblers. Both experimental (E) and theoretical [Poincaré sections (P) and computational results based on continuum model (C)] results are shown for circular (first row), elliptic (second row), and square (third to fifth rows) tumblers. The distinguishing parameter [i.e., density (D system) or size (S system)] is noted on the left. The D system consists of 2 mm glass and steel spheres while the S system consists of a ternary mixture of glass beads (0.8 mm, 1.2 mm, and 2 mm). The volume fraction is noted at the top. From Hill *et al.*, 1999.

binary mixture of glass and steel beads. While the patterns observed differed significantly from those observed in the circular configuration the interplay between the mechanisms of segregation and mixing was found to be similar. In particular, the study reinforced the empirical relationship between size and mass ratios found for circular drums [Eq. (14)]. Cisar, Umbanhowar, and Ottino (2006) expanded the work of Hill *et al.* (1999) to various regular polygonal geometries. Experiments were carried out with bidisperse spherical glass beads while simulations, based on the model developed by Khakhar *et al.* (1997a), were done on binary mixtures of spherical particle differing in density. Their work further verified the strong correlation between the observed segregation patterns and the computed Poincaré sections. Meier *et al.* (2006) complemented the information from the Poincaré sections with analysis of periodic points. Of particular interest are hyperbolic periodic points, which are related to stretching and compression of the flow and therefore correspond to chaotic regions. It was shown that segregation patterns correspond to the orientation of eigenvectors of hyperbolic points.

Recently, Meier *et al.* (2008) reported radial streak coarsening in circular and square tumblers. In the latter case, they used an equal volume bidisperse mixture of glass beads ($d_1/d_2 = 3$). The number of streaks was observed to reduced from five after seven revolutions to two after 2300 revolutions. In addition, as in the case of circular drums (see Sec. VI.B.1), they observed the occurrence of orientation periodicity of the streak pattern (relative to the orientation

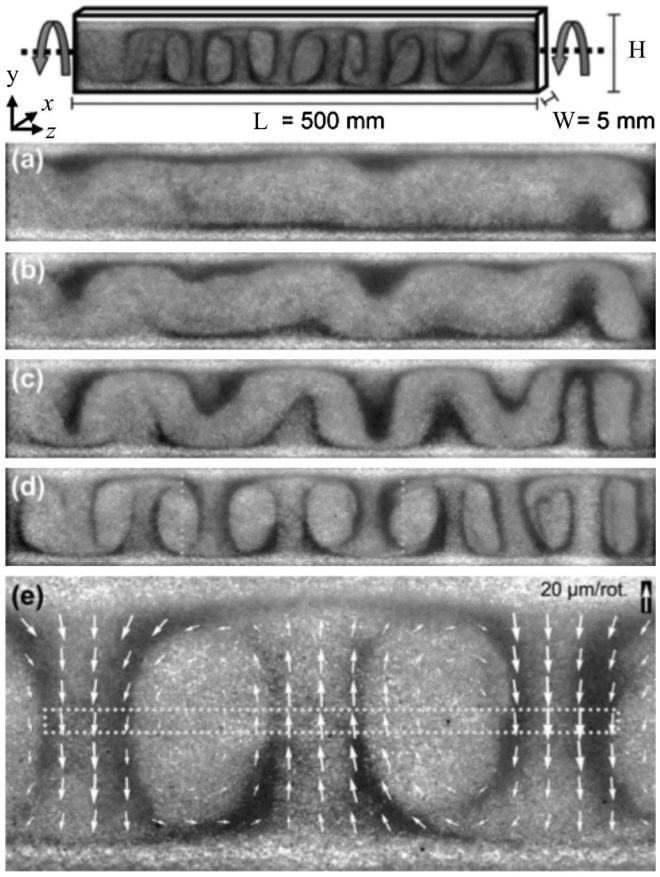

FIG. 40. Convection patterns in rotating Hele-Shaw cell. Evolution of pattern after (a) 2000, (b) 4000, (c) 6000, and (d) 12 000 revolutions. Dark areas have higher concentration of small particles and vice versa. (e) Enlarged central region of (d) with flow field represented by arrows. Adapted from Rietz and Stannarius, 2008.

of the tumbler). For a square tumbler rotating at 2 rpm, the orientation periodicity was approximately four revolutions.

A different 2D geometry which was the focus of recent studies on dense granular flows is the Hele-Shaw cell. Awazu (2000) numerically investigated segregation behavior of highly packed bidisperse mixtures placed in a thin 2D rectangular box rotating about its axis. The molecular dynamics simulations showed that, although the cell was almost completely full ($V_p^* = 0.84$), both radial and axial segregation occurred. Depending on the Froude number, the small particles were found either close to the walls ($\mathrm{Fr} > 1$) or in a stripe close to the axis of rotation ($\mathrm{Fr} < 1$). Furthermore, a large-scale convection was observed after the radial segregation was formed. Motivated by the work of Awazu, Rietz and Stannarius (2008) carried out an experimental investigation of segregation and pattern formation in a similar configuration. The equal volume, bidisperse mixture consisted of spherical glass beads. As the volume fraction was varied, two different flow regimes were found. The first, at $V_p^* < V_c^* = 0.6$, was characterized by interleaving band patterns, similar in appearance to the ones observed in bidisperse mixtures rotating in a cylindrical drum. The second regime, found at $V_p^* > V_c^*$, was characterized by 2D convection cells along the rotation axis (see Fig. 40). Here a core of larger particles is engulfed by a ring of smaller particles.

B. 3D tumblers

Three-dimensional tumblers can be divided into two groups. The first consists of containers having a uniform cross section. This group includes, for example, the circular and the square cross-section cylinders. The second group consists of tumblers with an axially varying cross section. Notable examples are the sphere and the bicone. In these containers the presence of a "preferred" plane (i.e., the midplane) orthogonal to the axis of rotation will be manifested in the dynamics of the contained bulk, be it granular mixtures or suspensions.[11]

Hill *et al.* (1999) and Fiedor and Ottino (2003) investigated segregation patterns of binary granular mixtures in a square cross-section cylinder. Hill *et al.* (1999) used a tube of aspect ratio $L/a = 6$ and a volume fraction $V_p^* = 0.5$. Surprisingly, while in the corresponding 2D scenario radial segregation was observed only for a short period (less than one revolution), in the 3D drum steady radial and axial segregation patterns were observed (see Fig. 41). Fiedor and Ottino (2003) investigated the long-time behavior of axial band patterns in circular and square cross-section drums, under both dry and wet conditions. They found a similar logarithmic rate of coarsening for all cases (cf. Sec. VI.B.2). The square cross-section geometry was also used by Seiden (2006) for investigating axial segregation of suspended particles in a fluid-filled drum. In a manner similar to the circular case, axial segregation was observed with the same characteristic sawtooth dependency of the wavelength on the drum length (see Sec. V.A.1). The scaled mean wavelength was $\bar{\lambda}/a = 2.2$.

Segregation of bidisperse granular mixtures in a spherical tumbler was investigated by Gilchrist and Ottino (2003), Chen *et al.* (2009), and Naji and Stannarius (2009). Gilchrist and Ottino (2003) investigated segregation in a bidisperse mixture of spherical glass beads contained in a spherical tumbler, which was both rotating and rocking. Rocking was applied in the form of periodic oscillations about an axis orthogonal to the rotation axis. The volume fraction was $V_p^* = 0.5$ and the composition ratio was $V_S/V_L = 1/3$. Both dry and wet (i.e., slurry) conditions were examined. In the former case, for a wide range of rotation rates and rocking amplitudes, they observed a robust band structure consisting of a central band of small particles surrounded on both sides by bands rich in large particles [large-small-large (LSL) configuration]. For high rocking amplitudes the segregated central band bifurcates into spots. When the granules were immersed in water, similar segregation behavior was observed, with the notable exception that an inversion of axial bands [small-large-small (SLS) structure] was observed under slurry conditions.

Naji and Stannarius (2009) investigated size segregation in a mixture of spherical glass beads under slurry conditions, which allowed for MRI measurements of the 3D segregation

[11] A particle adjacent to the wall will experience a normal force with an axial component causing it to migrate toward the midplane.

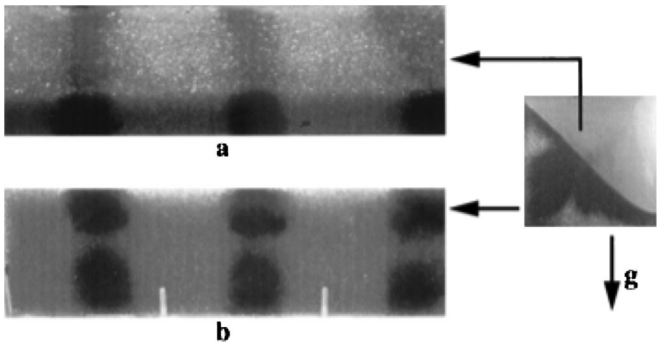

FIG. 41. Axial segregation of a binary granular mixture in a square cross-section drum. Right: Side view. Left: On-axis view. From Hill *et al.*, 1999.

structure. They studied the effect of volume fraction on the three-band structure observed by Gilchrist and Ottino and found a reversal from an SLS configuration at low volume fraction to an LSL structure at high volume fraction (see Fig. 42). The use of MRI revealed a segregated core of small particles which extends to the poles of the sphere. Naji and Stannarius identified three mechanisms which govern the segregation behavior: friction at side walls, sliding on a free surface, and ''Brazil nut'' sieving. Chen *et al.* (2009) carried out a similar experimental study, but under dry conditions. They also observed the inversion of the axial band structure and noted the dependency of the transition fill level on the

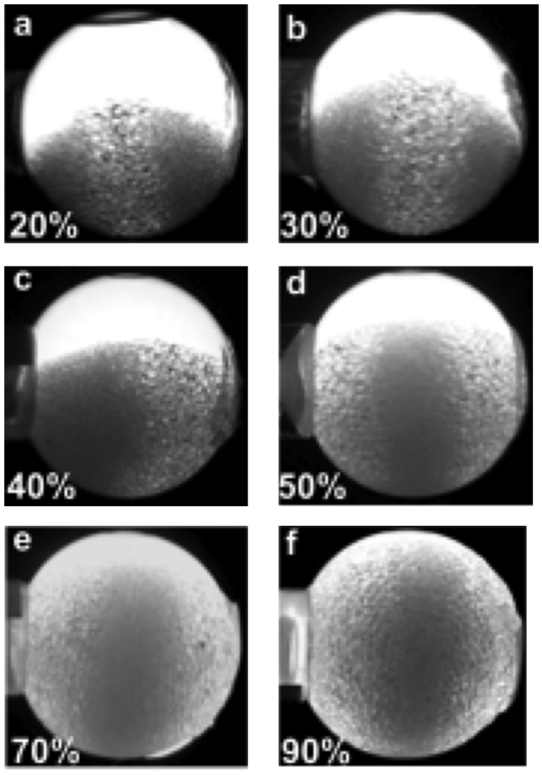

FIG. 42. Segregation of bidisperse granular mixture in spherical drum. At low volume fractions the SLS pattern is observed (dark regions have higher concentration of small beads), while at high volume fractions the LSL configuration is favored. At the transition ($V_p^* \approx 0.4$) different states can be observed (here a two-band configuration is shown). From Naji and Stannarius, 2009.

rotation rate and particle size. In order to investigate the origin of the segregation pattern, they utilized molecular dynamics simulations. These simulations revealed that at low volume fraction small particles drift laterally further toward the poles, as they flow down the free surface, than large particles. Thus the small particles occupy the outer bands and an SLS structure is formed. For high volume fractions, the paths of small and large particles down the inclined free surface almost coincide, though as segregation starts the large particles tend to drift further toward the poles. This slow relative drift results in the LSL band structure. Meier, Lueptow, and Ottino (2007) extended the dynamical-systems approach used for 2D tumblers [see, e.g., Meier *et al.* (2006)] to the sphere. Poincaré sections were calculated and periodic points found and analyzed. The results of continuum model simulations were shown to be in good agreement with the experimental findings [cf. Gilchrist and Ottino (2003)].

VIII. CONCLUDING REMARKS

The rotating horizontal drum is a unique experimental configuration which has served as a fertile tool in the investigation of various phenomena ranging from rimming flows in pure liquids, through segregation in dilute suspensions, to avalanches in granular matter. In the present work we attempted to review the existing literature on the different physical systems related to the rotating-drum configuration. In particular, we set out to compare and interrelate studies on the different realizations of rotating-drum flows.

The large variety of phenomena associated with the rotating-drum configuration includes stable, periodic, and chaotic dynamics. It includes processes having characteristic time scales ranging from $O(10^{-4}\ \Omega^{-1})$ to $O(10^{4}\ \Omega^{-1})$. The patterns observed in the different realizations of rotating-drum flows can be one, two, or three dimensional; they can be reversible or they can exhibit hysteresis.

In this review we put an emphasis on scaling laws governing the rich variety of dynamics observed for different realizations of rotating-drum flows. In particular, in Sec. II.B, we outlined a comprehensive dimensional analysis that treats the various realizations as different regions in a generic nondimensional parameter space. The use of such a comprehensive scaling approach sets a framework that might help to shed light on the relationships between the different systems. In addition, it naturally allows for experimental observations and theoretical investigations of vastly different systems, such as granular mixtures and dilute suspensions, to be treated with respect to a conventional system of dimensionless numbers, a fact that will help form a clear and consistent picture of the contemporary state of our understanding regarding complexity, segregation, and pattern formation in this rich experimental arrangement.

To date, the dimensionless numbers which were explored the most are the Froude and Reynolds numbers. This is in large part due to their dependency on the rotation rate, which can easily be varied in experiment. A relatively large number of studies focused on scaling laws which combined a few dimensionless numbers [see e.g., Alonso, Satoh, and Miyanami (1991) and Jain, Ottino, and Lueptow (2004)]. While these studies revealed important dependencies or

even manifolds in parameter space separating different states, there is concern that the reported laws might lack accuracy due to the multiple parameter intervals they attempt to cover.

It is interesting to compare the time scales characteristic of the different rotating-drum flows. Granular flows exhibit the shortest reported time scales [i.e., $O(10^{-4}\ \Omega^{-1})$ associated with critical behavior [i.e., duration of an avalanche; see, e.g., Jaeger, Liu, and Nagel (1989)]. For pure liquid rimming flows the reported time scales, which represent transient dynamics such as the formation of shark-teeth undulations from an unperturbed front, are $O(10\ \Omega^{-1})$ to $O(100\ \Omega^{-1})$ (Thoroddsen and Mahadevan, 1997). Similar intermediate time scales can be found for transient dynamics of particle-laden and dense granular flows [e.g., axial banding from an initially mixed state; see, e.g., Zik *et al.* (1994)]. Particle-laden and dense granular flows also exhibit longer time scales, associated with drift or coarsening of axial band patterns [see, e.g., Frette and Stavans (1997) and Guyez and Thomas (2008)], which can reach $O(10^4\ \Omega^{-1})$. Similar long time scales were not reported, to the best of our knowledge, for pure liquid rimming flows.

Apart from a few exceptions, theoretical analyses of rotating-drum flows relied on continuum models based on conservation laws, simplified governing equations derived from a constituent (or microscopic) equation (i.e., Navier-Stokes equation), or on phenomenological models. This can be attributed to the high complexity of the systems in question. While in most cases these simplified models succeeded in reproducing the general features of the phenomena observed experimentally, there were aspects that these models failed to explain. For example, various models have been successful in reproducing axial segregation in binary granular mixtures [see, e.g., Levitan (1998)]. However, the related phenomenon of traveling waves in granular mixtures has to date not been adequately explained. Segregation and axial banding of suspended particles in a fluid-filled rotating drum is yet another example. Here simplifying assumptions with respect to the governing Navier-Stokes equation were employed (Seiden, Ungarish, and Lipson, 2005; Lee and Ladd, 2007), which successfully reproduced the banding phenomenon. However, the related phenomenon of oscillating bands (Seiden, Lipson, and Franklin, 2004; Breu, Kreulle, and Rehberg, 2004), which is intrinsically nonlinear, was not accounted for by these approaches.

In this respect, it is important to note the increasing role of numerical simulations, especially during the last decade. While early works were restricted due to limited computer capacities, recent years have seen valuable contributions [see, e.g., Richard and Taberlet (2008)], including predictions which have been confirmed experimentally [i.e., Taberlet, Losert, and Richard (2004); see Sec. VI.B.2]. It is therefore anticipated that numerical simulations will in the coming years play a significant role in shedding light on important outstanding questions. In addition, numerical simulations could also serve as a valuable complementary tool to experiments in exploring the vast dimensionless parameter space.

In addition to unexplained phenomena, such as those described above, there are flow regimes (or, equivalently, regions in parameter space) that have attracted little or no attention at all. Examples include nondilute suspension flows and flows associated with drums containing more than one liquid. The use of a generic parameter space helps clarify what regions are yet to be explored. The former of the previous examples corresponds to $V_p^* \approx V_f^*$, while the latter implies $V_{f_2}^* \neq 0$. A further example is rimming flows of non-Newtonian liquids, such as polymer solutions. While rimming flows associated with these intriguing liquids were the focus of theoretical and numerical studies, experimental works on such liquids are few. The dimensionless parameter most associated with the latter is the Weissenberg number, which is the product of the polymer relaxation time and the characteristic shear rate and can readily be included in the generic set presented in Table I.

REFERENCES

Acrivos, A., 2002, Comment on "Theory of suspension segregation in partially filled horizontal rotating cylinders," Phys. Fluids **14**, 3750.

Acrivos, A., 2005 (private communication).

Acrivos, A., and B. Jin, 2004, "Rimming flows within a rotating horizontal cylinder: asymptotic analysis of the thin-film lubrication equations and stability of their solutions," J. Eng. Math. **50**, 99.

Aitta, A., 1991, "Nonlinear phenomena at an air-fluid interface in a horizontal, rotating cylinder," Eur. J. Mech. B, Fluids **10**, 175.

Aitta, A., *et al.*, 1988, "New bifurcations in a partially filled, horizontal, rotating cylinder," *Propagation in Non-Equilibrium Systems*, edited by J. E. Wesfreid *et al.* (Springer-Verlag, Berlin), p. 325.

Aldridge, K. D., and L. I. Lumb, 1987, "Inertial waves identified in the earth outer fluid," Nature (London) **325**, 421.

Alexander, A., F. J. Muzzio, and T. Shinbrot, 2004, "Effects of scale and inertia on granular segregation," Granular Matter **5**, 171.

Alexander, A., T. Shinbrot, and F. J. Muzzio, 2002, "Scaling surface velocities in rotating cylinders as a function of vessel radius, rotation rate, and particle size," Powder Technol. **126**, 174.

Alonso, M., M. Satoh, and K. Miyanami, 1991, "Optimum combination of size ratio, density and concentration to minimize free surface segregation," Powder Technol. **68**, 145.

Aranson, I., and L. S. Tsimring, 1999, "Continuum theory of axial segregation in a long rotating drum," Phys. Rev. Lett. **82**, 4643.

Aranson, I., L. S. Tsimring, and V. Vinokur, 1999, "Dynamics of axial separation in long rotating drums," Phys. Rev. E **60**, 1975.

Arndt, T., T. Siegmann-Hegerfeld, S. J. Fiedor, J. M. Ottino, and R. M. Lueptow, 2005, "Dynamics of granular band formation: Long-term behavior in slurries, parameter space and tilted cylinders," Phys. Rev. E **71**, 011306.

Arnold, V. I., 1963, "Small denominators and problems of stability of motion in classical and celestial mechanics," Russ. Math. Surv. **18**, 85.

Ashmore, J., A. E. Hosoi, and H. A. Stone, 2003, "The effect of surface tension on rimming flows in a partially filled rotating cylinder," J. Fluid Mech. **479**, 65.

Awazu, A., 2000, "Size segregation and convection of granular mixtures almost completely packed in a thin rotating box," Phys. Rev. Lett. **84**, 4585.

Bae, S. H., and D. H. Kim, 2007, "Computational study of the axial instability of rimming flow using Arnoldi method," Int. J. Numer. Methods Fluids **53**, 691.

Bagnold, R. A., 1954, "Experiments on a gravity-free dispersion of large solid spheres in a Newtonian fluid under shear," Proc. R. Soc. A **225**, 49.

Bak, P., C. Tang, and K. Wiessenfeld, 1987, "Self-organized criticality: an explanation of the $1/f$ noise," Phys. Rev. Lett. **59**, 381.

Baker, J., T. Oliver, L. Lin, R. Ponnapan, and J. Leland, 2001, "Correlations of critical Froude number of annular-rimming flow in rotating heat pipes," Trans. ASME: J. Fluids Eng. **123**, 909.

Balmer, R. T., 1970, "The hygrocyst—A stability phenomenon in continuum mechanics," Nature (London) **227**, 600.

Balmer, R. T., and T. G. Wang, 1976, "An experimental study of internal hygrocysts," Trans. ASME: J. Fluids Eng. **98**, 688.

Baumann, G., I. M. Janosi, and D. E. Wolf, 1994, "Particle trajectories and segregation in a two-dimensional rotating drum," Europhys. Lett. **27**, 203.

Benilov, E. S., 2004, "Explosive instability in a linear system with neutrally stable eigenmodes. Part 2. Multi-dimensional disturbances," J. Fluid Mech. **501**, 105.

Benilov, E. S., 2006, "Does surface tension stabilize liquid films inside a rotating horizontal cylinder? Part 2: Multidimensional disturbances," Stud. Appl. Math. **116**, 1.

Benilov, E. S., M. S. Benilov, and N. Kopteva, 2008, "Steady rimming flows with surface tension," J. Fluid Mech. **597**, 91.

Benilov, E. S., M. S. Benilov, and S. B. G. O'Brien, 2008, "Existence and stability of regularized shock solutions, with applications to rimming flows", J. Eng. Math. **63**, 197.

Benilov, E. S., N. Kopteva, and S. B. G. O'Brien, 2005, "Does surface tension stabilize liquid films inside a rotating horizontal cylinder?," Q. J. Mech. Appl. Math. **58**, 185.

Benilov, E. S., S. M. Lacey, and S. B. G. O'Brien, 2005, "Exploding solutions for three-dimensional rimming flows," Q. J. Mech. Appl. Math. **58**, 563.

Benilov, E. S., and S. B. G. O'Brien, 2005, "Inertial instability of a liquid film inside a rotating horizontal cylinder," Phys. Fluids **17**, 052106.

Benilov, E. S., S. B. G. O'Brien, and I. A. Sazonov, 2003, "A new type of instability: explosive disturbances in a liquid film inside a rotating horizontal cylinder," J. Fluid Mech. **497**, 201.

Benjamin, T. B., and S. K. Pathak, 1987, "Cellular flows of a viscous liquid that partly fills a horizontal rotating cylinder," J. Fluid Mech. **183**, 399.

Benjamin, T. B., W. G. Pritchard, and S. J. Tavener, 1993, " Steady and unsteady flows of a highly viscous liquid inside a rotating horizontal cylinder," Report No. AM 122, Department of Mathematics, Pennsylvania State University.

Bielenberg, J. R., G. M. Gladysz, and A. L. Graham, 2007, "A parametric study of axial segregation in granular systems," Chem. Eng. Sci. **62**, 4177.

Bird, R. R., R. C. Armstrong, and O. Hassager, 1987, *Dynamics of Polymeric Liquids*, Fluid Mechanics, Vol. 1 (Wiley, New York).

Boateng, A. A., and P. V. Barr, 1997, "Granular flow behaviour in the transverse plane of a partially filled rotating cylinder," J. Fluid Mech. **330**, 233.

Bodenschatz, E., W. Pesch, and G. Ahlers, 2000, "Recent Developments in Rayleigh-Bénard Convection," Annu. Rev. Fluid Mech. **32**, 709.

Boote, O. A. M., and P. J. Thomas, 1999, "Effects of granular additives on transition boundaries between flow states of rimming flow," Phys. Fluids **11**, 2020.

Bretz, M., J. B. Cunningham, P. L. Kurczynski, and F. Nori, 1992, "Imaging of avalanches in granular materials," Phys. Rev. Lett. **69**, 2431.

Breu, A. P. J., C. A. Kreulle, and I. Rehberg, 2003, "Pattern formation in a rotating aqueous suspension," Europhys. Lett. **62**, 491.

Breu, A. P. J., C. A. Kreulle, and I. Rehberg, 2004, "Oscillatory patterns in a rotating aqueous suspension," Eur. Phys. J. E **13**, 189.

Brown, R. A., R. C. Armstrong, N. A. Beris, and P.-W. Yeh, 1986, "Galerkin finite element analysis of complex viscoelastic flows.," Comput. Methods Appl. Mech. Eng. **58**, 201.

Buckingham, E., 1914, "On physically similar systems: Illustrations of the use of dimensional equations," Phys. Rev. **4**, 345.

Cantelaube, F., and D. Bideau, 1995, "Radial segregation in a 2d drum: an experimental analysis," Europhys. Lett. **30**, 133.

Caps, H., R. Michel, N. Lecocq, and N. Vandewalle, 2003, "Long lasting instabilities in granular mixtures," Physica A (Amsterdam) **326**, 313.

Charles, C. R. J., Z. S. Khan, and S. W. Morris, 2005, "Pattern scaling in axial segregation," Granular Matter **8**, 1.

Chen, P., B. J. Lochman, J. M. Ottino, and M. L. Lueptow, 2009, "Inversion of band patterns in spherical tumblers," Phys. Rev. Lett. **102**, 148001.

Chen, P.-J., Y.-T. Tsai, T.-J. Liu, and P.-Y. Wu, 2007, "Low volume fraction rimming flow in a rotating horizontal cylinder," Phys. Fluids **19**, 128107.

Chew, J. W., 1996, "Analysis of the oil film on the inside surface of an aero-engine bearing chamber housing," in *Proceedings of the International Gas Turbine and Aeroengine Congress, and Exhibition, Birmingham, UK* (American Society of Mechanical Engineers, New York), 96-GT-300, p. 1.

Choo, K., T. C. A. Molteno, and S. W. Morris, 1997, "Traveling granular segregation in a long drum mixer," Phys. Rev. Lett. **79**, 2975.

Chou, H., and C. Lee, 2008, "Cross-sectional and axial flow characteristics of dry granular material in rotational drums," Granular Matter **11**, 13.

Christov, I. C., J. M. Ottino, and R. M. Lueptow, 2010, "Streamline jumping: A mixing mechanism," Phys. Rev. E **81**, 046307.

Cisar, S. E., R. M. Lueptow, and J. M. Ottino, 2007, "Geometric effects of mixing in 2D granular tumblers using discrete models," AIChE J. **53**, 1151.

Cisar, S. E., P. B. Umbanhowar, and J. M. Ottino, 2006, "Radial granular segregation under chaotic flow in two-dimensional tumblers," Phys. Rev. E **74**, 051305.

Clément, E, J. Rajchenbach, and J. Duran, 1995, "Mixing of a granular material in a bidimensional rotating drum," Europhys. Lett. **30**, 7.

Das Gupta, S., D. V. Khakhar, and S. K. Bhatia, 1991, "Axial segregation of particles in a rotating cylinder," Chem. Eng. Sci. **46**, 1513.

Deiber, J. A., and R. L. Cerro, 1976, "Viscous flow with a free surface inside a horizontal rotating drum. I. Hydrodynamics," Ind. Eng. Chem. Fundam. **15**, 102.

Donald, M. B., and B. Roseman, 1962, "Mechanisms in a horizontal drum mixer," Br. Chem. Eng. **7**, 749.

Drahun, J. A., and J. Bridgwater, 1983, "The mechanisms of free surface segregation," Powder Technol. **36**, 39.

Dubrulle, B., and L. Valdettarol, 1992, "Consequences of rotation in energetics of accretion disks," Astron. Astrophys. **263**, 387.

Duong, N.-H. P., A. E. Hosoi, and T. Shinbrot, 2004, "Periodic knolls and valleys: Coexistence of solid and liquid states in granular suspension," Phys. Rev. Lett. **92**, 224502.

Duran, J., 1999, *Sands, Powders and Grains* (Springer-Verlag, New York).

Dury, C. M., and G. H. Ristow, 1997, "Radial segregation in a two-dimensional rotating drum," J. Phys. I (France) **7**, 737.

Dury, C. M., G. H. Ristow, J. L. Moss, and M. Nakagawa, 1998, "Boundary effects on the angle of response in rotating cylinders," Phys. Rev. E **57**, 4491.

Elperin, T., and A. Vikhansky, 1998, "Granular flow in a rotating cylindrical drum," Europhys. Lett. **42**, 619.

Evesque, P., and J. Rajchenbach, 1988 C.R. Acad. Sci. Ser. Gen., Ser. 2 **307**, 223.

Fiedor, S. J., and J. M. Ottino, 2003, "Dynamics of axial segregation and coarsening of dry granular material and slurries in circular and square tubes," Phys. Rev. Lett. **91**, 244301.

Fiedor, S. J., P. Umbanhowar, and J. M. Ottino, 2007, "Effects of fluid viscosity on band segregation dynamics in bidisperse granular slurries," Phys. Rev. E **76**, 041303.

Finger, T., and R. Stannarius, 2007, "Influences of the interstitial liquid on segregation patterns of granular slurries in a rotating drum," Phys. Rev. E **75**, 031308.

Finger, T., A. Voigt, J. Stadler, H. G. Nielssen, L. Naji, and R. Stannarius, 2006, "Coarsening of axial segregation patterns of slurries in a horizontally rotating drum," Phys. Rev. E **74**, 031312.

Fischer, D., T. Finger, F. Angenstein, and R. Stannarius, 2009, "Diffusive and subdiffusive axial transport of granular material in rotating mixers," Phys. Rev. E **80**, 061302.

Fomin, S., 2006, "Three regimes of non-Newtonian Rimming flow," Trans. ASME: J. Fluids Eng. **128**, 107.

Fomin, S., T. Hashida, and J. Watterson, 2003, "Fundamentals of steady-state non-Newtonian rimming flow," J. Non-Newtonian Fluid Mech. **111**, 19.

Fomin, S., K. Kilpatrick, and R. Hubbard, 2010, "Rimming flow of a power-law fluid: Qualitative analysis of the mathematical model and analytical solutions," Appl. Math. Comput. **216**, 2169.

Fomin, S., J. Watterson, S. Raghunathan, and E. Harkin-Jones, 2001, "The run-off condition for rimming flow of a power law fluid," Theor. Comput. Fluid Dyn. **15**, 83.

Fomin, S., J. Watterson, S. Raghunathan, and E. Harkin-Jones, 2002, "Steady-state rimming flow of the generalized Newtonian fluid," Phys. Fluids **14**, 3350.

Frette, V., K. Christensen, A. Malthe-Soreenssen, J. Feder, T. Jossang, and P. Meakin, 1996, "Avalanch dynamics in a pile of rice," Nature (London) **379**, 49.

Frette, V., and J. Stavans, 1997, "Avalanche-mediated transport in a rotated granular mixture," Phys. Rev. E **56**, 6981.

Fried, E., A. O. Shen, and S. T. Thoroddsen, 1998, "Wave patterns in a thin layer of sand within a rotating horizontal cylinder," Phys. Fluids **10**, 10.

Frisch, U., 1995, *Turbulence: The Legacy of A. N. Kolmogorov* (Cambridge University Press, Cambridge).

Gans, R. F., 1977, "On steady flow in a partially filled rotating cylinder," J. Fluid Mech. **82**, 415.

Gerashchenko, O. V., 2009, "Power-law distribution of the flux avalanches in a Josephson medium," J. Stat. Mech. 01, P01037.

Giesekus, H., 1982, "A simple constitutive equation for polymer fluids based on the concept of deformation dependent tensorial mobility.," J. Non-Newtonian Fluid Mech. **11**, 69.

Gilchrist, J. F., and J. M. Ottino, 2003, "Competition between chaos and order: mixing and segregation in a tumbler," Phys. Rev. E **68**, 061303.

Govindarajan, R., P. R. Nott, and S. Ramaswamy, 2001, "Theory of suspension segregation in partially filled horizontal rotating cylinders," Phys. Fluids **13**, 3517.

Gray, J. M. N. T., 2001, "Granular flow in partially filled slowly rotating drums," J. Fluid Mech. **441**, 1.

Gray, J. M. N. T., and A. R. Thornton, 2005, "A Theory for particle size segregation in shallow granular free-surface flows," Proc. R. Soc. A **461**, 1447.

Greenspan, H. P., 1969, *Theory of Rotating Fluids* (Cambridge University Press, Cambridge, UK).

Greenspan, H. P., 1976, "On a rotational flow disturbed by gravity," J. Fluid Mech. **74**, 335.

Gutenberg, B., and C. F. Richter, 1956, "Magnitude and energy of earthquakes," Ann. Geof. **9**, 1.

Guyez, E., and P. J. Thomas, 2008, "Spatitemporal segregation-pattern drift in particle-laden rimming flow," Phys. Rev. Lett. **100**, 074501.

Guyez, E., and P. J. Thomas, 2009, "Effects of particle properties on segregation-band drift in particle-laden rimming flow," Phys. Fluids **21**, 033301.

Hardin, M. T., T. Howes, D. A. Mitchell, and A. K. Whittaker, 2002, "Axial mixing in rotating drums using magnetic resonance imaging using bran as a model for solid state fermentation," Biotechnol. Lett. **24**, 521.

Held, G. A., D. H. Solina, D. T. Keane, W. J. Haag, P. M. Horn, and G. Frinstein, 1990, "Experimental study of critical-mass fluctuations in an evolving sandpile," Phys. Rev. Lett. **65**, 1120.

Henein, H., K. Brimacombe, and A. P. Watkinson, 1983, "Experimental study of transverse bed motion in rotary kinks," Metall. Mater. Trans. B **14**, 191.

Hill, K. M., A. Caprihan, and J. Kakalios, 1997a, "Bulk Segregation in a rotating granular material measured by Magnetic resonance imaging," Phys. Rev. Lett. **78**, 50.

Hill, K. M., A. Caprihan, and J. Kakalios, 1997b, "Axial Segregation of granular media rotated in a drum mixer: pattern evolution," Phys. Rev. E **56**, 4386.

Hill, K. M., G. Gioia, and D. Amaravadi, 2004, "Radial segregation patterns in rotating granular mixtures: waviness selection," Phys. Rev. Lett. **93**, 224301.

Hill, K. M., G. Gioia, D. Amaravadi, and C. Winter, 2005, "Moon patterns, sun patterns, and wave breaking in rotating granular mixtures," Complexity **10**, 79.

Hill, K. M., and J. Kakalios, 1994, "Reversible axial segregation of binary mixtures of granular materials," Phys. Rev. E **49**, R3610.

Hill, K. M., and J. Kakalios, 1995, "Reversible axial segregation of rotating granular media," Phys. Rev. E **52**, 4393.

Hill, K. M., D. V. Khakhar, J. F. Gilchrist, J. J. McCarthy, and J. M. Ottino, 1999, "Segregation-driven organization in chaotic granular flows," Proc. Natl. Acad. Sci. U.S.A. **96**, 11701.

Hosoi, A. E., and L. Mahadevan, 1999, "Axial instability of a free-surface front in a partially filled horizontal rotating cylinder," Phys. Fluids **11**, 97.

Inagaki, S., and K. Yohsikawa, 2010, "Traveling Wave of segregation in a highly Filled rotating drum," Phys. Rev. Lett. **105**, 118001.

Ivanova, A. A., V. G. Kozlov, and D. A. Polezhaev, 2005, "Vibrational dynamics of a centrifuged fluid layer," Fluid Dyn. **40**, 297.

Jaeger, H. M., Chu-heng Liu, and S. R. Nagel, 1989, "Relaxation at the angle of repose," Phys. Rev. Lett. **62**, 40.

Jaeger, H. M., S. R. Nagel, and R. P. Behringer, 1996, "Granular solids, liquids, and gases," Rev. Mod. Phys. **68**, 1259.

Jain, N., D. V. Khakhar, R. M. Lueptow, and J. M. Ottino, 2001, "Self-organization in granular slurries," Phys. Rev. Lett. **86**, 3771.

Jain, N., J. M. Ottino, and R. M. Lueptow, 2004, "Effect of interstitial fluid on a granular flowing layer," J. Fluid Mech. **508**, 23.

Jain, N., J. M. Ottino, and R. M. Lueptow, 2005a, "Regimes of segregation and mixing in combined size and density granular systems: an experimental study," Granular Matter **7**, 69.

Jain, N., J. M. Ottino, and R. M. Lueptow, 2005b, "Combined size and density segregation and mixing in noncircular tumblers," Phys. Rev. E **71**, 051301.

Jin, B., 2004 Ph.D. thesis, The City University of New York.
Jin, B., and A. Acrivos, 2004a, "Rimming flows with an axially varying viscosity," Phys. Fluids **16**, 633.
Jin, B., and A. Acrivos, 2004b, "Theory of particle segregation in rimming flows of suspensions containing neutrally buoyant particles," Phys. Fluids **16**, 641.
Johnson, R. E., 1988, "Steady-state coating flows inside a rotating horizontal cylinder," J. Fluid Mech. **190**, 321.
Johnson, R. E., 1990, "Coating flow stability in rotating molding," in *Engineering Science, Fluid Dynamics: A Symposium to Honor T. Y. Wu* (World Scientific, Singapore), p. 435.
Joseph, D. D., J. Wang, R. Bai, B. H. Yang, and H. H. Hu, 2003, "Particle motion in a liquid film rimming the inside of a partially filled rotating cylinder," J. Fluid Mech. **496**, 139.
Juarez, G., R. M. Lueptow, and J. M. Ottino, 2010, "Granular coarsening: Phase space and evolution analogies," Phys. Rev. E **81**, 012301.
Juarez, G., J. M. Ottino, and R. M. Lueptow, 2008, "Axial band scaling for bidisperse mixtures in granular tumblers," Phys. Rev. E **78**, 031306.
Karweit, M. J., and S. Corrsin, 1975, "Observation of cellular patterns in a partially filled, horizontal rotating cylinder," Phys. Fluids **18**, 111.
Kellay, H., Y. Amarouchene, and J. F. Boudet, 2007, "Intermittency of the velocity fluctuations in a granular surface flow," Phys. Fluids **19**, 078104.
Keunings, R., 1989, "Simulation of viscoelastic flow," in *Fundamentals of Computer Modeling for Polymer Processing*, edited by C. L. Tucker (Carl Hanser Verlag, Munich, Germany), p. 403.
Khakhar, D. V., J. J. McCarthy, J. F. Gilchrist, and J. M. Ottino, 1999, "Chaotic mixing of granular materials in two-dimensional tumbling mixers," Chaos **9**, 195.
Khakhar, D. V., J. J. McCarthy, and J. M. Ottino, 1997a, "Radial segregation of granular mixtures in rotating cylinders," Phys. Fluids **9**, 3600.
Khakhar, D. V., J. J. McCarthy, T. Shinbtot, and J. M. Ottino, 1997b, "Transverse flow and mixing of granular materials in a rotating cylinder," Phys. Fluids **9**, 31.
Khakhar, D. V., V. A. Orpe, and S. K. Hajra, 2003, "Segregation of granular materials in rotating cylinders," Physica A (Amsterdam) **318**, 129.
Khakhar, D. V., V. A. Orpe, and J. M. Ottino, 2001, "Continuum model of mixing and size segregation in a rotating cylinder: concentration-flow coupling and streak formation," Powder Technol. **116**, 232.
Khan, Z. S., and S. W. Morris, 2005, "Subdiffusive Axial Transport of Granular Materials in a Long Drum Mixer," Phys. Rev. Lett. **94**, 048002.
Khan, Z. S., W. A. Tokaruk, and S. W. Morris, 2004, "Oscillatory granular segregation in a long drum mixer," Europhys. Lett. **66**, 212.
Kistler, S. F., and P. M. Schweizer, Eds. 1997, *Liquid Film Coating: Scientific Principles and Their Technological Implications* (Chapman and Hall, London).
Kolmogorov, A. N., 1941, "The local structure of turbulence in incompressible viscous fluid for very large Reynolds numbers," C.R. Acad. Sci. URSS **30**, 301.
Kolmogorov, A. N., 1954, "On conservation of conditionally periodic motions for a small change in Hamiltonian's function," Dokl. Akad. Nauk SSSR **98**, 527 (in Russian).
Kovac, J. P., and R. T. Balmer, 1980, "Experimental studies of external hygrocysts," Trans. ASME: J. Fluids Eng. **102**, 226.
Kozlov, V. G., and D. A. Polezhaev, 2008, "Stability of rimming flow under vibration," Microgravity Sci. Technol. **21**, 79.
Krasnapol'skaya, T. S., G. J. F. van Heijst, J. H. Voskamp, and S. A. Trigger, 2001, "Similarities of patterns in fluid and granulated flow inside a horizontally rotating cylinder," International Applied Mechanics **37**, 929.
Lai, P. Y., L. C. Jia, and C. K. Cham, 1997, "Friction induced segregation of a granular binary mixture in a rotating drum," Phys. Rev. Lett. **79**, 4994.
Lawrence, C. J., and R. Mei, 1995, "Long-time behaviour of the drag on a body in impulsive motion," J. Fluid Mech. **283**, 307.
Lee, J., and A. J. C. Ladd, 2002, "Axial Segregation in a Cylindrical Centrifuge," Phys. Rev. Lett. **89**, 104301.
Lee, J., and A. J. C. Ladd, 2005, "Axial Segregation of a Settling Suspension in a Rotating Cylinder," Phys. Rev. Lett. **95**, 048001.
Lee, J., and A. J. C. Ladd, 2007, "Particle dynamics and pattern formation in a rotating suspension," J. Fluid Mech. **577**, 183.
Leighton, D., and A. Acrivos, 1987a, "Measurement of shear-induced self-diffusion in concentrated suspensions of spheres," J. Fluid Mech. **177**, 109.
Leighton, D., and A. Acrivos, 1987b, "The shear-induced migration of particles in concentrated suspensions," J. Fluid Mech. **181**, 415.
Levina, A., J. M. Herrmann, and T. Geisel, 2007, "Dynamical synapses causing self-organized criticality in neural networks," Nature Phys. **3**, 857.
Levine, D., 1999, "Axial segregation of granular materials," Chaos **9**, 573.
Levitan, B., 1998, "Segregation and coarsening of granular mixture in a rotating tube," Physica A (Amsterdam) **249**, 386.
Lin, Y.-Y., 1986, "Numerical solutions for flow in a partially filled, rotating cylinder," SIAM J. Sci. Stat. Comput. **7**, 560.
Lipson, S. G., 2001, "Periodic banding in crystallization from rotating supersaturated solutions," J. Phys. Condens. Matter **13**, 5001.
Lipson, S. G., and G. Seiden, 2002, "Particle banding in rotating fluids: a new pattern-forming system," Physica A (Amsterdam) **314**, 272.
Makse, H. A., 1999, "Continuous avalanche segregation of granular mixtures in thin rotating drums," Phys. Rev. Lett. **83**, 3186.
Malkin, B. A., 1937a, "The behaviour of condensate in paper machine dryers," *The Dominion Engineer* (Dominion Engineering Co. Ltd., Montreal), Vol. 4, No. 4, p. 8.
Malkin, B. A., 1937b, "The behaviour of condensate in paper machine dryers," *The Dominion Engineer* (Dominion Engineering Co. Ltd., Montreal), Vol. 4, No. 5, p. 8.
Maneval, J. E., K. M. Hill, B. E. Smith, A. Caprihan, and E. Fukushima, 2005, "Effects of end wall friction in rotating cylinder granular flow experiments," Granular Matter **7**, 199.
Matson, M., B. J. Ackerson, and P. Tong, 2008, "Measured scaling properties of the transition boundaries in a rotating suspension of non-Brownian settling particles," J. Fluid Mech. **597**, 233.
Matson, W. R., B. J. Ackerson, and P. Tong, 2003, "Pattern formation in a rotating suspension of non-Brownian settling particles," Phys. Rev. E **67**, 050301.
Matson, W. R., M. Kalyankar, B. J. Ackerson, and P. Tong, 2005, "Concentration and velocity patterns in a horizontal rotating suspension of non-Brownian settling particles," Phys. Rev. E **71**, 031401.
Meier, S. W., S. E. Cisar, R. M. Lueptow, and J. M. Ottino, 2006, "Capturing patterns and symmetries in chaotic granular flow," Phys. Rev. E **74**, 031310.
Meier, S. W., R. M. Lueptow, and J. M. Ottino, 2007, "A dynamical systems approach to mixing and segregation of granular materials in tumblers," Adv. Phys. **56**, 757.
Meier, S. W., D. A. Melani-Barreiro, J. M. Ottino, and R. M. Lueptow, 2008, "Coarsening of granular segregation patterns in quasi-two-dimensional tumblers," Nature Phys. **4**, 244.

Melo, F., 1993, "Localized states in a film-dragging experiment," Phys. Rev. E **48**, 2704.
Melo, F., and S. Douady, 1993, "From solitary waves to static patterns via spatiotemporal intermittency," Phys. Rev. Lett. **71**, 3283.
Metcalfe, G., and M. Shattuck, 1996, "Pattern formation mixing and segregation of flowing granular materials," Physica A (Amsterdam) **233**, 709.
Metcalfe, G., T. Shinbrot, J. J. McCarthy, and M. Ottino, 1995, "Avalanch mixing of granular solids," Nature (London) **374**, 39.
Midi, G. D. R., 2004, "On dense granular flows.," Eur. Phys. J. E **14**, 341.
Moffatt, H. K., 1977, "Behaviour of a viscous film on the outer surface of a rotating cylinder," J. Mec. **16**, 651.
Moser, J. K., 1962, "On invariant curves of area-preserving mappings of an annulus," Nachr. Akad. Wiss. Göttingen Math.-Phys. Kl. II **1962**, 1.
Mullin, T., Y. Li, C. Del Pino, and J. Ashmore, 2005, "An experimental study of fixed points and chaos in the motion of spheres in a Stokes flow," J. Appl. Math. Phys. **70**, 666.
Naji, L., and R. Stannarius, 2009, "Axial and radial segregation of granular mixtures in a rotating spherical container," Phys. Rev. E **79**, 031307.
Nakagawa, M., 1994, "Axial segregation of granular flows in a horizontal rotating cylinder," Chem. Eng. Sci. **49**, 2540.
Nakagawa, M., S. A. Altobelli, A. Caprihan, E. Fukushima, and E. -K. Jeong, 1993, "Non-invasive measurements of granular flows by magnetic resonance imaging," Exp. Fluids **16**, 54.
Newey, M., J. Ozik, S. M. Van Der Meer, E. Ott, and W. Losert, 2004, "Band-in-band segregation of multidisperse granular mixtures," Europhys. Lett. **66**, 205.
O'Brien, S. B. G., 2002a, "Linear stability of rimming flows," Q. Appl. Math. **60**, 201.
O'Brien, S. B. G., 2002b, "A mechanism for linear instability in two-dimensional rimming flow," Q. Appl. Math. **60**, 283.
O'Brien, S. B. G., and E. G. Gath, 1998, "The location of a shock in rimming flow," Phys. Fluids **10**, 1040.
Orpe, A., and D. V. Khakhar, 2001, "Scaling relations for granular flow in quasi-two-dimensional rotating cylinders," Phys. Rev. E **64**, 031302.
Orr, F. M., and L. E. Scriven, 1978, "Rimming flow: a numerical simulation of steady, viscous, free-surface flow with surface tension," J. Fluid Mech. **84**, 145.
Ottino, J. M., and D. V. Khakhar, 2000, "Mixing and segregation of granular materials," Annu. Rev. Fluid Mech. **32**, 55.
Oyama, Y., 1939, "Axial segregation of granular materials," Bull. Inst. Phys. Chem. Res. (Tokyo), Rept. 5, **18**, 600.
Parker, D. J., A. E. Dijkstra, T. W. Martin, and J. P. K. Seville, 1997, "Positron emission particle tracking studies of spherical particle motion in rotating drums," Chem. Eng. Sci. **52**, 2011.
Peng, S. W., K. Mizukami, W. Liu, N. Sebe, and T. Takeba, 1997, "An experimental study of condensation heat transfer in a horizontal rotating cylinder with a scraper," Exp. Therm. Fluid. Sci. **14**, 205.
Peratt, B. A., and J. A. Yorke, 1996, "Continuous avalanche mixing of granular solids in a rotating drum," Europhys. Lett. **35**, 31.
Phillips, O. M., 1960, "Centrifugal Waves," J. Fluid Mech. **7**, 340.
Plantrad, G., H. Saadaoui, and B. Pouligny, 2006, "Surface-roughness-driven segregation in a granular slurry under shear," Europhys. Lett. **75**, 335.
Pohlman, N. A., B. L. Severson, J. M. Ottino, and R. M. Lueptow, 2006, "Surface roughness effects in granular matter: Influence on angle of repose and the absence of segregation," Phys. Rev. E **73**, 031304.
Prasad, D. V. N., and D. V. Khakhar, 2008, "Granular flow in rotating cylinders with noncircular cross sections," Phys. Rev. E **77**, 041301.
Prasad, D. V. N., and D. V. Khakhar, 2010, "Mixing of granular material in rotating cylinders with noncircular cross-sections," Phys. Fluids **22**, 103302.
Press, W. H., 1978, "Flicker noises in astronomy and elsewhere," Comments Astrophys. **7**, 103.
Preziosi, L., and D. D. Joseph, 1988, "The run-off condition for coating and rimming flows," J. Fluid Mech. **187**, 99.
Prigozhin, L., 1993, "A variational problem of bulk solids mechanics and free-surface segregation," Chem. Eng. Sci. **48**, 3647.
Prigozhin, L., and H. Kalman, 1998, "Radial mixing and segregation of a binary mixture ia a rotating drum: model and experiment," Phys. Rev. E **57**, 2073.
Rajagopalan, D., R. J. Phillips, R. C. Armstrong, R. A. Brown, and A. Bose, 1992, "The influence of viscoelasticity on the existence of steady solutions in two-dimensional rimming flow," J. Fluid Mech. **235**, 611.
Rajchenbach, J., 1990, "Flow in powders: from discrete avalanches to continuous regime," Phys. Rev. Lett. **65**, 2221.
Rapaport, D. C., 2002, "Simulational studies of axial granular segregation in a rotating cylinder," Phys. Rev. E **65**, 061306.
Rapaport, D. C., 2007a, "Radial and axial segregation of granular matter in a rotating cylinder: A simulation study," Phys. Rev. E **75**, 031301.
Rapaport, D. C., 2007b, "Simulated three-component granular segregation in a rotating drum," Phys. Rev. E **76**, 041302.
Reynolds, O., 1885, "On the dilatancy of media composed of rigid particles in contact, with experimental illustrations," Philos. Mag. **20**, 469.
Richard, P., and N. Taberlet, 2008, "Recent advances in DEM simulations of grains in a rotating drum," Soft Matter **4**, 1345.
Rietz, F., and R. Stannarius, 2008, "On the brink of Jamming: granular convection in densely filled containers," Phys. Rev. Lett. **100**, 078002.
Ristow, G. H., 1994, "Particle mass segregation in a two-dimensional rotating drum," Europhys. Lett. **28**, 97.
Ristow, G. H., 1996, "Dynamics of granular materials in a rotating drum," Europhys. Lett. **34**, 263.
Ristow, G. H., 2000, *Pattern Formation in Granular Materials* (Springer-Verlag, Berlin).
Roberts, G. O., D. M. Kornfeld, and W. W. Fowlis, 1991, "Particle orbits in a rotating liquid," J. Fluid Mech. **229**, 555.
Rosato, A., K. J. Strandburg, F. Prinz, and R. H. Swendsen, 1987, "Why the Brazil nuts are on top: size segregation of particulate matter by shaking," Phys. Rev. Lett. **58**, 1038.
Rosendahl, J., M. Vekić, and J. Kelley, 1993, "Persistent self-organization of sandpiles," Phys. Rev. E **47**, 1401.
Rosendahl, J., M. Vekić, and J. E. Rutledge, 1994, "Predictability of large avalanches on a sandpiles," Phys. Rev. Lett. **73**, 537.
Rossby, C. G., 1939, "Relation between variations in the intensity of the zonal circulation of the atmosphere and the displacements of the semipermanent centers of action," J. Mar. Res. **2**, 38.
Ruschak, K. J., and L. E. Scriven, 1976, "Rimming flow of liquid in a rotating horizontal cylinder," J. Fluid Mech. **76**, 113.
Sanders, J., D. D. Joseph, and G. S. Beavers, 1981, "Rimming flow of a viscoelastic liquid inside a rotating horizontal liquid," J. Non-Newtonian Fluid Mech. **9**, 269.
Sanfratello, L., and E. Fukushima, 2008, "Experimental studies of density segregation in the 3D rotating cylinder and the absence of banding," Granular Matter **11**, 73.
Santomaso, A. C., and L. Petenó, 2006, "Radial segregation driven by axial convection," Europhys. Lett. **75**, 576.

Savage, S. B., and K. Hutter, 1989, "The motion of a finite mass of granular material down a rough incline," J. Fluid Mech. **199**, 177.
Schoklitsch, A., 1933, "Ueber die Verkleinerung der Geschiebe in Flusslaeufen," Akad. Wiss. Wien **142**, 343.
Seiden, G., 2006, Ph.D. Thesis, Technion, Israel.
Seiden, G., 2011, previously unpublished photograph.
Seiden, G., S. G. Lipson, and J. Franklin, 2004, "Oscillatory axial banding of particles suspended in a rotating fluid," Phys. Rev. E **69**, (R)015301.
Seiden, G., M. Ungarish, and S. G. Lipson, 2005, "Banding of suspended particles in a rotating fluid-filled cylinder," Phys. Rev. E **72**, 021407.
Seiden, G., M. Ungarish, S. G. Lipson, 2007, "Formation and stability of band patterns in a rotating suspension-filled cylinder," Phys. Rev. E **76**, 026221.
Sepúlvida, N, G. Krstulovic, and S. Rica, 2005, "Scaling laws in granular continuous avalanches in a rotating drum," Physica A (Amsterdam) **356**, 178.
Sethna, J. P., K. A. Dahmen, and C. R. Myers, 2001, "Crackling noise,"Nature (London) **410**, 242.
Shoichi, S., 1998, "Molecular-Dynamics Simulations of Granular Axial Segregation in a Rotating Cylinder," Mod. Phys. Lett. B **12**, 115.
Shrager, G. R., M. N. Shtokolova, V. A. Yakutenok, Yu. M. Milekhin, V. M. Merkulov, Yu. B. Banzula, S. V. Karyazov, and I. A. Glushkov, 2005, "Modeling of the viscous flow with a free surface inside a rotating horizontal cylinder," Theor. Found. Chem. Eng. **39**, 283.
Taberlet, N., W. Losert, and P. Richard, 2004, "Understanding the dynamics of segregation bands of simulated granular material in a rotating drum," Europhys. Lett. **68**, 522.
Taberlet, N., and P. Richard, 2006, "Diffusion of a granular pulse in a rotating drum," Phys. Rev. E **73**, 041301.
Third, J. R., D. M. Scott, and S. A. Scott, 2010, "Axial dispersion of granular material in horizontal rotating cylinders," Powder Technol. **203**, 510.
Third, J. R., D. M. Scott, S. A. Scott, and C. R. Müller, 2010, "Tangential velocity profiles of granular material within horizontal rotating cylinders modelled using the DEM," Granular Matter **12**, 587.
Thomas, N., 2000, "Reverse and intermediate segregation of large beads in a dry granular media," Phys. Rev. E **62**, 961.
Thomas, P. J., 2011a, previously unpublished photograph.
Thomas, P. J., 2011b, previously unpublished photograph.
Thomas, P. J., G. D. Riddell, S. Kooner, and G. P. King, 2001, "Fine structure of granular banding in two-phase rimming flow," Phys. Fluids **13**, 2720.
Thoroddsen, S. T., and L. Mahadevan, 1997, "Experimental study of coating flows in a partially-filled horizontally rotating cylinder," Exp. Fluids **23**, 1.
Thoroddsen, S. T., and Y.-K. Tan, 2004, "Free-surface entrainment into a rimming flow containing surfactants," Phys. Fluids **16**, L13.
Timberlake, B. D., and J. F. Morris, 2002, "Concentration band dynamics in free-surface Couette flow of a suspension," Phys. Fluids **14**, 1580.
Timberlake, B. D., and J. F. Morris, 2003, "Film depth and concentration banding in free-surface Couette flow of a suspension," Phil. Trans. R. Soc. A **361**, 895.
Tirumkudulu, M., 2001 Ph.D. thesis, The City University of New York.
Tirumkudulu, M., and A. Acrivos, 2001, "Coating flows within a rotating horizontal cylinder: Lubrication analysis, numerical results, and experimental measurements," Phys. Fluids **13**, 14.
Tirumkudulu, M., A. Mileo, and A. Acrivos, 2000, "Particle segregation in monodisperse sheared suspensions in a partially filled rotating horizontal cylinder," Phys. Fluids **12**, 1615.
Tirumkudulu, M., A. Tripathi, and A. Acrivos, 1999, "Particle segregation in monodisperse sheared suspensions," Phys. Fluids **11**, 507.
Tougher, C. H., S. K. Wilson, and B. R. Duffy, 2009, "On the approach to the critical solution in leading order thin-film coating and rimming flow," Appl. Math. Lett. **22**, 882.
Vallette, D. P., W. S. Edwards, and J. P. Gollub, 1994, "Transition to spatiotemporal chaos via spatially subharmonic oscillations of a periodic front," Phys. Rev. E **49**, R4783.
Vallette, D. P., G. Jacobs, and J. P. Gollub, 1997, "Oscillations and spatiotemporal chaos of one-dimensional fluid fronts," Phys. Rev. E **55**, 4274.
Villegas-Díaz, M., H. Power, and D. S. Riley, 2003, "On the stability of rimming flows to two-dimensional disturbances," Fluid Dyn. Res. **33**, 141.
Villegas-Díaz, M., H. Power, and D. S. Riley, 2005, "Analytical and numerical studies of the stability of thin-film rimming flow subject to surface shear," J. Fluid Mech. **541**, 317.
Weidenbaum, S. S., 1958, *Mixing of Solids, in Advances in Chemical Engineering II* (Academic Press, New York), p. 211.
Weinstein, S. J., and J. K. Ruschak, 2004, "Coating Flows," Annu. Rev. Fluid Mech. **36**, 29.
White, R. E., 1956, "Residual condensate, condensate behaviour, and siphoning in paper driers," Tech. Assoc. Pulp Paper Ind. **39**, 228.
White, R. E., and T. W. Higgins, 1958, "Effect of fluid properties on condensate behaviour," Tech. Assoc. Pulp Paper Ind. **41**, 71.
Wilhelmsson, B. I., J. F. McKibben, S. G. Stenström, and C. K. Aidun, 1995, "Condensate flow inside paper dryer cylinders," J. Pulp Pap. Sci. **21**, J1.
Williams, J. C., 1976, "The segregation of particulate material. A review," Powder Technol. **15**, 245.
Wilson, S. D. R., and J. Williams, 1997, "The flow of a liquid film on the inside of a rotating cylinder, and some related problems," Phys. Fluids **9**, 2184.
Wilson, S. K., R. Hunt, and B. R. Duffy, 2002, "On the critical solutions in coating flow and rimming flow on a uniformly rotating horizontal cylinder," Q. J. Mech. Appl. Math. **55**, 357.
Yamane, K., N. Nakagawa, S. A. Altobelli, T. Tanaka, and Y. Tsuji, 1998, "Steady particulate in a horizontal rotating cylinder," Phys. Fluids **10**, 1419.
Yanagita, T., 1999, "Three-Dimensional Cellular Automaton Model of Segregation of Granular Materials in a Rotating Cylinder," Phys. Rev. Lett. **82**, 3488.
Yariv, A., 1969, *Optical Electronics in Modern Communications* (Oxford University Press, New York).
Yih, C. S., 1960, "Instability of a rotating liquid film with a free surface," Proc. R. Soc. A **258**, 63, with Appendix by J. F. C. Kingman.
Zik, O., D. Levine, S. G. Lipson, S. Shtrikman, and J. Stavans, 1994, "Rotationally induced segregation of granular materials," Phys. Rev. Lett. **73**, 644.
Zuriguel, I., J. M. N. T. Gray, J. Peixinho, and T. Mullin, 2006, "Pattern formation by a granular wave in a rotating drum," Phys. Rev. E **73**, 061302.
Zuriguel, I. T., J. Peixinho, and T. Mullin, 2009, "Segregation pattern competition in a thin rotating drum," Phys. Rev. E **79**, 051303.